Technische Universität München

Genetically controlled iron uptake and storage in mammalian cells for magnetic resonance imaging and magnetic actuation

Christoph Massner

Fakultät für Medizin

Technische Universität München

Fakultät für Medizin

Genetically controlled iron uptake and storage in mammalian cells for magnetic resonance imaging and magnetic actuation

Christoph Massner

Vollständiger Abdruck der von der Fakultät für Medizin der Technischen Universität München zur Erlangung des akademischen Grades eines

Doktors der Naturwissenschaften

genehmigten Dissertation.

Vorsitzende: Prof. Dr. Gabriele Multhoff

Prüfende der Dissertation:
1. Prof. Dr. Gil Gregor Westmeyer
2. Prof. Dr. Wolfgang Wurst

Die Dissertation wurde am 13.07.2017 bei der Technischen Universität München eingereicht und durch die Fakultät für Medizin am 21.02.2018 angenommen.

Zusammenfassung

Das Verständnis von molekularen Prozessen in lebenden Organismen ist der Schlüssel zur Entwicklung von effektiven Medikamenten und der Heilung von Krankheiten. Um die Unversehrtheit zellulärer Netzwerke während der Beobachtung und der Interaktion mit diesen Prozessen beizubehalten, müssen nicht-invasive Bildgebungs- und Aktuierungsmethoden benutzt werden. Die Sensitivität und Spezifität dieser Methoden kann durch spezifische Kontrastmittel und Aktuatoren stark verbessert werden. Magnetische Kontrastmittel und Aktuatoren ermöglichen zusätzlich Interaktionen durch Magnetfelder auf zellulärer Ebene. Da magnetische Felder frei durch Gewebe propagieren, haben sie das Potenzial nicht-invasive Bildgebung und Zellaktuierung zu ermöglichen. Ein außergewöhnlicher Ansatz um spezifische Zellnetzwerke zu adressieren und physikalische Barrieren komplexer Organe zu überwinden, ist die genetische Kodierung der gewünschten Kontrastmittel und Aktuatoren. Das Forschungsfeld Magnetogenetik kombiniert die genetische Kodierung mit magnetischen Eigenschaften, um mit den neu entwickelten Systemen biomedizinische Probleme zu lösen.

Das Ziel meiner Doktorarbeit war die Modifikation der eukaryontischen Eisenhomeostase, um Zellen anhand von Magnetresonanzbildgebung (MR-Bildgebung) zu detektieren und die Manipulierbarkeit durch Magnetfelder zu ermöglichen. Dafür habe ich die zelluläre Eisenhomeostase genetisch mit dem Ziel manipuliert, den intrazellulären Eisengehalt zu erhöhen und das zusätzliche Eisen in einer nicht-toxischen, hochmagnetischen Form zu organisieren.

In dem ersten Teil meiner Doktorarbeit wurde er Transferrin-abhängige

Eisentransportweg untersucht. Dieser Transportweg kommt am häufigsten vor und transportiert maximal zwei Eisenatome nach einem Endozytosezyklus in das Zytosol. Es konnte gezeigt werden, dass die zelluläre Eisenladung durch Supplementation mit Eisen(III) und Transferrin erhöht wurde. Gleichzeitig wurde durch diese Methode der T_2-abhängige MR-Kontrast erhöht. Die Grenzen dieses Ansatzes wurden jedoch erreicht, da, wahrscheinlich auf Grund von starken zellulären Regulationsmechanismen, keine effektiven genetischen Veränderungen vorgenommen werden konnten.
Eine Art diesen hochregulierten Transportweg zu umgehen war die Einführung von Eisen(II)-abhängigen Transportproteinen. Das Protein Zip14 wurde wegen seines pH-Optimums dem gut bekannten Protein DMT1 vorgezogen. Durch den Zip14-abhängigen Eisentransport konnte die zelluläre Eisenbeladung stark erhöht werden. Jedoch führten hohe, unkontrollierte Eisenmengen im Zytosol zu starker Toxizität. Dieser Effekt konnte durch die Überexpression von Eisenspeicherproteinen, hauptsächlich Heavy Chain Ferritin, reduziert werden. Durch den Eisen(II)-abhänigen Transportweg konnte die Eisenladung 2-3-fach erhöht werden und gleichzeitig wurde der MR-Kontrast ca. 3,5-fach im Vergleich zu Kontrollzellen verstärkt. Obwohl die Eisenladung zusätzlich durch die Benutzung von Ascorbinsäure erhöht werden konnte, war Zelltot, wahrscheinlich durch die Toxizität von freiem Eisen im Zytosol, der limitierende Faktor dieses Ansatzes.
Im Gegensatz dazu erlaubt der Ferritin-abhängige Transportweg einen sicheren Transport von Eisen in das Innere der Zellen, in Kombination mit einer gesteigerten Endozytoseeffizienz von bis zu 4500 Eisenatomen pro Zyklus. Die zusätzliche genetische Kontrolle durch die Überexpression der Ferritinrezeptoren TfR1, Tim-2 und Scara5 ermöglichte hohe zelluläre Eisenladungen, die einen ca. 5-fach erhöhten MR-Kontrast während TfR1 Überexpression und eine ca. 10-fache Erhöhung während der Überexpression von Tim-2 oder Scara5 zur Folge hatte. Interessanterweise wurde der beobachtete MR-Effekt wahrscheinlich durch lysosomale Kluppung des endozytierten Ferritins verstärkt. Um die Sensitivität von MRT zu erhö-

hen und um magnetische Interaktionen zu ermöglichen, wurde der Ferrihydritkern von Ferritin durch superparamagnetisches Magnetit ersetzt. Dadurch entstand hFTH-Mag. Durch magnetische Wechselwirkungen konnten 30% der TfR1 und Tim-2 überexprimierende Zellen spezifisch absortiert werden. Zusätzlich war es durch Tim-2 induzierte hFTH-Mag Aufnahme möglich ca. 10% der untersuchten Zellen durch magnetische Hyperthermie gezielt abzutöten. Zusätzlich wurde durch die Veränderung der optische Absorption und des Brechnungsindexes des intrazellulären, eisengeladenen Ferritins optoakustische und Frequenzverdreifachungsmikroskopie, sowie spezifische Zellabtötung ermöglicht.

Zusammenfassend habe ich unterschiedliche Möglichkeiten untersucht, die Magnetisierung von Zellen durch genetische Veränderungen zu erhöhen und diese Magnetisierung für nicht-invasiven Bildgebungs- und Aktuierungsmethoden zu benutzen. Dafür wurden drei verschiedene Eisentransportwege evaluiert, von denen der Ferritintransportweg der effizienteste war. Die Kombination dieses Transportweges mit hFTH-Mag ermöglichte magnetische Interaktionen auf zellulärer Ebene. Die Ergebnisse meiner Doktorarbeit beschreiben die vielfältigen Einsatzmöglichkeiten der neuentwickelten, synthetisch-biologischen Werkzeuge für nicht-invasive Bildgebungs- und Aktuierungsmethoden, die zusätzlich genetisch und biosynthetisch angepasst werden kann. Die Kombination aus genetischer Kontrolle der subzellulären Lokalisation und dem Einsatz von modifiziertem Ferritin ist dadurch ein robustes Werkzeug für Untersuchungen von zellulären Netzwerken ohne diese bei der Untersuchung zu verändern oder zu verzerren.

Summary

The understanding of molecular processes in living organisms is the key to developing effective medical treatment and cure disease. To maintain the integrity of cellular networks during the observation and interaction with these processes, non-invasive imaging and actuation methods need to be used. The sensitivity and the specificity of these methods can be strongly improved with the help of contrast agents and specific actuators. Magnetic contrast agents and actuators, for instance, introduce cellular susceptibility to magnetic fields. Therefore, they have the potential to enable non-invasive imaging and cell actuation since magnetic fields to not suffer from tissue attenuation. An exceptional approach to address specific cellular networks and to overcome physical barriers in complex organs is the genetic encoding of the desired contrast agents and actuators. The field of magnetogenetics combines genetic encoding with desired magnetic properties to address biomedical problems with newly developed systems.
The aim of my doctoral thesis was the modification of the eukaryotic iron homeostasis, to enable their detection through magnetic resonance imaging (MRI) and render them receptive for magnetic fields. To achieve this goal, I genetically manipulated the cellular iron homeostasis, to increase cellular iron content and organize the excess iron in a non-toxic, highly magnetic form.
In the first part of my doctoral project, the transferrin-dependent iron uptake pathway was investigated. It is the most abundant iron uptake pathway and transports a maximum of two iron atoms after endocytosis to the cytosol. It could be shown that cellular iron loading was elevated after ferric iron and transferrin supplementation. Also, T_2-derived MR-contrast was increased

through this method. However, this system reached its limits due to the lack of genetic modification possibilities, which were probably caused by effective cellular regulation mechanisms.
To bypass this highly regulated pathway, ferrous iron transport proteins were introduced. The protein Zip14 was favored to the well known DMT1 protein because of its physiological pH optimum. High cellular iron loading could be achieved through Zip14 mediated iron transport, but iron mishandling caused severe iron toxicity. This effect could be reduced through the overexpression of iron storage proteins, mainly heavy chain ferritin. The use of the ferrous iron pathway led to a 2 to 3-fold elevation of intracellular iron content and cellular MR-contrast was approx. 3.5-fold enhanced compared to control cells. Even though the iron loading could be further increased through the addition of ascorbic acid, cell death, probably caused by mishandling of high intracellular iron concentration, was the major obstacle to this approach.
In contrast to that, the ferritin uptake pathway allowed for the safe introduction of iron into the cells, combined with an enhanced endocytosis efficiency of up to 4500 Fe-atoms in one cycle. Additionally, the genetic control through the overexpression of the ferritin receptors TfR1, Tim-2 and Scara5 enabled high cellular iron content, which caused an approx. 5-fold increased in MR-contrast during TfR1 overexpression and 10-fold increased during Tim-2 or Scara5 overexpression. Interestingly, the observed MR-contrast enhancement was probably pronounced due to lysosomal clustering of endocytosed ferritin. To increase the sensitivity of MRI and enable magnetic interactions, the ferrihydrite core was substituted with superparamagnetic magnetite, creating hFTH-Mag. Through magnetic interactions, 30% of TfR1 and Tim-2 expressing cells could be sorted. Furthermore, Tim-2 mediated hFTH-Mag uptake allowed for magnetic hyperthermic cell ablation of approx. 10% of the examined cells. Additionally, it was possible to achieve optoacoustic and third harmonic imaging with specific photoablation through the change of optical absoprtion and refractive index properties of intracellular, iron loaded ferritin.
In conclusion, I investigated different possibility to enhance cellular mag-

netisation through genetic modifications and to use this magnetisation for non-invasive imaging and actuations methods. Therefore, three different iron uptake pathways were evaluated and the ferritin uptake pathways proved to be the most efficient. The combination of this pathway with the use of hFTH-Mag enabled magnetic interactions on cellular levels. The findings of this thesis describe the broad possible use of the newly developed bioengineered toolbox for multimodal, non-invasive imaging and and actuation which can be tailored genetically and biosynthetically. The combination of genetic control over the subcellular localization and the use of modified ferritn is thereby a robust tool for cellular network studies without interruption and potential distortion of the systems under investigation.

Contents

List of Figures

List of Tables

Abbreviations

3' UTR	3' untranslated region
5' UTR	5' untranslated region
BBB	Blood brain barrier
CFS	Cerebrospinal fluid
CP	Ceruloplasmin
DAB PB	Diaminobenzidine enhanced Prussian Blue Staining
DcytB	Duodenal cytochrom B
DMEM	Dulbecco's modified Eagle's medium
DMT1	Divalent metal transporter
DNA	Desoxyribonucleic acid
DPBS	Dulbecco's phosphate-buffered saline
EDTA	Ethylenediaminetetraacetic acid
eFTH+L	Horse spleen ferritin, equine ferritin heavy chain + light chain
FAS	Ferrous ammonium sulfate
FBS	Fetal bovine serum
FC	Ferric citrate
FDA	Federal Drug Administration
FLVCR2	feline leukemia virus subgroup C receptor-related protein 2
G418	Geneticin
GECI	Gnetically encoded calcium indicators
GFP	Green fluorescent protein
H-chain	Heavy chain
HCP1	Heme carrier protein-1
HEK293	Human embryonic kidney cells
HEPES	4-(2-hydroxyethyl)-1-piperazineethanesulfonic acid
HFE	Hemochromatosis protein
hFT	Human heavy chain ferritin

hFTH-Mag	Magnetoferritin, human ferritin heavy chain – magnetic
HRG1	Heme-responsive gene 1 protein homologue
ICP-MS	Inductively coupled plasma mass spectrometry
IPTG	Isopropyl-β-D-thiogalactopyranoside
IRE	Iron responsive element
IRP	Iron responsive protein
ISC	Iron sulfur cluster
L-chain	Light chain
LDH	Lactate dehydrogenase
LHFT	Chimeric ferritin composed of L- and H-chain ferritin
LRP1	Pro-low-density lipoprotein receptor-related protein
MFP	Mean free path
MGE	Multiple gradient echo
MNP	Magnetic nanoparticle
MRI	Magnetic resonance imaging
mRNA	Messenger RNA
MSME	Multi-slice multi-echo
NHS-ester	N-hydroxysuccinimide ester
NTBI	Non-transferrin bound iron
OA	Optoacoustic
OCD	Obsessive-compulsive disorder
PCBP	Poly (rC)-binding portein
PCR	Polymerase chain reaction
PET	Positron emission tomography
PFA	Paraformaldehyde

RNA	Ribonucleic acid
ROI	Regions of interests
ROS	Reactive oxygen species
Scara5	Scavenger receptor member 5
SDS PAGE	Sodium dodecly sulfate polyacrylamid gel electrophoresis
SPECT	Single photon emission computed tomography
SPIO	Superparamagnetic iron oxide
TAE	Tris-Acetate-EDTA
TBS	Tris buffered saline
Tf	Transferrin
TfR1	Transferrin receptor 1
THG	Third harmonic generation
Tim-2	murine T cell immunoglobulin-domain and mucin-domain 2
TMFP	Transport mean free path
TrpV1	Transient receptor potential cation channel subfamily V member 1
VSM	Vibrating Sample Magnetometer
WB	Western blotting
XCT	X-ray computed tomography
YFP	Yellow fluorescence protein
Zip	ZRT, IRT1-like protein

Chapter 1

Introduction

Biological and medical research is a highly interdisciplinary field of science facing the great challenge of explaining how complex molecular and cellular networks operate to realize complicated physiological functions. For a deeper understanding of correlative and causal relationships, various imaging and manipulation techniques are used. Each of them harboring inherent physical limitations in penetration depth, resolution or sensitivity. Some limitations can be overcome with the help of contrast agents. These contrast agents, on the other hand, introduce a different set of inherent limitations e.g. in specificity, delivery or addressability. Genetically encoded contrast agents are an elegant tool to overcome the major limitations of synthetic contrast agents in complex biological systems like the brain. If they can be used with non-invasive imaging and interaction techniques simultaneously, it would be possible to gain profound knowledge of the systems in question through observation and interaction in its most natural state.

1.1 Molecular Imaging and Manipulation in Neuroscience

Molecular imaging emerged as a discipline combining molecular biology and *in vivo* imaging. It is a biomedical discipline that provides the visualization, characterization, and quantification of biologic processes at cellular and subcellular levels within living subjects [Blasberg & Gelovani-Tjuvajev, 2002; Kang & Chung, 2008]. Nowadays a diverse set of imaging and actuation techniques can be used, depending on the research interest. The most used imaging techniques in neuroscience are fluorescent imaging, magnetic resonance imaging (MRI), computed tomography (CT), Ultrasound (US), Positron emission tomography (PET) and single photon emission computed tomography (SPECT) [Rudin & Weissleder, 2003]. Actuation techniques are mostly used in research areas for instance in the form of optical or ultrasound actuation [Deisseroth, 2011; Yoo et al., 2011; Lakshmanan et al., 2016], but electrical stimulation, which is the oldest known and used stimulation technique, is also approved by the Federal Drug Administration (FDA) for deep brain stimulation patients with essential tremor, Parkinson's disease, dystonia and obsessive-compulsive disorder (OCD). Furthermore, transcranial magnetic stimulation is FDA approved for treatment of clinical depression.

1.1.1 Optogenetics

To date, the most powerful *in vivo* imaging and interaction tools for preclinical molecular neuroscience are summarized under the name of optogenetics. Optogenetics is the combination of genetic and optical methods to achieve gain or loss of function of well-defined events in specific cells of living tissue [Deisseroth, 2011].

Optogenetic sensors enable for instance imaging of intracellular calcium transients in neurons [Tian et al., 2009]. This can be correlated with neuronal activity because voltage-gated calcium channels open upon the arrival of an action potential and cause a calcium influx. This generates

further calcium release from intracellular storages and finally results the migration and fusion of vesicles filled with neurotransmitter with the presynaptic cleft [Rusakov, 2006]. Calcium imaging with synthetic calcium indicators has been used for decades to measure neuronal activation *in vivo* and *in vitro* [Yuste et al., 1992; Stosiek et al., 2003; Fetcho et al., 1998]. The more recent development of genetically encoded calcium indicators (GECIs) made it possible to target distinct neuronal populations and circumvent neuronal damage during delivery of the dye. This combination enabled long-term *in vivo* studies [Mank et al., 2008]. The GCaMP proteins found the broadest range of use among GECIs. GCaMPs were initially fusions of the green fluorescent protein (GFP), calmodulin, and M13 -a peptide sequence from myosin light chain kinase- but have nowadays advanced to different spectral properties [Nakai et al., 2001; Zhao et al., 2011].

Optogenetic actuators, on the other hand, help to achieve gain or loss of function in specifically targeted cells in the tissue of living organisms with high spatial and temporal resolution [Deisseroth, 2011]. Therefore, light-sensitive ion channels like channelrhodopsin, halorhodopsin and archaerhodopsin are expressed in cells of interest [Mancuso et al., 2011]. Channelrhodopsins, for instance, are naturally occurring light sensors in unicellular green algae [Nagel et al., 2002]. They are mostly unspecific for H^+, Na^+, K^+ and Ca^{2+} ions, but it was possible to alter ion selectivity as well as kinetics, wavelength and photocurrent amplitude through protein engineering and make them, a widely usable tool in neuroscience [Lin, 2011].

It is unquestionable how much the field of brain science advanced using optogenetic tools, but they bare an inherent limitation: the propagation of light in tissue. Dependent upon the wavelength, the distance for light to become highly diffuse in tissue, is typically between a few hundred micrometers and one millimeter [Ntziachristos et al., 2005]. This means that very limited information can be received or transmitted outside of these limits. Through the use of organisms like *Caenorhabditis elegans*, zebrafish larvae or transparent adult zebrafish these restrictions could be avoided, but for studies of deeper brain regions in mouse or rats highly invasive optical

windows and surgical implantation of optical fibers are used [Hove et al., 2003; Jain et al., 2002].

1.2 Towards Magnetogenetics

The need for photon-independent control of cellular processes resulted in numerous affords to sense and actuate defined cell populations in living tissue and lead to the birth of the field magnetogenetics. The biggest advantage of magnetic actuators as compared to optical actuators is that magnetic fields only weakly interact with tissue, meaning that magnetic actuation and sensing techniques do not suffer for tissue attenuation and can, therefore, enable non-invasive studies of intact cellular systems. The use of magnetic actuators enables the exertion of mechanic forces, heat generation through magnetic hyperthermia and the use as contrast agent for non-invasive imaging, namely MRI [Dobson, 2008; Jordan et al., 1999; Pankhurst et al., 2003].
Most attempts to realize the idea of magnetogenetics relied on chemically synthesized magnetic micro- or nanoparticles with very high magnetic moments. The coating of magnetic particles with molecules that enable binding to certain receptors allows for genetic targeting. Through targeting of the extracellular part of integrin with magnetic nanoparticles (MNPs), it was possible to measure the force needed to twist the magnetic particles and therefore mechanical properties of the cytoskeleton could be quantified [Wang & Ingber, 1995; Wang et al., 1993]. Furthermore, mechanosensitive receptors on the cell surface could be activated through deformation of the whole cell membrane [Pankhurst et al., 2003]. This approach was further improved through the targeting of specific mechanosensitive ion channels and their subsequent opening through the interaction with a magnetic field gradient [Hughes et al., 2008]. Another example of the potential use of magnetic interaction was published by Mannix et al. The authors showed membrane receptor clustering in RBL-2H3 mast cells and the onset of a calcium second messenger signal cascade after binding

of 30 nm MNPs and exposure to high gradient magnetic field [Mannix et al., 2008]. Besides mechanical interaction, it is also possible to influence cell signaling through heat. Heat can be generated by hysteresis loss of many magnetic materials when subjected to a magnetic field that alternates direction [Carrey et al., 2011]. Nevertheless, there is usually no hysteresis loss observed in MNP, and the dominant factors for heat generation in MNP are Brownian and Néel relaxation [Rosensweig, 2002]. Heat-sensitive ion channels on the cell membrane, e.g. the transient receptor potential cation channel subfamily V member 1 (TrpV1), can be targeted by magnetic nanoparticles such that ion channels open and allow calcium influxes when their temperature threshold is exceeded [Huang et al., 2010]. Magnetic particles can also be used as contrast agents for MRI. MRI is a powerful tool for non-invasive whole organ imaging with high resolution and superior soft tissue contrast, thereby relying solely on energy tissue interaction [Rudin & Weissleder, 2003]. There are two different relaxation mechanism that result in conventional MR-contrast, namely spin-lattice relaxation (T_1-relaxation) and spin-spin relaxation(T_2-relaxation) [Bloch, 1946; Bloembergen et al., 1948]. After excitation from its equilibrium in an external magnetic field, each tissue returns to the equilibrium by these two independent processes [Bloembergen et al., 1948]. To overcome the limitations in the sensitivity of MRI and therefore make it a powerful molecular imaging device, contrast agents are widely used [Muller et al., 2001; Lauffer, 1987]. A special form of contrast agents are MNPs, more precisely superparamagnetic iron oxides (SPIOs), which are used to enhance the so-called T_2-contrast in MR-applications. T_2-contrast agents have high magnetic susceptibilities and induce local magnetic field distortions [Roch et al., 1999]. Water molecules diffusing near these particles experience rapid dephasing by the induced field inhomogeneities, and signal loss occurs [Roch et al., 1999]. SPOIs are widely used in research for non-invasive cell tracking [Heyn et al., 2006; Ramos-Gómez & Martínez-Serrano, 2016; Vera et al., 2014]. With the help of SPIOs induced contrast, it was further possible to detect single cells in the mouse brain via MRI [Heyn et al., 2006].

These achievements in interaction through magnetic forces and imaging of magnetic particles associated with cells are remarkable demonstrations on the versatility of biomagnetic actuators. However, the central weakness of current approaches is the need to use synthetic nanoparticles to achieve sufficiently strong magnetization. As discussed before, synthetic approaches display weaknesses in addressability, delivery, and specificity and additionally suffer from dilution and asymmetrical distribution in tissue [Goodfellow et al., 2016]. Semi-genetic approaches of magnetogenetics give researchers a glimpse of future possibilities to conduct experiments and gather knowledge. But to truly keep pace and eventually outcompete optogenetics, a fully genetic solution must be developed with a robustness close to optogenetic tools.

The Bases for the Development of a Biomagnetic Contrast Agents and Actuators There are only three elements that could potentially form magnetic structures in mammalian organisms: nickel, cobalt and iron. Very little is known about nickel or cobalt homeostasis, besides the essential role of cobalt in humans as an integral part of vitamin B12 and the formation of thyroid hormones. However, low additional amounts of nickel and cobalt are highly toxic [Romero et al., 2014]. In contrast, iron homeostasis is fairly well understood and the knowledge can be used as a starting point for the development of a genetically encoded biomagnetic contrast agents and actuators.

1.2.1 Mammalian Iron Homeostasis

Iron is an essential element of life. It functions as co-factor for DNA replication, oxygen transport, oxygen sensing and hypoxic regulation, intermediary metabolism and detoxification, energy generation, synthesis of neurotransmitter and hormones, host defense and inflammation and cell division [Salvador, 2010; Madsen & Gitlin, 2007; Ganz & Nemeth, 2015]. It has a broad range of oxidation states, ranging from -2 to +6. In biological systems, the +2 and +3 oxidations states are the most common ones

and therefore making iron either an electron donor or electron acceptor for redox reactions, hydrolysis and polynuclear complex formation [Aisen et al., 2001]. The accessibility of iron varies greatly between the ferrous form (Fe^{2+}), which is highly active and soluble in water and the ferric (Fe^{3+}) form, which is insoluble and more stable under physiological conditions [Aisen et al., 2001]. As membrane transport, storage and heme synthesis are dependent on ferrous iron, redox-chemistry of iron is critical [Aisen et al., 2001]. It is highly regulated on systemic and cellular levels because excessive free ferrous iron can result in the uncontrolled generation of reactive oxygen species (ROS) due to Fenton chemistry [Finazzi & Arosio, 2014]. In this reaction, a superoxide is formed after oxidation of ferrous iron. This superoxide leads then to hydrogen peroxide formation and in the last step to hydroxyl radicals. These radicals have the potential to destroy proteins, nucleic acids, and carbohydrates and initiate lipid peroxidation [Aisen et al., 2001].

$$Fe^{2+} + O_2 \longrightarrow Fe^{3+} + {O_2}^{-\cdot}$$
$$2\,{O_2}^{-\cdot} + 2\,H_2 \longrightarrow H_2O_2 + O_2$$
$$Fe^{2+} + H_2O_2 \longrightarrow OH^{\cdot} + OH^{-} + Fe^{3+}$$

To make this fine balancing, iron homeostasis is transcriptionally and translationally regulated on systemic and on cellular levels.

Systemic Iron Homeostasis - Uptake, Trafficking and Storage

Iron is a highly abundant element on earth, but mostly poorly accessible for living organisms. For this reason, many different iron accumulation strategies have evolved in the three domains of life. Systemic iron homeostasis in vertebrates is dominated by iron retention and recycling [Ganz & Nemeth, 2015]. This keeps the total body iron levels relatively constant and correlates with a steady demand of iron which is only enhanced during pregnancy and childhood. Constant iron loss is very little and happens mainly through the skin and intestinal cell death. Iron loss becomes only

significant during bleeding, for instance during menstruation, child birth or injuries [Ganz & Nemeth, 2015].
Systemic iron uptake happens in the jejunum and the duodenum on the apical membrane of enterocytes [Frazer & Anderson, 2005]. Dietary iron is either taken up after reduction by ascorbate through Duodenal cytochrome B (DcytB) by ferrous iron transporters (e.g. DMT1, Zip8 and Zip14) or in the form of heme through heme transporters (e.g. HCP1) [Evstatiev & Gasche, 2011; von Haehling et al., 2015; Garrick, 2011]. After uptake, the iron is trafficked through the cytoplasm, probably inside the iron storage protein ferritin and subsequently, ferrous iron is released into the plasma by ferroportin on the basolateral membrane [McKie et al., 2000; Ganz, 2013]. Iron which is not released into the plasma by enterocytes is lost during 2-5 days due to cellular turn over [Creamer, 1967; Donovan et al., 2005]. If ferrous iron is released, it undergoes oxidation to ferric iron through hephaestin on the cell membrane and is then bound with an association constant of $4.7 \cdot 10^{20}$ M^{-1} to the main blood plasma iron transport protein, namely transferrin (Tf) [Vulpe et al., 1999; Aisen et al., 1978]. Transferrin mainly delivers iron to the liver, which is the main iron storage organ, or to the bone marrow where it is utilized for erythropoiesis [Ganz & Nemeth, 2015]. Adults normally store 3-5 g iron in their body. Mainly in erythrocytes, hepatocytes and marcophages [Ganz & Nemeth, 2006]. This means that systemic iron levels are regulated on the level of duodenal absorption through enterocytes and iron release form macrophages and hepatocytes.

Hecidin- the Main Systemic Iron Regulator

The key regulation step of systemic iron homeostasis is the release of iron from enterocytes, macrophages and hepatocytes to the plasma [Ganz, 2013]. This step is controlled by the liver hormone hepcidin [Ganz & Nemeth, 2015]. Hepcidin is a 2.7 kDa peptide which is synthesized in hepatocytes and released in the blood stream [Ganz, 2013]. Hepcidin binds to ferroportin and causes its endocytosis and lysosomal degrada-

tion [Nemeth et al., 2004]. This leads to diminishing iron release to the plasma and enables the control over the totally available iron in the body [Ganz, 2013]. Hepcidin itself is regulated on the transcriptional level. HAMP transcription is increased during high body iron conditions and inflammation and declined over erythropoietin-stimulated expansion of erythroid precursors [Ganz & Nemeth, 2015]. To date, this transcriptional regulation is the only one known for hepcidin [Ganz, 2013]. During inflammation, for instance, macrophages secrete hepcidin through the TLR-4 pathway [Lin et al., 2007]. These increased levels of hepcidin prevent iron absorption in the gut as well as iron release from iron-recycling macrophages and results in an iron restriction for invading pathogens [Worthen & Enns, 2014].

Iron Homeostasis in the Brain

Iron plays a crucial role in the maintenance of the high metabolic and energetic requirements of neuronal tissues. It is also vital for myelination, neurotransmitter synthesis and metabolism [Gerlach et al., 1994; Belaidi & Bush, 2016]. The highest concentrations of iron are found in the substantia nigra pars compacta and basal ganglia, with levels comparable to the liver [Drayer et al., 1986; Griffiths & Crossman, 1993; Haacke et al., 2005; Singh et al., 2014]. During the process of aging, iron is accumulated in the brain mainly in ferritin and neuromelanin [Connor et al., 1992; Zecca et al., 2001, 2004]. All the regions in which iron is accumulated, namely the substantia nigra, putamen, globus pallidus, caudate nucleus, and cortices, are associated with neurodegenerative disorders [Berg & Youdim, 2006; Rodrigue et al., 2011; Ward et al., 2014; Hare et al., 2015]. There is a clear correlation between increased cellular iron content and resulting cellular damage through oxidative stress in neurodegenerative diseases like Parkinson's, Alzheimer's, Huntington's and Friedreich ataxia [Zecca et al., 2004; Barnham et al., 2004; Greenough et al., 2013]. Nevertheless, it remains unclear whether increased iron concentrations are a primary or secondary cause. Only two of the ten known forms of neurodegenerative diseases with increased pathological iron levels involve mutation of genes

directly involved in iron homeostasis: neuroferritinopathy and aceruloplasminemia [Singh et al., 2014]. In the other forms lipid metabolism, mitochondrial function, lysosomes and autophagosomes are impaired [Singh et al., 2014].

The brain has two major barriers: the blood-brain barrier (BBB) and the brain cerebrospinal fluid (CSF) [McCarthy & Kosman, 2015]. To enter the brain iron has to cross the BBB. This is mediated through the transferrin receptor 1 (TfR1) which is highly expressed on the luminal side of endothelial cells [Moos et al., 2007]. The mechanism of the subsequent release of iron of the abluminal side is still elusive [Belaidi & Bush, 2016]. There are two models for its description:

The transcytosis, which is based on the lack of the divalent metal transporter (DMT1) staining, proposes that transferrin bound iron is transported through the cytosol in endosomes and release on the abluminal side [Belaidi & Bush, 2016]. It should be noted that this model could not be verified through transferrin transport studies over the BBB [Moos et al., 2007].

The receptor-mediated transferrin endocytosis model is in accordance with the major iron uptake pathway used in other organs and cells discussed in 1.2.1. It is supported by the proven need for iron in brain endothelial cells, DMT1 expression in Belgrade rat and the expression of ferroportin and ferroxidases in cultured brain endothelial cells [Burdo et al., 2001; Wu et al., 2004; McCarthy & Kosman, 2013; McCarthy et al., 2014]. In consequence, this model defines the brain endothelial cells as a regulatory site for brain iron homeostasis [Simpson et al., 2015].

Both models assign an important role to astrocytes in the process of iron uptake and distribution in the brain. It was proposed that the tight association of astrocytes and endothelial cells enable the formation of a microenvironment which facilitates iron transport as low molecular weight complexes with citrate, adenosine triphosphate or ascorbate, towards astrocytes and away from them [Moos et al., 2007; Ward et al., 2014]. Astrocytes do not express TfR1 but express ferroportin and glycophosphatidylinositol-anchored ceruloplasmin (CP), which oxidizes ferrous iron and facilitates binding to circulating transferrin [Wong & Duce, 2015; Belaidi & Bush,

2016]. During inactivation of ceruloplasmin iron accumulated in astrocytes and no iron accumulation was observed in oligodendrocytes and neurons in the deep nuclei [Patel et al., 2002]. Once iron is released from astrocytes in the brain, it is bound by transferrin, which is secreted from the choroid plexus, and trafficked to neurons which are expressing TfR1, DMT1 and ferroportin [Belaidi & Bush, 2016]. Even though the role of transferrin is similar in the brain as in periphery, iron levels in the brain are not tightly coupled to peripheral iron levels [Belaidi & Bush, 2016]. Transferrin-iron saturation in the brain is close to saturation, whereas iron saturation of transferrin in the periphery is about 30% and only reaches high saturation in diseases[Batey et al., 1980; Brissot et al., 1985; Moos et al., 2007]. In consequence, this means that the buffering capacity of circulating iron in the brain is very low and that there is probably another mechanism in place, which prevents toxic effects of excess iron.

In search of on alternative iron transport system in the brain, Tim-2 was identified as ferritin heavy-chain (H-chain) receptor in rodent [Todorich et al., 2008]. Tim-2 is expressed in oligodendrocytes, which are the cells with the highest content of iron in the brain [Connor & Menzies, 1995; Connor et al., 1995]. Probably this results from the usage of iron as a cofactor for enzymes required for myelination [Connor & Menzies, 1996]. This can be reasoned through iron uptake peaks during periods of strongest myelination [Crowe & Morgan, 1992]. Despite the high demands of iron, there is neither evidence for Tf-binding nor TfR1 mRNA in the white matter of rodents and humans [Hulet et al., 1999; Han et al., 2003]. Furthermore, there is no effect of transferrin receptor expression in myelin-deficient rat model, and iron uptake continues in hypotransferrinemic mice which show no myelin defect [Roskams & Connor, 1992; Takeda et al., 1998]. Functionally Tim-2 is also a negative regulator of T-cell proliferation, which is in agreement with its role as an H-chain receptor because ferritin H-chain is reported to inhibit proliferation of lymphocytes [Rennert et al., 2006; Recalcati et al., 2008].

The source of H-chain ferritin for oligodendrocytes is believed to be microglia. Iron staining is shifted from microglia to oligodendrocytes during

brain development and microglia respond in the adult brain to increased iron levels with ferritin secretion, which promotes the growth of oligodendrocytes [Connor & Menzies, 1995; Zhang et al., 2006]. More evidence is provided by hypoxia/ischemia animal models showing iron enriched microglia in damaged areas of the brain and iron enrichment in microglia when oligodendrocyte development is impaired [Bidmon et al., 2001; Cheepsunthorn et al., 2001; Connor et al., 1990]

Cellular Iron Homeostasis

The understanding of cellular iron homeostasis is the first and most crucial step for the creation of genetically encoded iron-based biomagnetic contrast agents and actuators. Cellular iron homeostasis can differ in detail among cell types but consists mainly of iron import, storage and sometimes export.

Iron Sensing and Signaling Intracellular iron sensing and signaling is carried out by the HIF pathway and heme signaling but mainly by the iron-responsive element (IRE)/iron responsive protein (IRP) system [Hentze et al., 1988; Theil & Eisenstein, 2000; Evstatiev & Gasche, 2011]. IREs are regulatory mRNA elements on proteins involved in iron homeostasis on which IRPs bind according to intracellular iron levels. The position of the IRE determines thereby whether the translation is blocked or carried out. If the IRE is located in the 5' untranslated region (UTR), as for H-chain and L-chain ferritin, binding of the IRP blocks ribosomal formation and therefore inhibits translation [Evstatiev & Gasche, 2011]. As opposed to this, IRP binding on a IRE located on the 3'UTR prevents mRNA from endonucleotic digestion and enhances translation [Evstatiev & Gasche, 2011]. This posttranscriptional regulation mechanism is used for the expression of major iron transport proteins (TfR1 and DMT1), storage proteins (H-chain and L-chain ferritin), iron utilization proteins (ALAS-2, succinyl dehydrogenase, mitochondrial aconitase) and the iron export protein (ferroportin) [Sanchez et al., 2006]. Furthermore, the IRE/IRP sys-

tem is involved in the control of the transcription factor HIF-2α, cell cycle phosphatase cdc14A, the cytoskeleton-regulating kinase MRCK-α and the amyloid precursor protein [Evstatiev & Gasche, 2011]. Currently, there are two IRP known, namely IRP1 and IRP2. The main difference is the form of iron sensing. When there is enough intracellular iron, the iron-sulfur cluster (ISC) synthesis functions normally and IRP1 binds ISCs as cofactor. This causes a change in its function from an mRNA binding protein to a cytosolic aconitase [Paraskeva & Hentze, 1996]. In contrast, IRP2 is controlled by ubiquitination and degradation via the proteasome under iron-replete condition [Salahudeen et al., 2009; Vashisht et al., 2009].

Import Iron import can be categorized according to the chemical state of transported iron. Iron is either transported over the cell membrane in the form of transferrin-bound ferric iron, free ferrous iron, heme-bound ferrous iron or ferritin-bound ferric iron in the form of ferrihydrite [Ganz, 2013; Evstatiev & Gasche, 2011; Liuzzi et al., 2006; Todorich et al., 2008]. All these processes require different transport proteins which are transcriptional and translational regulated.

Transferrin-dependent Iron Import Most cells acquire iron from the blood stream through the so-called transferrin-dependent iron uptake pathway [Garrick, 2011]. This pathway is essential for development because deletion of TfR1 is embryonically lethal at E11-E12 [Levy et al., 1999]. A maximum of two transferrin-bound ferric iron atoms are taken up through transferrin receptor-mediated endocytosis after transferrin binding. Until now it is not clear whether, after acidification of the endosome, ferric iron is released from transferrin and reduced by Steap3, or Steap3 causes the release and reduction of ferric iron from transferrin [Garrick, 2011; Dhungana et al., 2004]. However, ferrous iron is trafficked via DMT1 and/or Zip14 into the cytosol after reduction [Fleming et al., 1998; Zhao et al., 2010]. Transferrin and the transferrin receptor are recycled to the cell membrane and plasma, respectively [Hopkins, 1983; Yamashiro et al., 1984; Dunn et al., 1989]. Inside the cell, iron is either used as a cofactor or stored inside

ferritin [Evstatiev & Gasche, 2011]. Iron uptake via this pathway can be enhanced via ascorbic acid or 2-phosphoascorbate *in vivo* and in cell culture, probably through the facilitation of endosomal reduction of ferric iron to ferrous iron [Hallberg et al., 1986; Frikke-Schmidt & Lykkesfeldt, 2010; Lane et al., 2013].

The transferrin-dependent iron uptake pathway is well understood for many years, but it refers to the function of TfR1. The function of TfR2, which structure shares 45% homology in total and 66% in the ectodomain with TfR1, is not well understood and remains a topic of intense research [Kawabata et al., 1999; Evstatiev & Gasche, 2011; Worthen & Enns, 2014]. In contrast to TfR1, TfR2 is not ubiquitously present but only expressed in liver, erythrocytes, lung and muscle [Kawabata et al., 1999, 2001]. The mRNA is not directly regulated by iron and the expression patterns are opposite to TfR1. Meaning that TfR1 expression is upregulated during iron depletion condition, whereas TfR2 is stabilized during binding with diferric-Tf and therefore reaches higher levels during iron-repleted conditions [Johnson et al., 2007]. Both Tf-receptors interact with another important iron sensing protein, HFE (hemochromatosis protein, HFE stands for *High Fe*). HFE is an MHC class I protein which is brought to the cell surface through interaction with β2-microglobulin [Bhatt et al., 2009]. Binding to TfR1 occurs during low serum iron concentrations and is prohibiting HAMP transcription [Goswami & Andrews, 2006]. During high serum iron concentrations, HFE binds to TfR2, which leads finally to HAMP transcription and subsequent hepcidin production [Goswami & Andrews, 2006; Gao et al., 2009]. TfR2 is considered more an iron sensor than an iron transporter [Worthen & Enns, 2014], because it is stabilized when bound with iron-loaded Tf, its mutations lead to low hepcidin expression and prevent the organism to respond to acute iron-loading [Worthen & Enns, 2014]. Even though TfR2 is also able to mediate cellular iron uptake, its binding affinity is 25-fold lower than that of TfR1 [Kawabata et al., 1999]. This difference may be advantageous for iron sensing and modulation abilities, because it extends the dynamic range of sensing [Worthen & Enns, 2014].

Ferrous Iron Import The ferrous iron uptake pathway is predominately present in enterocytes of the duodenum and is responsible for the systemic acquisition of dietary iron and acquisition of iron in iron overload disorders [Evstatiev & Gasche, 2011; Ganz & Nemeth, 2015]. Non-transferrin bound iron (NTBI) is mainly transported into the cytoplasm by DMT1 and the more recently discovered Zip14(Slc39a14) [Andrews, 1999; Liuzzi et al., 2006]. Ascorbic acid also enhances this iron uptake route, probably through its reducing capabilities which allow iron to be kept in the ferrous state [Lane et al., 2010].
DMT1 is the best characterized mammalian iron transporter, more specifically DMT1 is a ferrous iron transporter. It is also known under the names DCT1 and Nramp2 [Gunshin et al., 1997; Fleming et al., 1997; Gruenheid et al., 1995]. Besides its primary physiological role as an ferrous iron transporter, it also transports Fe^{2+}, Zn^{2+}, Mn^{2+}, Co^{2+}, Cd^{2+}, Cu^{2+}, Ni^{2+} and Pb^{2+} [Gunshin et al., 1997]. DMT1 plays a major role in duodenal iron uptake, is the main responsible protein for the exit of iron during the Tf-dependent iron uptake pathway and plays a role in NTBI-uptake [Garrick, 2011]. For each iron also one proton is transported in the same direction, which make DMT1 a proton-coupled symporter [Picard et al., 2000]. This might explain the natural trafficking of DMT1 to early and late endosomes where the low pH is favorable for its function and close to its pH optimum of 6.75 [Aisen et al., 2001; Worthington et al., 2000].
The Zip family (SLC39) encompasses 14 mammalian transmembrane proteins which function as metal-ion importer [Jenkitkasemwong et al., 2012]. The family name (Zip) is derived from the first characterized member of this protein family namely, ZRT, IRT1-like protein. IRT1 (iron-regulated transporter) is an Arabidopsis cation transporter that is expressed in the roots of iron-deficient plants [Guerinot, 2000]. Generally, Zip proteins are predicted to have eight transmembrane domains with short extracellular C-termini and long extracellular N-termini [Eide, 2004]. Zip14 and Zip8 are broad range metal ion transporters and transport Zn^{2+}, Fe^{2+}, Mn^{2+}, Co^{2+} and Cd^{2+}, but not Cu^{2+} or Cu^{1+}, with a pH optimum of approx. pH 7 [Pinilla-Tenas et al., 2011; Wang et al., 2012; Jenkitkasemwong et al.,

2012]. While Zip14 and Zip8 share basic mechanistic features, they differ in tissue, cellular and subcellular distribution. Luizzi et. al showed highest expression of Zip14 in duodenum [Liuzzi et al., 2006], whereas most studies agree that in humans Zip14 is most abundant in liver, pancreas and heart [Jenkitkasemwong et al., 2012]. In contrast, Zip8 is most abundantly expressed in lung, testis and kidney [Jenkitkasemwong et al., 2012]. In isolated cells or cell lines Zip14 and Zip8 are mostly present in the cell membrane, after expression from overexpression systems and from endogenous loci [Jenkitkasemwong et al., 2012]. Nevertheless, there are reports of cell type-specific differences in Zip14 and Zip8 trafficking, which show protein localization at the cytoplasm, endosome, lysosome and even in mitchondria [Jenkitkasemwong et al., 2012]. It is well understood that the 14 members of ZIP family and the ten members of the ZNT family are the key regulators of zinc homeostasis, but their role in iron homeostasis is still not completely understood [Fukada & Kambe, 2011]. As discussed, DMT1 is essential for intestinal iron absorption and cannot be substituted if knocked-out in adult mice, so they become iron deficient and anemic [Shawki et al., 2012]. In contrast, DMT1 does not seem to be essential for iron uptake from milk during early development [Thompson et al., 2007]. The high expression for Zip14 in the duodenum could explain a possible compensation during this period, before the acid microenvironment is formed and the pH shifts below 6.5, which limits transports capabilities drastically [Pinilla-Tenas et al., 2011; Zhao et al., 2010; Collins et al., 1997]. In adult animals, Zip14 is the primary NTBI transporter into liver, pancreas and heart during iron overload disorders [Jenkitkasemwong et al., 2012]. A different role of Zip14 was shown in Hep-G2 cells. In transfected cells Zip14 was found in early endosomes, colocalized with transferrin and showed the ability, despite the low pH, to transport iron into the cytosol [Zhao et al., 2010]. Nevertheless, it is not expected that Zip14 plays a major role in TBI (transferrin bound iron) uptake because it is weakly expressed in the bone marrow, where most TBI of the body is taken up by erythroid cells, and cannot compensate for DMT1 loss [Taylor et al., 2007; Gunshin et al., 2005]. The role of Zip8 in iron metabolism is

even less defined. Zip8 is strongly expressed in the placenta and might therefore function as a mediator of metal transfer between mother and fetus, because downregulation causes the death of the fetus in the neonatal period, whereas knockout mice of DMT1 and Zip14 are born with normal iron levels [Begum et al., 2002; Wang et al., 2012]. High expression of Zip8 in lung, kidney, testis and pancreas could elute to an impact in iron homeostasis of these organs, but very little is known up to now about it.
Iron absorption via porphyrin-bound iron plays an important role in dietary iron uptake. The sources of porphyrin-bound iron (heme) are mainly vegetables, fruits, cereals and legumes and to a minor account red meat. Heme is mainly taken up by enterocytes in the duodenum in a non- competing manner to inorganic iron [Arredondo et al., 2008; Raffin et al., 1974; Morgan & Oates, 2002]. In total, 60% of the entire iron in the body is bound in heme and functions as a prosthetic group in hemoglobin, myoglobin, cytochromes, catalase, peroxidase and nitric oxide synthase [Padmanaban et al., 1989]. It also has vital functions in transcription, translation and cellular differentiation [Padmanaban et al., 1989]. Up to date, cellular heme import is the least understood iron import mechanism, and the knowledge is almost entirely restricted to macrophages and erythrocytes [Crielaard et al., 2017]. On macrophages, the scavenger receptor CD163 takes up hemoglobin in a complex with haptoglobin [Kristiansen et al., 2001; Andersen et al., 2012]. If heme is bound to hemopexin a very similar uptake happens through pro-low-density lipoprotein receptor-related protein (LRP1) [Hvidberg et al., 2005]. LRP1 is highly expressed in CD163-positive macrophages and is suggested to aid iron clearance [Hvidberg et al., 2005]. Furthermore, heme-responsive gene one protein homolog (HRG1) and feline leukemia virus subgroup C receptor-related protein 2 (FLVCR2) were also identified as heme transporter proteins [Rajagopal et al., 2008; Duffy et al., 2010]. There is evidence that HRG1 is a transporter of heme across the lysosomal membrane after phagocytosis of senescent erythrocytes by macrophages [White et al., 2013]. It has also been proposed that heme carrier protein-1 (HCP1) takes over the part of heme import [Shayeghi et al., 2005]. However, it is well established that this protein

is a proton-coupled folate transporter called PCFT or SLC46A1 [Inoue et al., 2008; Nakai et al., 2007; Qiu et al., 2006]. Recent experiments suggest that the transporter is not constrained to folate transport but also involved in heme-Fe transport and could play a physiological role in iron nutrition as a low-affinity heme transporter [Le Blanc et al., 2012].

Ferritin-dependent Iron Import Another alternative iron uptake pathway is the ferritin uptake pathway. Even though there is no consensus about the exact physiological role of circulating ferritin, it has been reported that cells in the intestine [San Martin et al., 2008], white matter [Hulet et al., 1999], in the capsule of the adult kidney [Kobayashi, 1978] and in the stroma of embryonic capsule [Li et al., 2009] as well as hepatocytes [Mack et al., 1983; Sibille et al., 1989], lymphoid cells [Moss et al., 1992] and erythroid precursors [Meyron-Holtz et al., 1999] take up ferritin. In all of these cell types, ferritin uses an endocytic pathway [Hulet et al., 2000; Gelvan et al., 1996; Bretscher & Thomson, 1983] and delivers iron to the cytoplasm [Radisky & Kaplan, 1998; San Martin et al., 2008; Li et al., 2009]. To date, there are three ferritin receptors described in human and mice: murine scavenger receptor member 5 (Scara5) [Li et al., 2009], murine T cell immunoglobulin-domain and mucin-domain 2 (Tim-2) [Chen et al., 2005] and human transferrin receptor 1 (TfR1) [Li et al., 2010]. It seems that the ferritin uptake mechanisms evolved independently in mouse and human because Tim-2 and Scara5 are not expressed in humans and murine TfR1 does not function as an H-chain receptor [Chen et al., 2005; Li et al., 2010].
As discussed in 1.2.1, transferrin is the major distributor of iron in the body, nevertheless ferritin can provide sufficient iron, e.g. during erythropoiesis, to compensate for the lack of transferrin [Leimberg et al., 2008, 2003]. Research from Li and colleges showed that the role of the human transferrin receptor 1 in iron homeostasis is not restricted to the mediation of transferrin uptake. They prove that H-chain ferritin can bind to TfR1 with subsequent internalization and trafficking to endosomes and lysosomes [Li et al., 2010]. Interestingly the binding of H-chain ferritin was not reduced

through HFE interaction with TfR1, which reduces transferrin binding to TfR1 [Li et al., 2010]. On the other hand, transferrin can diminish ferritin binding to TfR1 up to 70% but not completely [Li et al., 2010].
Scara5 belongs to the structurally diverse group of scavenger receptors [Pearson, 1996]. These membrane proteins were associated with the recognition of low-density lipoprotein and therefore with the development of vascular disease [Krieger, 1994]. Furthermore specific scavenger receptors, e.g. Scara5, exhibit binding to microbe-associated molecules and it is possible that they, therefore, play a role in innate immunity [Krieger, 1997; Jiang et al., 2006]. It was first shown in 2009 from Li and colleges that Scara5 can function as an L-chain but not as an H-chain ferritin receptor [Li et al., 2009]. By injecting GFP-labeled TfR1$^{(-/-)}$ ES cells into wild-type blastocysts, they were able to conduct studies beyond E11-E12, where a knockout of TfR1 is usually lethal [Li et al., 2009; Levy et al., 1999]. It was shown, that L-chain ferritin was endocytosed in capsular cells in the kidney expressing TfR1 and also by those not expressing TfR1 but showing GFP fluorescence [Li et al., 2009]. Also, iron was obtained for the activation of iron responsive elements through ferritin endocytosis after intracellular trafficking to the lysosomes [Li et al., 2009]. These results suggest that cells can, organ specifically, compensate for TfR1 loss through alternative iron uptake mechanism. The selective uptake of ferritin elutes to ferritin as a non-transferrin source of iron during development, since the ferritin levels are 3-8-fold higher in fetal blood than in that of the mother [Li et al., 2009].
Tim-2 belongs to type 1 transmembrane proteins and is expressed on B cells, on Th2-differentiated T-lymphocytes and as well in the liver, kidney and in the brain [Chakravarti et al., 2005; Chen et al., 2005]. After binding of H-chain ferritin, ferritin undergoes endocytosis and is trafficked to the lysosomes [Chen et al., 2005]. To date, no human ortholog for mouse Tim-2 has been found. Recently Tim-2 was used as a reporter gene for MRI [Patrick et al., 2015]. In this study, Patrick and colleges showed elevated uptake of horse spleen ferritin in HEK293T cells overexpressing Tim-2. Due to the higher ferritin load of cells, they reported higher iron loading

and stronger T_2 derived MR-contrast [Patrick et al., 2015]. Furthermore, they show aggregation of ferritin in the lysosomes after endocytosis and speculate about an enhanced magnetic effect [Patrick et al., 2015]. The ferritin nanocage was also used as a manganese carrier to enhance selectively T_1-drevied MR-contrast, but due to toxic effects, *in vivo* experiments were only conducted with horse spleen ferritin and xenografted HEK293T cells in SCID mice as a proof of concept [Patrick et al., 2015].

Cellular Iron Storage- Ferritin and Hemosiderin Once inside the cell, iron can be utilized or stored. Mitochondria use most of the iron inside the cell as a cofactor for ISC-synthesis, the respiratory chain, and heme-synthesis [Crielaard et al., 2017]. The mitochondrial iron import is realized through mitoferrin 1 and 2 [Shaw et al., 2006].
When intracellular iron exceeds cellular requirements, excess iron must be stored safely but still bioavailable. In all three kingdoms of life the protein ferritin functions as the main cellular iron storage and its expression is regulated on transcriptional levels by IRPs [Finazzi & Arosio, 2014; Evstatiev & Gasche, 2011]. Mammalian ferritins consist of 24 subunits of two types, namely the heavy chain subunit (H-chain) and the light chain subunit (L-chain) [Aisen et al., 2001]. They assemble to a spherical molecule with a mean molecular weight of 450000 kDa, an inner diameter of 7-8 nm and an outer diameter of 12 nm [Aisen et al., 2001]. Most mature ferritin is found in the cytoplasm but also in the nucleus and the mitochondria [Pountney et al., 1999; Drysdale et al., 2002]. The exact composition of ferritin varies depending upon species, organ and inflammation state [Aisen et al., 2001; Harrison & Arosio, 1996]. Iron is stored in a polynuclear form that closely resembles of ferrihydrite, in the cavity of ferritin, after cytosolic ferrous iron is delivered, probably through the iron chaperone poly (rC)-binding portein1 (PCBP1) and PCBP2 [Towe, 1981; Leidgens et al., 2013]. Despite the high homology between the ferritin subunits, they have different purposes. H-chain ferritin has ferroxidase activity and catalyzes oxidization of ferrous iron to ferric iron with hydrogen as an electron donor, producing hydrogen peroxide [Chasteen & Harrison, 1999]. The L-chain subunit har-

bors additional glutamate residues on the interior surface, which produce a microenvironment that facilitates mineralization [Harrison & Arosio, 1996; Ford et al., 1984]. The ferrihydrite core inside ferritin can consist of a maximum of 4500 iron atoms. However, under physiological conditions, it bears 2000-2500 iron atoms and is usually disrupted in its regular structure through phosphate and maybe traces of magnetite and hematite [Aisen et al., 2001]. In case cellular processes require more iron than available in the cytosolic labile iron pool, iron is mobilized from ferritin. This happens through ferritin degradation during ferritinophagy, a form of autophagy, or through the proteasome [Mancias et al., 2014; De Domenico et al., 2006]. Autophagy is the process in which organelles and large proteins are segregated in membrane structures called autophagosomes and delivered to lysosomes for degradation [Yang & Klionsky, 2010]. Recently the protein NCO4, which is known from interactions and co-activation of several nuclear hormone receptors and the control of DNA replication [Bellelli et al., 2014; Heinlein et al., 1999; Lanzino et al., 2005], was identified as cargo receptor, that interacts with ferritin and promotes its transport to the autophagosomes [Mancias et al., 2014; Dowdle et al., 2014]. This was further confirmed in an *in vivo* study where the loss of NCO4 function resulted in ferritin accumulation in all analyzed tissue [Bellelli et al., 2016]. Furthermore, lysosomal activity and therefore the degradation of the ferritin shell where proven to be necessary for the mobilization of iron [Kidane et al., 2006; Asano et al., 2011]. If lysosomal iron mobilization from ferritin is defective, hemosiderin is formed [Richter, 1986]. Hemosiderin is insoluble, consists mainly of denatured H-chain ferritin and is more variable in its phosphate and mineralized structure [Ward et al., 2000; Miyazaki et al., 2002].

Iron Export Iron export is most entirely restricted to enterocytes as described in 1.2.1. After the release of ferrous iron, ceruloplasmin (serum and astrocytes), hephaestin (intestine, placenta, heart, brain and pancreatic β-cells) and zyklopen (placenta) oxidize ferrous iron to ferric iron and therefore enable transferrin loading [Crielaard et al., 2017]. But there are

also less well-understood iron export pathways like the ferritin export pathway. As discussed in 1.2.1 ferritin can be imported into certain cells and this ferritin is believed to be exported from hepatocytes, macrophages and kidney proximal tube cells through release via the secretory lysosomal pathway [Ghosh et al., 2004; Cohen et al., 2010; Mancias et al., 2014]. Erythroid cells apparently use FLVCR1B as heme exporter, if heme concentration reaches critically high levels [Keel et al., 2008]. Macrophages also use this pathway to supply iron directly to erythroblasts [Keel et al., 2008].

1.2.2 Genetically Encoded Biomagnetic Contrast Agents and Actuators

Numerous studies showed that due to overexpression of ferritin, MR-contrast could be increased in cell culture conditions and *in vivo* [Cohen et al., 2005; Genove et al., 2005; Cohen et al., 2007; Naumova et al., 2010; Iordanova & Ahrens, 2012; Feng et al., 2012]. In all studies, iron loading was realized through the transferrin-dependent iron uptake pathway (discussed in 1.2.1) and cells were supplemented with ferric iron. An explanation of the increased iron uptake was given through an endogenous upregulation of transferrin receptor as a result of cellular iron depletion caused by overexpressed ferritin [Cozzi et al., 2000; Feng et al., 2012]. On the other hand, there are no reports of bioengineered TfR1 overexpressing cells showing enhanced MR-contrast due to possible ferritin upregulation. Even though evoked MR-contrast by ferritin is measurable but weak, there are very few reports using an overexpression of TfR1 in combination with ferritin overexpression to enhance ferritin iron loading and therefore MR-contrast [Deans et al., 2006]. The same research group that published ferritin as an *in vivo* MRI gene reporter or to be precise a genetically encoded MRI contrast agent worked extensively on the improvement of the relaxivity of ferritin through bioengineering [Iordanova et al., 2010; Iordanova & Ahrens, 2012; Iordanova et al., 2013]. They reported a chimeric ferritin composed of L- and H-chain ferritin (LHFT), as

well as a cytosolically, targeted mitochondrial ferritin to have an increased T_2-relaxivity [Iordanova et al., 2010, 2013]. However, profound statements about the exact mechanism of contrast enhancement were challenging. The use of non-mammalian ferritin and the screen for iron loading enhancing mutations was carried out recently and lead to evidence for an improved iron loading of this mutated version [Matsumoto et al., 2015]. But since iron loading in the studies was carried out differently than in most mammalian cells, it remains unclear whether the results are generally applicable.

To address the shortcoming of ferritin-evoked MRI contrast and therefore make it an eGFP-like MRI marker, the iron loading of ferritin can be improved, or the ferrihydrite core (which has a weak magnetization [Gossuin et al., 2009]) could be exchanged for instance through a superparamagnetic magnetite core.

Ferritin was also used to evoke responsiveness for magnetic fields in cells. To provide more intracellular iron for ferritin loading the iron transporter DMT1 was used in combination with H-chain ferritin [Kim et al., 2012]. After transient overexpression of both genes, cells were artificially loaded in an iron incorporation buffer containing three mM ferrous iron and nifedipine, which is a controversially discussed DMT1 activator [Ludwiczek et al., 2007; Mackenzie et al., 2010]. After this procedure, cells could be magnetically attracted and sorted [Kim et al., 2012]. Even though the technical details are not compatible with a physiological experimental setup in cell culture or *in vivo*, the potential benefit in direct trafficking of iron into the cytosol, which could result in a higher iron loading of ferritin, was recognized. In other studies, it was even possible to activate heat-sensitive and mechano-sensitive ion channels in cell culture and in *in vivo* experiments through potential interactions of magnetic fields with overexpressed and engineered ferritins [Stanley et al., 2012, 2015, 2016; Wheeler et al., 2016]. The underlying mechanisms of these results remain questionable after detailed biophysical calculations and the lack of reproducibility from other laboratories [Meister, 2016].

1.3 Iron-based Nanostructures as Reporters for Optical Imaging and Actuation

New insights about the cellular interaction and complex biological networks can be gathered with the help of molecular imaging techniques. Amongst others, a tradeoff between resolution, sensitivity and penetration depth has to be made during these studies [Willmann et al., 2008]. Photon-dependent conventional imaging has a physical limit derived from the mean free path (MFP) [Ntziachristos, 2010]. This parameter describes the average distance that a photon travels between two consecutive scattering events [Ntziachristos, 2010]. Since the mean MFP in tissue is 100 µm, photons that travel 100 µm through tissue experience at least one scattering event which results in the blurring of the acquired image [Ntziachristos, 2010]. Techniques like multiphoton and confocal microscopy have been developed to overcome these obstacles. These techniques are facing a different physical limit called transport mean free path, which considers the MFP and the angle by which photos are scattered in each scattering event [Ntziachristos, 2010]. Imaging beyond the limit of 1 TMFP which translates to approx. 1 mm in biological tissue could only be achieved with non-optical approaches like x-ray computed tomography (XCT), ultrasound imaging, positron emission tomography and magnetic resonance imaging [Ntziachristos, 2010]. An emerging molecular imaging modality relies on photon absorption and the detection of an ultrasonic wave after thermoelastic expansion of the absorbing molecules [Ntziachristos, 2010]. This so-called optoacoustic imaging allows for deep tissue imaging with a resolution of approx. 50-200 µm at depths of 10 TMFP [Ntziachristos, 2010]. The development of gene reporters for this imaging modality has been an intense field of research in the last years [Jathoul et al., 2015; Deliolanis et al., 2014; Yao et al., 2016; Jiang et al., 2015]. Iron-based contrast agents have a reddish or black color and can therefore also be used as contrast agents for optoaccoustic imaging [Ha et al., 2012]. Furthermore, they can also be used as a targeted interface for high energy

absorption and subsequent ablation of labeled cells [Huang et al., 2014]. Another non-invasive imaging technique is third harmonic generation (THG). THG relies on an energy conserving, nonlinear coherent scattering process which results in the combination of the energy of three photons and the emission of one photon with triple the energy and one third of the excitation wavelength [Weigelin et al., 2016]. The energy-conserving nature of THG helps to overcome the shortcomings of absorbing and fluorescent materials like bleaching, blinking and signal saturation [Pu & Psaltis, 2013]. THG occurs at interfaces between two structures with different refractive indexes or different third-order nonlinear susceptibilities [Weigelin et al., 2016]. For biological applications, THG microscopy is used for label-free imaging of lipid-rich structures, cellular membranes, calcified bones and enamel in teeth with an imaging depth of approx. 1 mm [Weigelin et al., 2016]. Also, the interface between water and protein agglomerations at the size range of the excitation wavelength (approx. 1 µm) are known to cause this non-linear optical effect [Weigelin et al., 2016].

1.4 Aims of the Thesis

This thesis will be focused on the development of genetically encoded biomagnetic contrast agents and actuators required in the research area of magnetogenetics. Furthermore, the use of this contrast agents and actuators for optoacoustic and third harmonic generation microscopy will be evaluated. The bases of the development lay in the knowledge of mammalian iron homeostasis, and the modification of it will be the starting point. A genetically encoded contrast agents and actuators will enable non-invasive sensing and actuation with high penetration depths without the need for surgical interference. In contrast to state of the art technologies, magnetic fields do not suffer from tissue attenuation [Hove et al., 2003; Jain et al., 2002; Pankhurst et al., 2003]. Genetically controlled biomineralization combines these features with distinct genetic addressability and simplified delivery in complex organs like the brain.

To achieve this goal, cells of interest have to be equipped with an effective iron transport system while being able to store big amounts of iron in a non-toxic manner, preferably in a highly magnetic and inert structure. Control over the crystalline structure of iron and subcellular location of the contrast agents and actuators would bring further improvements of sensitivity and control over distinct cellular processes.
The cavity of ferritin will be explored as an effective iron storage. Bioengineered ferritins have already been used for the generation of stronger MR-contrast than native ferritin, [Iordanova et al., 2010, 2013; Matsumoto et al., 2015] but the MR-contrast of overexpressed ferritin is not only limited by the properties of ferrihydrite but also by the accessible iron at cellular and systemic levels.
Through the most abundant iron uptake pathway only a maximum of two iron atoms can be trafficked through into the cytosol in one endocytosis cycle, but there is the need for high intracellular iron concentrations for the desired contrast agents and actuators. To overcome potential iron limitations, bioengineering of ferrous iron transport pathways will be a central part of this doctoral thesis. During the introduction of a novel, highly effective route of iron import into cells the cytosolic labile iron pool must be tightly controlled and kept very low to prevent harmful Fenton chemistry as discussed in 1.2.1. Recently it was reported that each member of the Poly-r(C)-binding protein (PCBP) family exhibits iron chaperone activity towards ferritin [Leidgens et al., 2013]. Under elevated iron concentration in the cytosol, this could enable effective ferritin loading and the maintenance of a low labile iron.
A different approach to engineer cells as reporter cells for non-invasive imaging and actuation will be the genetically controlled direct uptake of ferritin. This uptake pathway is used in this project for the possibility of obtaining up to 4500 Fe-atoms with a single endocytosis cycle while introducing the storage protein directly in the system. The currently known three ferritin receptors, TfR1, Tim-2 and Scara5 will be used for this approach1.2.1. Ferritin can also be used as a nanocage for the synthesis of superparamagnetic magnetite [Cao et al., 2010]. Magnetite has a higher

magnetic susceptibility than ferrihydrite and therefore the so-called magnetoferritin generates a stronger MR-contrast than native ferritin [Cao et al., 2014]. This improves the sensitivity of MRI dramatically. The stronger magnetic susceptibility probably also enables a wider use of this system as an energy converter for non-invasive cellular actuation.
Besides genetic manipulations, the robust establishment of intracellular iron measurements, qualitative ferritin iron loading determination, MR- measurements on cell pellets, *in vivo* and hyperthermia experiments will be parts of this doctoral project.

Chapter 2

Materials and Methods

All chemicals were purchased in the highest possible grade, mostly from Sigma-Aldrich and Carl Roth. An alphabetical list can be found in the appendix (Table 2). An alphabetical list molecular biological kits and analytical kits can be found in the appendix (Table 4). An alphabetical list of laboratory equipment used can be found in the appendix (Table 5). An alphabetical list of cell culture equipment and items can be found in the appendix (Table 6). All solutions and buffers were prepared with ddH_2O, autoclaved and stored at 4 ℃, if not stated otherwise.

2.1 Molecular Biological Techniques

Plasmid DNA was produced by One Shot Top10 chemically competent *E. coli* (Thermo Fisher Scientific) after transfection and appropriate antibiotics selection. A list of antibiotic concentrations used for bacterial and mammalian cultures can be found in the appendix (Table 5). Plasmid preparation was conducted with Miniprep and Maxi Prep Kits (Qiagen) following the user's manual. For gene expression in mammalian cells, the pcDNA3 backbone (Invitrogen) was used, harboring either a geneticin (G418) or hygromycin antibiotic resistance. The gene of interest was inserted via HiFi DNA Assembly in the multiple cloning site. Two primer pairs were designed using the program NEBuilder Assembly Tool. In short,

one primer pair was designed for the linearization of the plasmid via polymerase chain reaction (PCR). The second primer pair was used for PCR amplification of the gene of interest, introducing a 15 base pair overhang to the linearized plasmid. PCRs were carried out with Q5 Mastermix (New England Biolabs, NEB). The reaction contained 25 µl Q5 Mastermix, 2.5 µl forward and reverse primer (10 µM) and approx. 500 pg template DNA. The final reaction volume of 50 µl was reached by adding ddH_2O. The temperature profile started with an initial denaturation for 30 s at 98℃, followed by 34 cycles of denaturation (30 s at 98 ℃), primer annealing (for 30 s at a temperature according to NEB Tm calculator and elongation (for 30 s/kilo base at 72 ℃). The PCR ended with a final extension for 2 min at 72 ℃ and was afterward stored until further use at 4 ℃. The insert DNA was mixed with plasmid-DNA (50 ng) in molar ratios of 2:1. A volume of 10 µl was used of the HiFi Assembly Mastermix, and the whole reaction mixture was adjusted to 20 µl with ddH_2O. The assembly was routinely carried out for 1 h at 50℃. Chemically competent One Shot Top10 *E. coli* (Thermo Fisher Scientific) were transformed with 2 µl of the reaction mixture following the user's manual. Correct integration of the desired DNA sequence was checked via colony PCR using PCR Master Mix (Genaxxon) and sequencing. For colony PCR single colonies of transformed *E. coli* were used as template DNA. The reaction contained 12.5 µl PCR Mastermix, 2.5 µl forward and reverse primer (10 µM) and 7.5 µl ddH_2O. The temperature profile started with an initial denaturation for 10 min at 95℃ to release DNA from bacteria, followed by 34 cycles of denaturation (30 s at 95 ℃), primer annealing (30s at 53 ℃) and elongation (1 min / kilo base at 72 ℃). The PCR ended with a final extension for 10 min at 72 ℃ and was afterward stored until further use at 4 ℃. A list of primers can be found in the appendix (Table 7). DNA sequencing was carried out by Eurofins Scientific.

Gel Electrophoresis

For electrophoresis of DNA 1% agarose (Carl Roth) gels were prepared in tris-acetate-EDTA (TAE) buffer. Electrophoresis of proteins was performed in a Mini-PROTEAN Tetra cell system (Bio-Rad). Protein extractions from HEK293T or HEK293 cell were conducted with M-Per Mammalian Protein Extraction Reagent (Thermo Fisher Scientific), containing protease inhibitor cocktail (Sigma-Aldrich), according to the user's manual. The protein extracts were stored until further experiments were conducted at -20 ℃ . For analysis of whole cell lysates approx. 30 µg total protein was loaded on polyacrylamide gels. Protein assays were carried out with the BCA-Kit (Pierce BCA Protein Assay Kit, Thermo Fisher Scientific) according to the user's manual.

Sodium Dodecyl Sulfate Polyacrylamide Gel Electrophoresis (SDS-PAGE) Protein samples were mixed with equal volumes of Laemmli sample buffer (Sigma-Aldrich) and heated for 3 min at 95 ℃. Mini-Protean TGX precast (12% polyacrylamide, Bio-Rad) gels were used with a running buffer containing 2.5 mM Tris, 19.2 mM glycine, 0.01% SDS at pH 8.3. Proteins were separated for 45 min at 200 V. Protein were visualized with Coomassie R-250 stain if not used for further analysis.

Native PAGE Protein samples were mixed with native samples buffer (Bio-Rad) and loaded onto Mini-Protean TGX precast (12% polyacrylamide, Bio-Rad) gels. The running buffer contained 25 mM Tris-base and 192 mM glycine. Protein separation was carried out for 45 min at 200 V. Proteins were visualized with Coomassie R-250 stain if not used for further analysis.

Diaminobenzidine enhanced Prussian Blue Staining For iron staining of proteins from whole cell lysates 7 µg protein was loaded per well. DAB-enhanced Prussian Blue (Perls') staining was adapted from Meguro et al. with minor modifications [Meguro et al., 2007]. For Prussian blue

staining, the gels were incubated with freshly prepared 2% potassium hexacyanoferrate (II) solution in 10% HCl for 30 minutes at room temperature. Gels were washed 3×5 min with ddH_2O. For DAB (diaminobenzidine)-enhancement stained gels were incubated in the dark in a freshly prepared solution of phosphate buffered saline, containing 0.025% DAB and 0.005% H_2O_2, for 30 min.

Western Blotting

After SDS-PAGE or native PAGE proteins were blotted, for 1 h at 100 V, on methanol activated Immun-Blot® PVDF Membrane (Bio-Rad). Afterward, the membrane was washed 3×5 min in ddH_2O and blocked for 1 h in tris buffered saline (TBS, 50 mM Tris-HCl, 150 mM NaCl, pH 7.4) containing 5% non-fat milk (Carl Roth). After blocking, the membrane was incubated for 1 h with the desired antibody, diluted in blocking solution, to a final concentration of 0.5-1 µg/ml. After washing 6×5 min with TBS, the membrane was incubated with the secondary antibody conjugated to horse radish peroxidase with a concentration of 0.5 µg/ml for 1 h. After 4×5 min washing with TBS, ECL Prime Western blotting detection reagent (Amersham, GE Health Care) was used for chemiluminescent-based signal detection in the FUSION-SL 7 advanced system (Vilber).

Cell Culture

Human embryonic kidney cells (HEK293T, ATCC: CRL-11268) were cultivated in advanced Dulbecco's modified Eagle's medium, (DMEM, Thermo Fisher Scientific) supplemented with 10% fetal bovine serum, 2 mM Glutamax (Thermo Fisher Scientific) and 100 U/ml penicillin/streptomycin (Thermo Fisher Scientific) solution at 37 °C in a humidified atmosphere containing 5% CO_2. For detachment of cells, accutase solution (Sigma-Aldrich) was used.

Transfection Lipofectamine 3000 (Thermo Fisher Scientific) was used for transient expression, following the producer's manual. Plates in all formats were poly-L-lysine coated (Sigma-Aldrich) during experiments. To minimize stress during transfections, the amount of DNA was always kept on the lower end of the recommended range, (e.g. 2.5 µg/6-well dish and 14 µg/10 cm dish) as well as the amount of lipofectamine 3000 used (1 µg/12-well dish, 3.75 µl/6 well dish and 21.7 µl/10 cm dish). For transfections carried out with Xfect (Clontech) 2.5 µg DNA/6-well dish and 20 µg DNA/10 cm dish were used in combination with 0.3 µl Xfect-Polymer for every 1 µg plasmid DNA. Cells were loaded with iron or ferritin for 24 h, 48 h after transfection.

Confocal Microscopy

For confocal microscopy the Leica SP5 system, equipped with lasers emitting light at wavelengths of 408 nm, 488 nm and 561 nm was used.

Cellular Localization of Transiently Expressed Proteins For the detection of transiently overexpressed proteins, HEK293T cells were prepared as described in 2.1. Cells were permeabilized with 1% TritonX-100 (Sigma-Aldrich). The primary antibodies (Anti-FLAG or anti-human ferritin) were diluted to a final concentration of 0.5 µg/ml in Superblock, based on TBS (Thermo Fisher Scientific) and incubated overnight. After 6$\times$5 min washing in tris-buffered saline (TBS, 50 mM Tris, 150 mM NaCl, pH 7.4), the secondary antibody was used at a final concentration of 0.5 µg/ml in Superblock, based on TBS and incubated for 2 h. After three washing steps (5 min each) in TBS, cells were mounted with Aqua-Poly/Mount (Polysciences, Inc.) on cover slides and imaged on an EVOS microscope or the Leica SP5 confocal microscopy system.

Fluorescent protein labeling Horse spleen- or magnetoferritin was conjugated to Alexa Fluor 488 N-hydroxysuccinimidyl (NHS) ester (Thermo Fisher Scientific), according to the user's manual and dialyzed overnight

against 50 mM HEPES with Slide-A-Lyser (Thermofisher Scientific). HEK 293T cells were grown on poly-L-lysine coated glass chips (BD Bioscience). After 48 h transient overexpression of Tim-2 or TfR1, cells were incubated for 24 h with labeled ferritin (0.4 mg/ml). Excessive ferritin was removed through 3×5 min washing with DPBS before the cell nuclei were stained with Hoechst 33258 (20 µM in PBS) for 5 min and cells were fixed with 4% paraformaldehyde (PFA) (Thermo Fisher Scientific) in PBS for 10 minutes. For imaging, cells were mounted on cover slides with Aqua-Poly/Mount (Polysciences, Inc.).

2.2 Preparation of Magnetoferritin

For the preparation of magnetoferritin (hFTH-Mag), human heavy-chain ferritin was expressed in *E. coli* and purified. After synthesis, magnetoferritin was purified again from other by-products.

2.2.1 Expression and Preparation of Recombinant H-chain Ferritin

Recombinant human heavy-chain ferritin (hFt) was expressed in *E. coli* BL21(DE3) based on Rucker et al. with modifications [Rucker et al., 1997]. In short, the gene encoding for human hFt was cloned into the multiple cloning side of pET151 via HiFi Assembly (NEB) and protein expression was induced with 0.5 mM isopropyl-β-D-thiogalactopyranoside (IPTG) overnight at room temperature. Cells were sonicated in lysis buffer (50 mM Tris-HCl, 150 mM NaCl and protease inhibitor cocktail (cOmplete EDTA-free, Roche). After cell lysis, the lysate was spun down for 20 minutes at 20,000 g. The supernatant was heated for 15 min at 65℃ for heat precipitation of less heat-stable proteins and centrifuged again for 20 min at 20,000 g. The cleared supernatant, containing the recombinant protein, was dialyzed over night at 4℃ against 50 mM HEPES buffer with 150 mM NaCl, using a Spectra/Por cellulose ester membrane (MWCO 300,000 Da;

Spectrum Labs). The protein concentration was determined via BCA protein assay kit (Pierce BCA Protein Assay Kit, Thermo Fisher Scientific).

2.2.2 Magnetoferritin Synthesis

The protocol for the magnetoferritin synthesis with recombinant human heavy-chain ferritin (hFt) was developed based on Fan et al. [Fan et al., 2012]. All solutions were carefully degassed with nitrogen and the reaction vessel was closed hermetically to maintain an oxygen-free atmosphere. The synthesis was performed at 65 °C and pH 8.5 in 50 ml 100 mM NaCl solution with 0.25 mg/ml apo-hFt. Ferrous iron was added in the form of a 25 mM ferrous ammonium solution with a rate of 100 Fe/(protein/min). Stoichiometric equivalents of 1 H_2O_2 : 3 Fe^{2+} were added to ensure correct oxidation conditions (8.33 mM H_2O_2) and the pH was kept stable with 50 mM NaOH using a TitroLine 7000 (SI Analytics). Five minutes after the theoretical loading of 3000 Fe/protein, 200 µl of 300 mM sodium citrate was added to the reaction to chelate free iron. The synthesized magnetoferritin particles were centrifuged stepwise at 20,000 and 80,000 g to remove aggregates and dialyzed against 50 mM HEPES with 150 mM NaCl over night at 4 °C. For final purification, the synthesis was applied on a Superdex 200 Increase 10/300 GL size exclusion column (GE Healthcare Life Sciences). Before sample loading, the column was pre-equilibrated with one column volume of buffer. The column run was performed isocratic with filtered and degassed buffer (100 mM HEPES, 50 mM NaCl, pH 7.4) at a flow rate of 0.5 ml/min. Absorbance was measured in-line at 280 nm for protein content.

2.3 Analysis of Magnetic Properties

After genes of interest were expressed and/or cells were loaded with iron, the magnetic properties of these cells were characterized in different ways.

2.3.1 Colorimetric Quantification of Cellular Iron Content

Iron assays were always carried out with two technical replicates for each biological replicate. Cells for these biological replicates were always counted before seeding and the seeding number was the same of every experimental condition. $4 \cdot 10^5$ cells were plated 24 h before transfection in 6-well plates. Cells were incubated with experimental amounts of the desired iron species 48 h after transfection. If experiments were conducted with ferrous iron, ferrous ammonium sulfate (FAS) was used. If experiments were conducted with ferric iron, ferric citrate (FC) was used in combination with 2 mg/ml human transferrin (Sigma-Aldrich). Both iron forms and transferrin were dissolved in cell culture media and sterile filtered before applying onto the cells.
After 24 h incubation cells were washed three times in Dulbecco's Phosphate-Buffered Saline (DPBS). Cells were detached with accutase and spun down for 5 min at 400 g. Afterward, cells were resuspended and counted according to the user's manual of the Countess II FL Automated Cell Counter (Life Technologies). Cells were spun down again at 2834 g and cell pellets were frozen until iron assay was conducted. The iron assay was carried out according to Riemer et al. [Riemer et al., 2004]. For cell lysis, pellets were resuspended in 200 µl of a 50 mM NaOH solution and incubated for 2 h on a shaker. Afterward the samples were split in half for technical replicates, and 100 µl of a 10 mM HCl solution was added for pH adjustment. This mixture was incubated with 100 µl of iron releasing solution (1.4 M HCl with equal volume of 4.5% (w/v) $KMnO_4$) for 2 h at 60 ℃ under the fume hood. This step is required for the release of protein-bound iron and iron bound in low-molecular weight complexes. After the samples had been cooled down to room temperature, they were mixed with 30 µl freshly prepared iron detection solution (6.5 mM ferrozine, 6.5 mM neocuproine, 2.5 M ammonium acetate, 1 M ascorbic acid) and incubated for 30 min. The absorption of the Fe(II)-ferrozine complexes was measured at a wavelength of 550 nm. The assay was calibrated with freshly prepared calibration solutions diluted from a 10 g/l iron in 1 M HCl

analytical stock solution, ranging from 300 µM to 10 µM iron. Through the determination of the iron concentration in the tested solutions and the assumption that all the iron in these solutions is derived from the harvested cells, the amount of cellular iron could be calculated, because the exact number of cells in the assay was known.
The colorimetric iron assay was cross-validated via ICP-MS.

2.3.2 Inductively Coupled Plasma Mass Spectrometry

Samples for inductively coupled plasma mass spectrometry (ICP-MS) were adjusted to contain approx. 200 µg/l iron in a total sample volume of 400 µl. The iron concentration was estimated based on the colorimetric assay. Samples were incubated with equal amounts of 65% nitric acid overnight at 60℃ and then sent for analysis. Measurements were performed by Christine Sternkopf (Institute of Hydrochemistry and Chair of Analytical Chemistry, Technische Universität München).

2.3.3 Extraction of Lysosomes

Lysosomes were prepared using a lysosome isolation kit (Sigma-Aldrich) according to the user's manual. In short, cells were incubated with 18 µg eFTH+L or hFTH-Mag for 24 h, afterward detached with accutase and pelleted. The pellet was washed twice with ice-cold PBS and resuspended in extraction buffer (3×packed cell volume). Cell lysates were prepared with a 7 ml Dounce homogenizer using Pestle B (Sigma-Aldrich). At approx. 80% cell lysis, the sample was centrifuged for 10 min at 1,000 g. The supernatant was transferred to a fresh tube and centrifuged for 20 min at 20,000 g. The pellet containing a crude lysosomal fraction was resuspended in extraction buffer and kept until further use at 4℃.

2.3.4 Magnetic Resonance Imaging

MR images were acquired at a Bruker BioSpec 94/20 USR, 9.4 T system equipped with an RF RES 400 1H 112/072 Quad TR AD resonator.
For relaxivity calculations of protein solutions four different concentrations between 1.8 and 0.2 mg/ml were measured in modified 384 well plates (Thermo Fisher Scientific). For accurate buffer correction, all wells surrounding a sample were filled with corresponding sample buffer (50 mM HEPES, 150 mM NaCl, pH 7.4). For crude lysosomal fractions (2.3.3), extraction buffer from the lysosome isolation kit (LYSISO1, Sigma-Aldrich) was used as a reference value. T_2-measurements were performed using a multi-slice multi-echo (MSME) sequence with a repetition time (TR) of 6000 ms, 30 echoes, an echo spacing of 20 ms, a flip angle of 90°, a field of view of 60×60 mm and an image size 256×256 pixels.
For T_2*-measurements of cells, $4 \cdot 10^6$ HEK293T cells were seeded 24 h prior to transfection on 10 cm dishes. Cells were incubated with the substance of interest for 24 h, two days after transfection with the gene of interest. After three washes with DPBS, cells were detached with accutase and centrifuged for 4 min at 500 g. The pellets were resuspended in 800 µl DPBS and transferred to cryobank vials (Thermo Fisher Scientific) containing 50 µl 1% agarose. Cells were then spun down for 2 min at 2000×g and immediately used for MRI. Agarose was filled in the tubes to flatten the bottom of the vials. Therefore cell pellets appeared in an angular shape in the take images and with a clear contrast difference to the agarose. This facilitated image analysis. Measurements were conducted in a custom-made holder filled with DPBS. T_2*-values were calculated based on a multiple gradient echo (MGE) sequence with a TR of 800 ms, 12 echoes with an echo spacing of 4.5 ms, a flip angle of 50°, a field of view of 65×65 mm and an image size of 256×256 pixels. Higher order shims were used for all measurements. Relaxation times were calculated with Image Sequence Analysis Tool from Bruker BioSpin MRI GmbH.

2.3.5 Magnetic Cell Sorting

Magnetic sorting of cells was performed with MS columns (Miltenyi Biotec). The column matrix consists of superparamagnetic beads which can amplify an applied external magnetic field and induce a high gradient within the column. Therefore, cells are retained through magnetic interactions in the column matrix if an external magnetic field is applied. For elution, the external magnetic field is removed. In consequence, the magnetically retained cells do not experience the strong, induced magnetic field anymore and can be removed without mechanical stress.
HEK293T transiently overexpressing Tim-2, TfR1, Scara5 or EYFP were loaded with 50 µg/ml eFTH+L or hFTH-Mag for 24 h. Cells were washed twice with PBS and detached with accutase. Cells were resuspended in 4% PFA in PBS for fixation and kept at 4 ℃ until sorting.
For magnetic sorting, MS columns were placed in a MiniMACS separator (Miltenyi Biotec) and equilibrated with 0.5 ml PBS (pH 7.4). The column was loaded with cells and washed with 0.5 ml PBS. The flow through was collected as one fraction. After removing the column from the magnetic separator, cells were eluted with 1 ml PBS using the provided plunger. The total number of cells before sorting as well as the cell numbers in flow through and eluate were determined. If cells were fixed, they were counted manually using a C-Chip disposable counting chamber (Biochrom AG). After life cell sorting, death cells were stained with trypan blue and the total number of cells before sorting as well as the cell numbers in flow through and eluate were determined with a Countess II FL Automated Cell Counter (Life Technologies).

2.3.6 Magnetic Hyperthermia Experiments

For RF-treatment the Tru Heat 3010 generator (Trumpf-Hüttinger) was used. The coil in use had 4 windings with a diameter of 10 cm and a height of 6 cm (Sketch can be found in the appendix (Figure 18)). To maintain steady temperature conditions during the experiment, the coil

was water cooled with a flow rate of 4 l/min. For ablation experiments, $2{\cdot}10^5$ cells were seeded in 24-well plates 24 h before transfection. Cells were then transfected and loaded with 300 µg/ml hFTH-Mag, eFTH+L or eFTH+L-apoferritin 48 h after transfection. After incubation for 24 h, cells were washed with DPBS and supplied with fresh medium before applying an RF-pulse (318 kHz, 18-21 mT or 1.8-2.1 mT) for 30 min. Control cells were left at room temperature for the duration of the RF-pulse. After treatment, cells were incubated another 24 h before cellular toxicity was determined via LDH cytotoxicity detection kit (Roche).

2.3.7 Vibrating sample magnetometer

VSM measurements were conducted by Prof. Dr. Michael Winklhofer and Dr. Ulf Wiewald from the Faculty of Physics and Center for Nanointegration (CENIDE), University of Duisburg-Essen. Samples were lyophilised before measurement.

2.4 Optoacoustic and third Harmonic Microscopy and Photoablation

Transiently overexpressing cells were loaded with 150 µg/ml eFTH+L or hFTH-Mag for 24 h before the experiments. As described in Seeger, 2016 57Tserevelakis, 2014 58Soliman, 2015 59, optical-resolution optoacoustic microscopy and third harmonic generation microscopy imaging was performed on a custom-built hybrid microscope. The beam of an actively triggered 532 nm laser (Elforlight) utilized for the OA modality is co-aligned and merged with a 1043 nm laser (Time-Bandwidth) used for THG by a longpass dichroic mirror (Thorlabs). Both beams are attenuated by neutral density filters to desired pulse energies and guided over a set of high-speed galvanometric mirrors (Cambridge Technology), enlarged by a telescopic arrangement of lenses and focused by microscopic objective lenses (Plan Apochromat 10X/0.45 and W Plan Apochro-

mat 20X/1.0, Zeiss) placed in an inverted microscope (AxioObserver.D1, Zeiss). For image generation, both laser beams are consecutively raster-scanned across the sample hold by a xyz-stage (Thorlabs) using the galvanometric mirrors controlled by a 16 bit data acquisition card (National Instruments) with an averaging of 100. OA signals are detected by a spherically focused 100 MHz transducer (SONAXIS), amplified (Miteq) and acquired by a 12 bit data acquisition card (SP Devices). THG detection is performed by a highly sensitive photomultiplier tube (Hamamatsu) equipped with an optical bandpass filter (Thorlabs) and digitized by the previously mentioned 16 bit data acquisition card. The system is fully controlled in Matlab (Mathworks); image post processing is carried out in ImageJ (Wayne Rasband).

Cell ablation induced by photothermolysis: To investigate the feasibility of selective cell ablation by means of photothermolysis within the dual-modal microscopy framework, cells were first imaged with both OA and THG modalities. Next, the pulse energy of the previously mentioned 532 nm laser utilized to excitate OA signals was increased about 15.4 fold (imaging: 18.5nJ/pulse; ablation 285nJ/pulse). The beam was raster scanned across a smaller area centered within the imaging FOV analogously to the OA imaging procedure. The ablation scan was carried out with 100 pulses per position to ensure strong photothermolysis effects. Finally, the sample was examined again with OA and THG as described above, whereas the OA laser power was reduced to the imaging power. Due to loose contact of the cells to the used glass bottom petri dishes (IBL Baustoff+Labor GmbH) in combination with slight heat induced convection, images had to be co-registered by an affine transformation carried out in ImageJ.

The OA and THG measurements and data analysis were carried out with the help of Markus Seeger (Institute of Biological and Medical Imaging, Helmholtz Zentrum München).

2.5 Statistical Methods

Statistical analysis was conducted with GraphPad Prism. If not stated otherwise, two-tailed, unpaired, parametric t-tests assuming same standard deviations for both populations were calculated.

Table 1: P values and statistical significance

P value	Asterisks	Significance
< 0.001	***	Very significant
0.001 - 0.01	**	Very significant
0.01 - 0.05	*	Significant
0.05	ns	Not significant

Chapter 3

Results

The results of this doctoral thesis are structured by the different iron uptake pathways. As pointed out in 1.4, at first an effective iron loading of cells was explored, and then safe storage of iron inside cells was addressed. Iron loading of cells was mainly assessed by a colorimetric iron assay. Afterwards, MR-measurements were carried out to assess possible MR-contrast changes evoked by the bioengineered pathways. These measurements were also used as a first approximation of altered magnetic properties of the cells since magnetic particles evoke T_2-contrast. As further assessment of cellular magnetization, the cells were magnetically sorted in high gradient magnetic fields and additional magnetic analysis was carried out.

3.1 Transferrin-dependent Iron Uptake Pathway

Most cells acquire iron through the transferrin-dependent iron uptake pathway. This pathway was used as a benchmark for bioengineering approaches in the following sections (3.2 and 3.3).
HEK293T cell express endogenously TfR1 and use this route to acquire iron from the culture medium. The supplementation with 2 mg/ml holotransferrin in combination with 1 mM ferric citrate (FC) for 48 h, lead to an increased intracellular iron content of 0.22 ± 0.04 iron/cell in comparison

with unloaded cells (0.04 ± 0.04 pg iron/cell). Cells only incubated with holo-transferrin but without ferric citrate contained 0.03 ± 0.01 pg iron/cell (Figure 1). To further elevate this pathway, TfR1 was transiently overexpressed. This approach did not lead to a clearly increased MR-contrast when compared to mock transfected HEK293T cells which were also incubated with ferric citrate and holo-transferrin (ΔR_2=11 s^{-1}). Nevertheless, a positive effect of ferric citrate could be identified. HEK293T cells, incubated only with holo-transferrin, showed an ΔR_2 of 6 s^{-1} and cell incubated with both showed ΔR_2 of 11 s^{-1}(Figure 1). These results suggest that the iron loading can be correlated with increased MR-contrast to a certain extent.

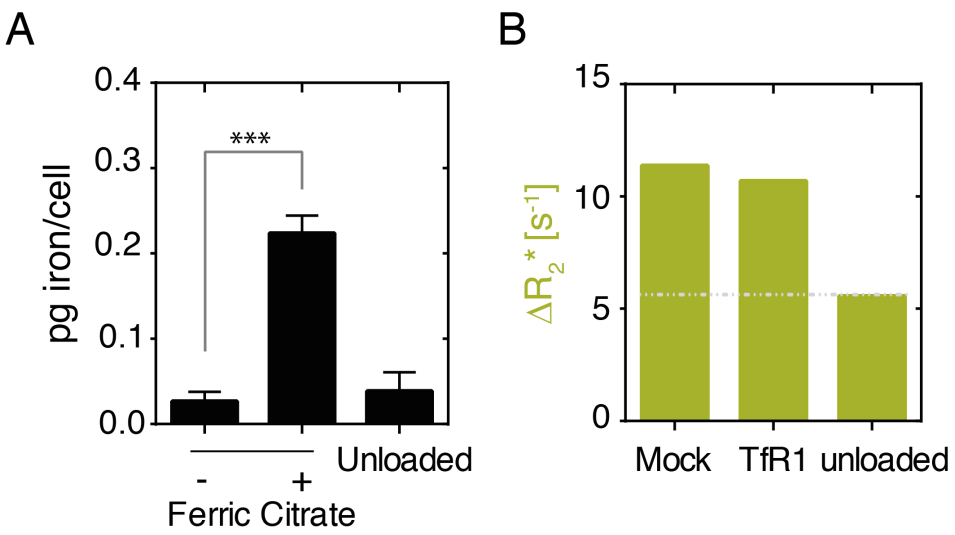

Figure 1: Transferrin dependent iron uptake. (A) HEK293T cells increase cellular iron content during incubation with ferric citrate and holo-transferrin. Error bars according to SEM. p=0.0008. n=3. (B) Transient overexpression of TfR1 leads to same MR-contrast enhancement like mock transfection. Enhanced cellular iron can be correlated with MR-contrast enhancement.

Since TfR1 is highly negatively regulated during iron repletion, heavy chain ferritin and a P2A-construct of PCBP1 and PCBP2 (PCBP) were overexpressed to induce an artificial iron depletion in cells. Co-expressions of TfR1 and hFt or TfR1, hFt and PCBP were compared to EYFP overexpressing control cells. The total amount of DNA was kept constant and was therefore adjusted EYFP coding DNA. The overexpression of TfR1 and hFt was carried out through co-transfection or through a P2A-construct enabling TfR and hFt expression from the same plasmid. During overexpression of TfR1 and hFt no differences in cellular iron loading (approx. 0.2 pg iron/cell) and T_2^*-derived MR-contrast could be detected.(Figure 2A). During co-expression of all three constructs, ferritin overexpression could be verified via Western blotting, but iron loading of ferritin could not be shown on native PAGE after DAB PB staining (Figure 2 B). Also the T_2^*-derived MR-contrast remained at approximately $\Delta R=20\ s^{-1}$ and was not significantly different from control cells. Nevertheless, a proliferative effect of transferrin supplementation with iron could be shown, indicating iron uptake under the detection level of the iron assay and MR-measurements.

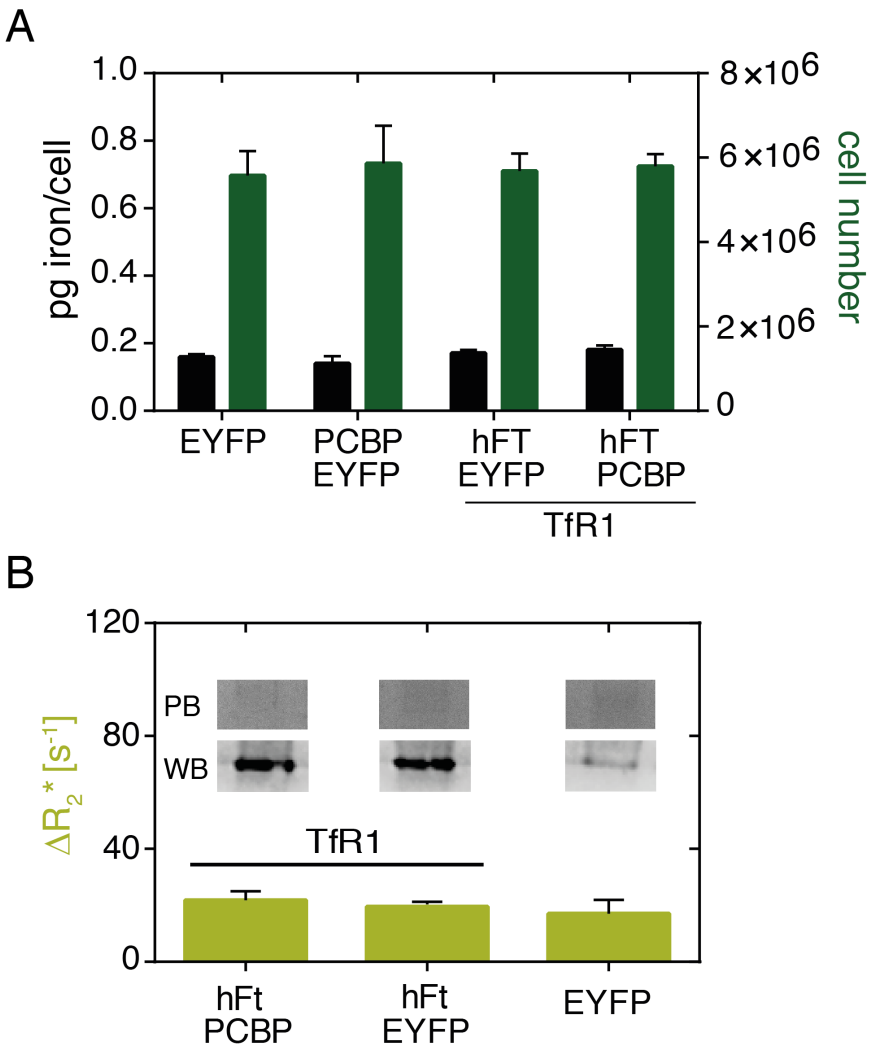

Figure 2: Modification of transferrin-dependent iron uptake. (A) The overexpression of hFt, the iron chaperones PCBP1-PCBP2 (PCBP) in combination with the overexpression of TfR1 did not lead to enhanced cellular iron loading. (B) T_2^*-derived MR-contrast was also not enhanced during the overexpression of hFT and PCBP. The overexpression of hFt was verified through WB, but iron loading could not be visualized through DAB PB staining of ferritin after native PAGE.

3.2 Ferrous Iron Transport Pathways

Ferrous iron transporters were used to bypass the highly regulated Tf-dependent iron uptake pathway. It was tested whether the ferrous iron transport pathway can be used for more effective iron loading through the direct delivery of ferrous iron into the cytosol without going through an endocytosis cycle which can transport only a maximum of two iron atoms into the cytosol.

3.2.1 DMT1

To test the suitability of DMT1, the protein was overexpressed in HEK293 cells and the cells were incubated with iron. During normal conditions in cell culture, the pH is at a physiological range (approximately pH 7.4) and far away from the optimal pH of DMT1, which is at pH 6.75. To achieve maximal iron loading, an iron loading buffer described in Kim et al. [2012] was used. Through this loading condition, it was possible to show that iron loading could be correlated with increased DNA coding for DMT1 (Figure 3). Iron was elevated to 0.37 ± 0.13 pg iron/cell, if half the DNA used for transfection was coding for DMT1. If all the DNA transfected coded for DMT1, 0.67 ± 0.16 pg iron/cell could be detected. During the increase of DMT1 and therefore cellular iron, the cell numbers gradually decreased. A decrease in cell number during iron loading is correlated with cell death induced by iron loading. The positive effect of nifedipine (dissolved in DMSO) could not be verified because the loading control (DMSO without nifedipine) showed similar iron loading than the iron loading buffer containing nifedipine (0.7 pg iron/cell vs. 1.2 pg iron/cell). The addition of ascorbic acid in combination with the iron loading buffer did not lead to a clear increase in iron loading. To further explore the possibilities for iron loading under more physiological conditions, the ferrous iron transporter Zip14 was evaluated.

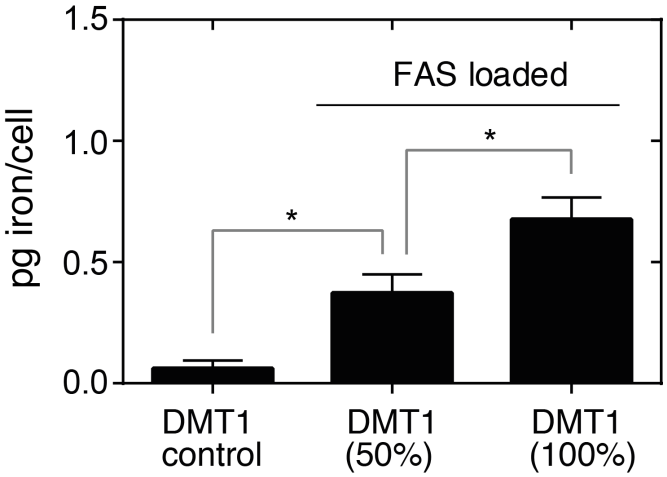

Figure 3: Iron loading through DMT1. The cellular iron loading could be gradually increased through the use of increasing DNA amounts coding for DMT1 during transfection. An iron loading buffer was used, which simulated optimal pH conditions for DMT1. Error bars according to SEM. $p<0.02$. n=3

3.2.2 Zip14

The pH optimum of Zip14 is at pH 7.4. This makes Zip14 a more promising candidate for effective cellular iron loading under physiological conditions. Zip14 has not been used for bioengineering purposes before, therefore membrane localization of CMV-driven, transient overexpressed Zip14 was tested and confirmed via immunocytochemical detection through a C-terminally introduced FLAG-tag (Figure 4 A)
Cellular iron loading could be increased if Zip14 coding DNA was increased during transfection. Iron was elevated 3-fold during the use of 50% Zip14 coding DNA of the total amount of DNA transfected. If all the DNA transfected consisted of Zip14 conding DNA, an approximately 5-fold higher cellular iron content could be detected. During the increase of Zip14, and as a direct consequence of intracellular iron, the cell numbers decreased to approximately a third of the control condition (100% Zip14 without iron loading) (Figure 4 B) The reduction in cell number during iron loading is correlated with cell death induced by iron loading.

High iron loading could be realized through Zip14 mediated iron transport into cells under physiological pH-conditions. Nevertheless, a pronounced iron-dependent cell death was observed. To lower induced toxicity and for the introduction of a scaffold for magnetic biomineralization, hFT and a chimera of light- and heavy-chain ferritin (LHFT) were co-expressed in combination with Zip14.

During co-expression of Zip14 and hFT, cell numbers reached the level of control cell numbers and an increase of iron loading from 0.1 ± 0.012 pg iron/cell to 0.3 ± 0.15 pg iron/cell could be detected. The coexpression of Zip14 and LHFT did not show the same cell rescue abilities as Zip14 in combination with hFT. However cellular iron content was also increased to 0.3 ± 0.1 pg iron/cell (Figure 5 A).

The iron loading of Zip14 and hFT cells could be increased gradually during incubation with 1 mM FAS if ascorbic acid was added as a reductive agent to the cell culture media in concentrations of 25 µM, 50 µM and 100 µM. However, this increase of iron correlated with increased cell death (Figure 5 B). During incubation with 3 mM FAS, no enhancing effect of ascorbic acid could be detected.

It was shown that the overexpression of hFt as an acceptor protein could abolish the toxic effect of increased intracellular iron. This effect was observed during 1 mM FAS loading for 24 h, leading to an intracellular iron content of approx. 0.3 pg iron/cell. For the purpose of an MRI gene reporter and biomagnetic actuator for magnetogenetics the non-toxic iron loading of cells had to be increased further.

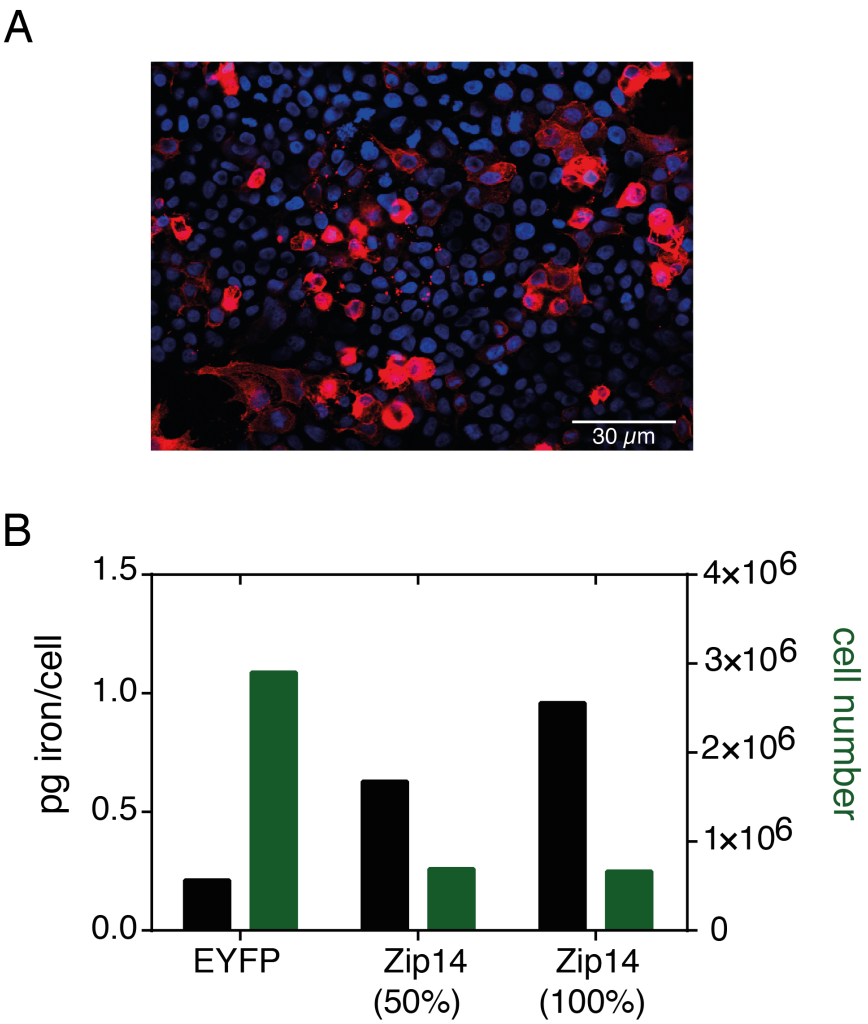

Figure 4: Iron loading via Zip14. (A) Immunocytological detection of transiently overexpressed Zip14 through a C-terminally induced FLAG-tag. (B) Iron loading was gradually increased during the elevation von Zip14 conding DNA in transfections. The increased iron concentration correlated with a decrease in cell viability.

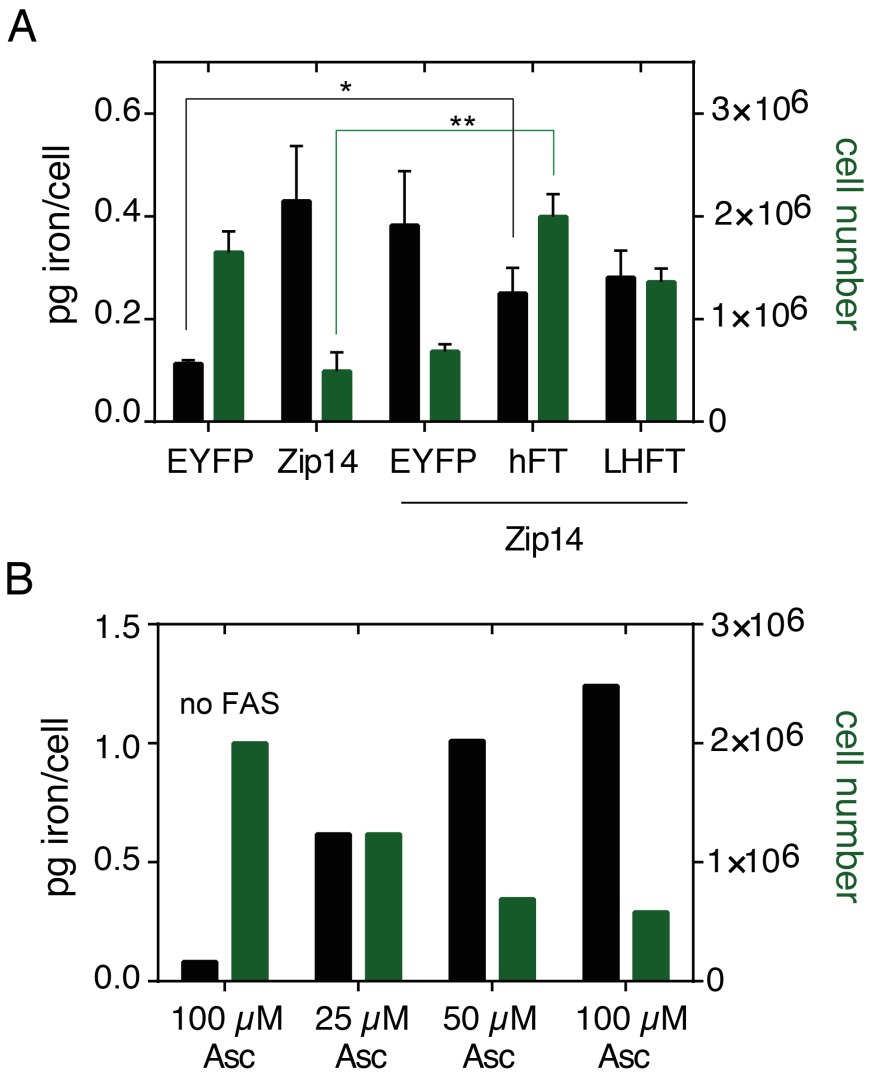

Figure 5: Zip14 with iron acceptors and ascorbic acid. (A) The combination of hFT and Zip14 lead to an increased iron loading compared to EYFP (one-tailed unpaired, parametric t-test. p=0.027. n=3) and could increase cell viability compared to cells overexpressing only Zip14 (two-tailed, unpaired, parametric t-test. p=0.0012. n=3) to values comparable with EYFP overexpressing control cells. (B) Iron loading of Zip14 and hFt overexpressing cells could be further increased through the use of ascorbic acid as a reducing agent in the cell culture media. The overexpression of hFt could not abolish toxic effects during this conditions.

To minimize toxic effects of transient transfection and to increase protein expression simultaneously, the transfection agent was changed from X-fect to lipofectamine3000. Furthermore, it was attempted to minimize the variability caused by multi-plasmid transfections. Zip14 and hFt were expressed from the same plasmid harboring a P2A-side. The effect of the iron chaperones PCBP1 and PCBP2 was also evaluated in a P2A construct (PCBP). The iron loading could be increased to 0.74 ± 0.18 pg iron/cell during Zip14 and hFt expression. It showed a slight, but not significant, decrease during Zip14, hFt and PCBP expression (Figure 6 A). The total cell numbers decreased in comparison to unloaded control cells, but still reached values comparable to control cells from experiments carried out with X-fect as a transfection reagent (Figure 5 A). A beneficial effect of PCBP1 and PCBP2 expression on cell death could not be determined from these experiments. T_2^*- MR-measurements showed a strong increase in contrast during Zip14-mediated iron loading of cells compared to EYFP control cells (ΔR_2^*=58 s^{-1} for hFt and Zip14 cells; ΔR_2^*=14 s^{-1} for control cells). Albeit PCBP overexpressing cells showed less MR-contrast during the expressing with Zip14 and hFt. In this constellation, PCBP did not show a pronounced improvement of either cell viability, iron loading nor MR-contrast. Even though the iron chaperones did not lead to an improvement of the system, the iron loading through Zip14 could be elevated to 0.74 pg iron/cell compared to 0.3 pg (as shown in 5) iron/cell maintaining cell viability. Furthermore, MR-contrast increased strongly in comparison to control cells (Figure 6 B).

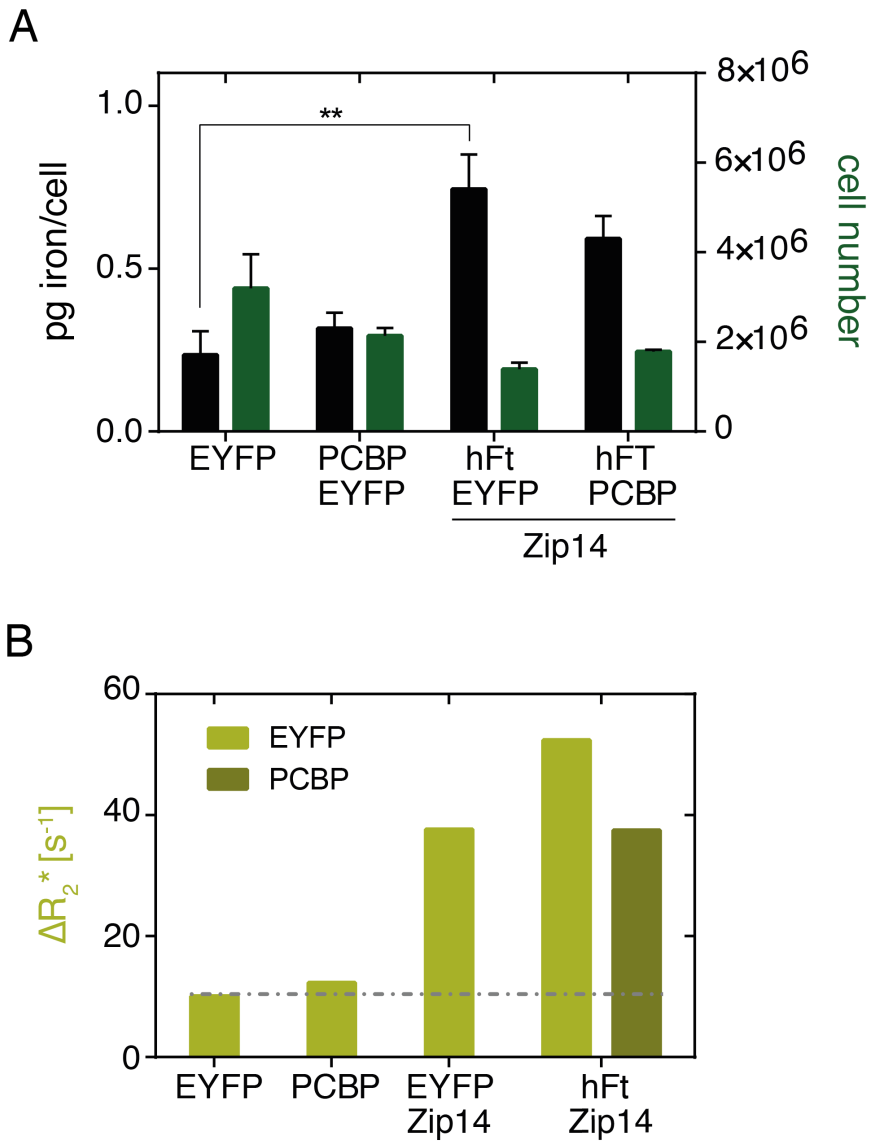

Figure 6: P2A constructs of Zip14 and hFt. (A) Cellular iron loading could be increased through the expression of the P2A-contruct of Zip14 and hFt, while maintaining cell viability at high levels. Error bars according to SEM. p=0.0084. (B) MR-contrast could be increased after the expression of Zip14 in either P2A-constructs compared to EYFP overexpressing control cells. PCBP did not lead to an additional enhancement.

To further evaluate Zip14, hFt and PCBP, coexpression of all three constructs from different plasmids was realized. Cells overexpressing Zip14 or Zip14 and hFt show 2 to 3-fold enhanced cellular iron loading

(Zip14+hFt=0.51 ± 0.06 pg iron/cell; Zip14+EYFP=0.71 ± 0.03 pg iron/cell) compared with control cells overexpressing EYFP (0.26 ± 0.02 pg iron/cell) (Figure 7). DAB-enhanced Prussian blue stainings after native PAGE of whole cell lysates show that the transported iron is stored to a certain extend inside overexpressed hFt.

Cellular evoked T_2^*-contrast increased dramatically after overexpression of Zip14 and hFT compared to control cells (Figure 8). The relaxation rates (ΔR_2^*) rose approximately 3.5-fold to a mean of ΔR_2^*=94 ± 11.3 s^{-1} compared to ΔR_2^*=23.5 ± 4.2 s^{-1} derived from EYFP cells.

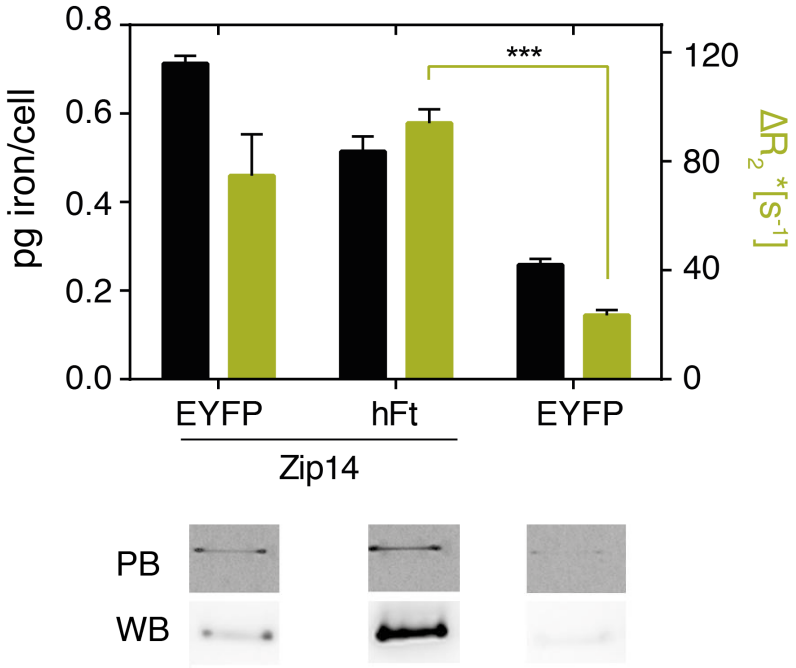

Figure 7: Zip14 and hFt evoked iron uptake and MR-contrast. Cotransfection of Zip14 and hFt elevated cellular iron loading and increased T_2^* derived MR-contrast. Newly introduced iron could be partly stored in overexpressed hFt. Cell overexpressing Zip14 -but no hFt- show upregulation of native heavy chain ferritin and increased iron incorporation. Error bars according to SEM. p=0.0065. n=5

Cells overexpressing Zip14, hFt and PCBP, show also enhanced iron loading (0.78 ± 0.12 pg iron/cell) compared to EYFP control cells. It remains unclear from these experiments whether the P2A-construct of PCBP1

and PCBP2 has a positive effect on ferritin loading in this system because cells overexpressing Zip14, hFt and EYFP show similar iron loading (0.65 ± 0.07 pg iron/cell). Notably, the amount of DNA encoding for Zip14 could be reduced to a third of total transfected DNA maintaining increased cellular iron loading and approximately same ferritin loading. This opens possibilities for more genes to be evaluate in a combinatorial way. Iron loading after overexpression of Zip14, hFT, and PCBP enhances cellular evoked T_2^*-contrast compared to EYFP overexpressing cells. The relaxation rates rose approximately 4-fold to a mean of ΔR_2^*=101.2 ± 26.8 s^{-1} compared to ΔR_2^*=23.5 ± 4.2 s^{-1} derived from EYFP cells.
The ferrous iron transport pathway proved to be a very efficient pathway to achieve cellular iron loading in a bioengineering context. However, a quick elevation of intracellular iron leads to iron-induced cell death. This cell death can be brought to an acceptable level, but never completely prevented, through the overexpression of hFT.

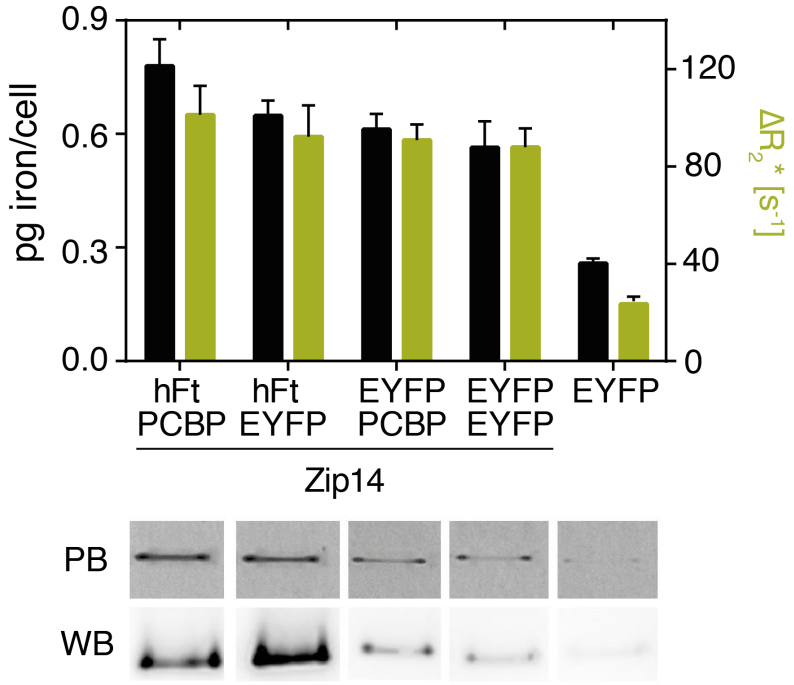

Figure 8: Iron uptake and MR-contrast via ferrous iron uptake. Transfections with three plasmids resulted in pronounced cellular iron elevation and iron incorporation in ferritin. Error bars according to SEM.

3.3 Ferritin Uptake Pathway

As described in 3.2.2 cells suffer under quick elevation of intracellular iron. This is probably a result of Fenton chemistry. The ferritin uptake pathway is another way of cellular iron loading. In this pathway, the iron storage protein ferritin is directly endocytosed into cells. This could prevent iron toxicity, increase the efficiency of each endocytosis cycle from two iron atoms to up to 4500 iron atoms and also open doors for the use of the ferritin cavity as a nanocage for the delivery of other substances.

3.3.1 Native Ferritin

HEK293T cell endogenously express the ferritin heavy-chain receptor TfR1. It was tested whether endogenous uptake of horse spleen ferritin (eFTH+L), which consists of heavy- and light chain ferritin, was sufficient to detect changes in cellular iron loading, cell viability and MR-contrast.
The incubation of HEK293T cells with eFTH+L (750 µg/ml) for two days resulted in a significant cell proliferation and a rise of intracellular iron from 0.04 ± 0.04 pg iron/cell to 0.23 ± 0.01 pg iron/cell (Figure 9 A). Also MR-contrast was enhanced approximately 3-fold from ΔR_2=6.6 ± 1.1 s^{-1} for unloaded control cells to ΔR_2=30.7 ± 3.1 s^{-1} for eFTH+L loaded cells (Figure 9 B).
To further asses whether it was possible to enhance iron loading and MR-contrast and simultaneously lower the amount of supplemented ferritin, ferritin receptors were overexpressed. HEK293T cells overexpressing the respective transporters were incubated with 150 µg eFTH+L/ml media. As a result transferrin receptor overexpressing cells increased their relaxation rate approximately 5-fold to 53.5 ± 16.5 s^{-1} compared to EYFP overexpressing cells (ΔR_2^*=10.2 ±3.2 s^{-1}) while the iron content was only slightly elevated to 0.2 ± 0.03 pg iron/cell. Cells overexpressing the mouse ferritin receptors Tim-2 or Scara5 showed a 10-fold higher relaxation rate of approximately ΔR_2^*=110 s^{-1} with cellular iron content of approximately 0.75 pg iron/cell in contrast to EYFP cells which only harbored 0.13 pg ± 0.01

iron/cell. Apparently, the correlation of intracellular iron and MR-contrast in cells loaded with ferritin is different from cells loaded via Zip14. More specifically it seems that a stronger MR-contrast is evoked with less intracellular iron.

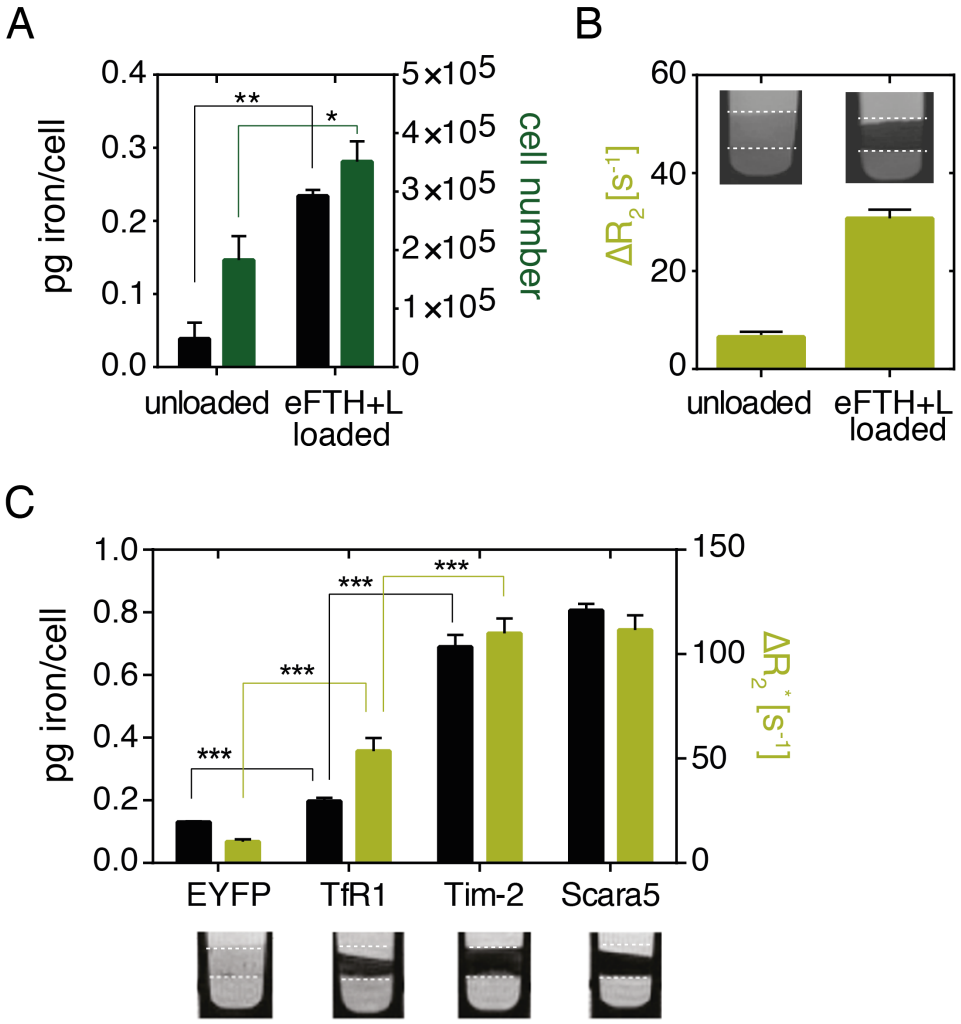

Figure 9: Ferritin uptake pathway. (A) Increased iron loading via endogenous ferritin receptor on HEK293T cells. A proliferative effect could be detected after iron loading over this pathways. Error bars according to SEM. p=<0.035. n=3 (B) Uptake of eFTH+L over endogenous TfR1 caused increased MR-contrast after two days of incubation. Error bars according to SEM. (C) Overexpression of ferritin receptors TfR1, Tim-2 and Scara5, enabled higher iron loading and stronger MR-contrast. Error bars according to SEM. p=<0.0011. n=6

Intracellular Iron Localization

To investigate the effect described above, the localization of endocytosed ferritin was determined. To test, if ferritin is trafficked to lysosomes under overexpression and high ferritin loading conditions, a lysosomally targeted mCherry (mCherryLT) was used. At first, it was shown that mCherryLT is colocalized with LysoTracker Green DND-26 and therefore trafficked to lysosomes (Figure 10 Aa-Ac). The designed mCherryLT does not show background signal from the cytosol, neither the lysosomes appear in an abnormally large shape. A weak fluorescent signal is derived, from the membrane because proteins with the dileucine-motive of the lysosomal acidic phosphatase (LAP) are trafficked first over the cell membrane and subsequently to the lysosomes. Tim-2 and mCherryLT overexpressing cells incubated with fluorescently labeled eFTH+L show colocalization of both fluorescent signals (Figure 10 Ad-Af)
Under physiological condition ferritin is degraded in lysosomes and iron is released. It was checked whether endocytosed ferritin could be detected or if introduced ferritin was rapidly degraded. Through Western blotting heavy- and light chain ferritin could be shown (Figure 10 B). Also, iron loading of ferritin could be proven through DAB enhanced PB staining after native PAGE. The detection of L-chain ferritin suggested that eFTH+L is not completely degraded during this experimental setup because non-modified HEK293T cells express only marginal amounts of light chain ferritin. Despite the detection of iron-loaded ferritin, lysosomal degradation was inhibited with bafilomycin A1 (50 nM and 100 nM) and chloroquine, (10 µM and 30 µM) which in consequence did not alter MR-contrast evoked by ferritin uptake (Figure 10 C). On the other hand, MR-measurements of isolated lysosomes from Tim-2 expressing cells, incubated with a concentration of 300 µg eFTH+L/ml media for 24 h, showed clear contrast enhancement compared to lysosomes from control cells (Figure 20 A in appendix). This suggests that iron is retained in the lysosomes and probably not released in significant amounts into the cytoplasm.

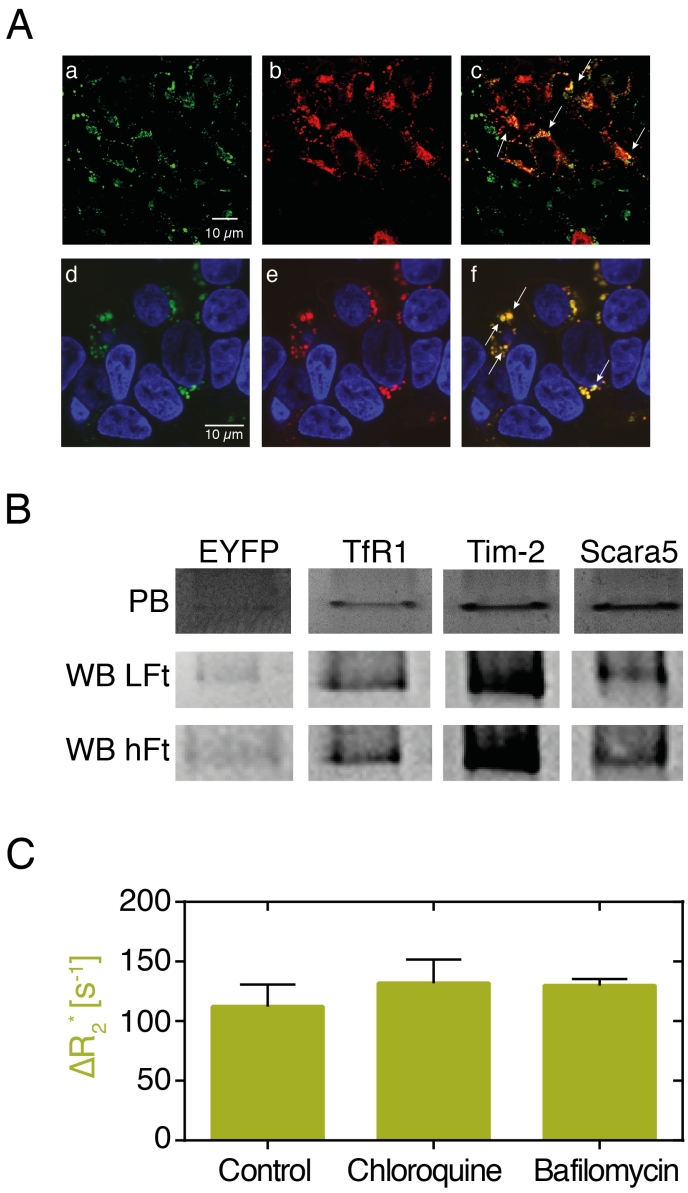

Figure 10: Intracellular eFTH+L localisation. (Aa) LysoTracker Green DND-26 derived fluorescent signal. (Ab) mCherryLT derived fluorescent signal. (Ac) Overlay of LysoTracker Green DND-26 and mCherryLT signals shows lysosomal trafficking. (Ad) Fluorescent signal from Alexa-488-eFTH+L. (Ae) Fluorescent signal from mCherryLT. (Af) Overlay of eFTH+L and mCherryLT signal. Colocalization (white arrows) shows lysosomal trafficking. (B) Detection of heavy- and light-chain ferritin through WB after ferritin endocytosis. DAB PB shows iron loading of endocytosed ferritin. (C) Inhibition of lysosomal proteases did not alter MR-contrast. Error bars according to SEM.

It was further tested whether expressed and loaded hFt could be directed to a cell compartment to mimic lysosomal clustering. The peroxisomal targeting signal PTS2 from the human acetyl-Coenzyme A acyltransferase 1 (ACAA1) was fused the N-terminus of hFt to direct ferritin after expression to the peroxisomes. Expression of the construct could be verified after Western Blotting, but iron loading was not achieved.
Through the ferritin uptake pathway, it was possible to increase cellular iron uptake approximately 8 times in a non-toxic manner and increase MR-contrast approximately one order of magnitude.

3.3.2 Magnetoferrtin

The exchange of the native ferrihydrite core of ferritin to a superparamagnetic magnetite core could help to overcome physical limits of ferritin as a biomagnetic contrast agent and actuator for non-invasive imaging and actuation.

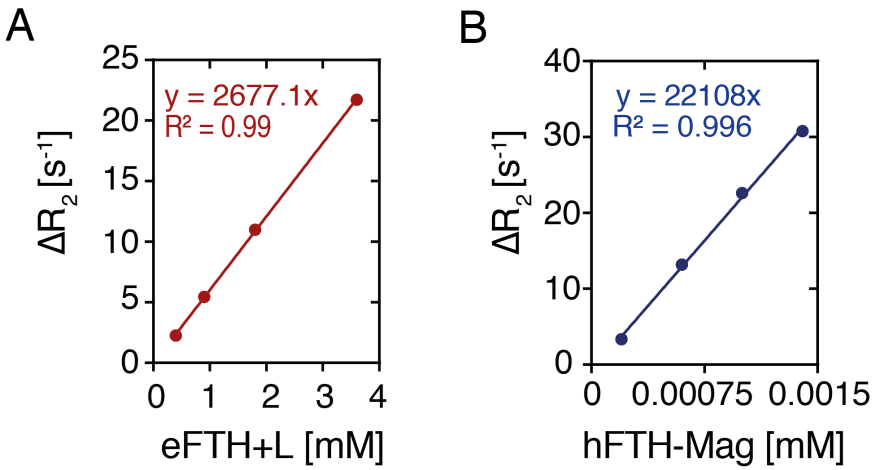

Figure 11: Relaxivity measurements of eFTH+L and hFTH-Mag. (A) eFTH+L showed a relaxivity of 2677 $mM^{-1}s^{-1}$. (B) hFTH-Mag showed a relaxivity of 22108 $mM^{-1}s^{-1}$.

Characterization of Magnetoferritin

After synthesis of magnetoferritin (hFTH-Mag), the synthesis batch was concentrated to a volume of 250 µl for purification through size exclusion chromatography. The parallel detection of absorbance at a wavelength of 280 nm and 410 nm enabled confirmation of iron loading of the newly synthesized ferritin online (appendix Figure 21). Iron staining after native PAGE also confirmed iron loading of ferritin, whereas no iron loading could be detected in ferritin before synthesis. The relaxivity of hFTH-Mag was calculated via T_2-measurements of four different concentrations (Figure 11). The T_2-relaxivity of hFTH-Mag was approximately 10-fold enhanced compared to eFTH+L (r_2 (hFTH-Mag)=22108 $mM^{-1}s^{-1}$; r_2 (eFTH+L)=2677 $mM^{-1}s^{-1}$). The newly synthesized hFTH-Mag displayed superparamagnetic behavior during measurements in vibrating sample magnetometer (VSM), whereas native eFTH+L was antiferromagnetic (Figure 12 A and B). To test whether hFTH-Mag is still recognized by ferritin receptor after synthesis and purification procedures, hFTH-Mag was fluorescently labeled with Alexa488, and the localization was compared with mCherryLT (Figure 12 C). Magnetoferritin was colocalized with mCherryLT and showed the same cellular localization pattern as native endocytosed ferritin.

Magnetoferritin as an MRI-Contrast Agent

After the functional validation of hFTH-Mag in combination with the heavy chain receptor Tim-2, hFTH-Mag was used as a contrast agent for MRI. HEK293T cells show a strong increase of T_2^*-derived MR-contrast after overexpression of the heavy chain receptors TfR1 and Tim-2 and loading with hFTH-Mag (TfR1: ΔR_2^*=120.3 ± 44.4 s^{-1}, Tim-2: $\Delta R2^*$=126.7 ± 41.1 s^{-1}) compared to EYFP overexpressing control cells (ΔR_2^*=12.7 ± 3.6 s^{-1}) (Figure 13 A). In these experiments a concentration of 1.875 µg/ml hFTH-Mag in the media was used for a 24 h incubation. This concentration is approximately 80-fold lower than the concentration of eFTH+L required to generate comparable contrast enhancement shown in 3.3.1.

Even though, cells overexpressing the light chain receptor Scara5 show high contrast enhancement, when incubated with eFTH+L, the contrast did not increase significantly during hFTH-Mag incubation, which is only composed of heavy chain ferritin (ΔR_2^*=15.1 ± 4.7 s^{-1}).

To test a possible contrast-enhancing effect of ferritin entrapment inside lysosomes, cells were incubated with different concentrations of both eFTH+L (r_2=2677 mM^{-1} s^{-1}) and hFTH-Mag (here (r_2=4849 mM^{-1} s^{-1}) (Figure 13 B and C). The pseudo-r2 ratio of these two monodisperse protein solutions is 1.81. However, the ratio of r_2 derived from cell pellets (eFTH+L r_2=184.7 (mg/ml)s^{-1}; hFTH-Mag r_2=2561 (mg/ml)s^{-1}) is 13.32. Regarding the linear enhancement of MR-contrast with increasing concentrations of ferritin, it can be assumed that all ferritin is taken up by the cells and that the conditions were in a non-saturating range. Therefore, these experiments suggest an amplifying effect of lysosomal entrapment of ferritin regarding MR-contrast.

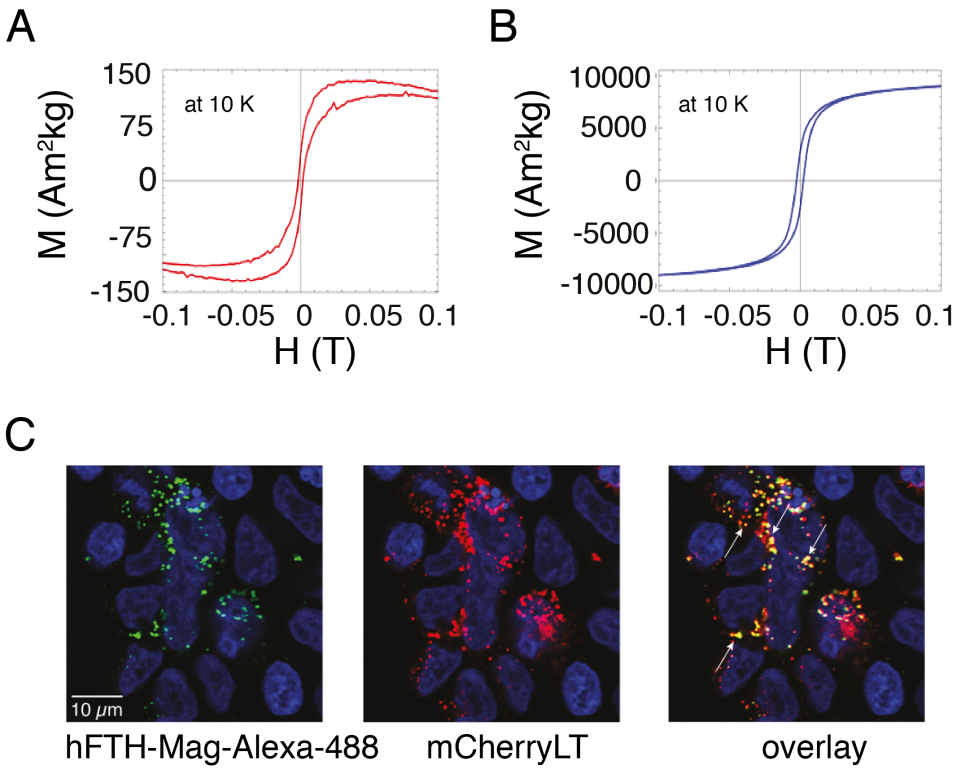

Figure 12: VSM measurements and cellular localization of hFTH-Mag. (A)VSM measurements at 10 K suggest a mainly paramagnetic behavior of eFTH+L. (B)VSM measurements at 10 K show superparamagnetic behavior of hFTH-Mag. (Ca) Fluorescent signal derived from Alexa-488 labeled hFTH-Mag. (Cb) Fluorescent signal derived from mCherryLT. (Cc) Overlay of fluorescent signals from Ca and Cb colocalization (white arrows) of hFTH-Mag and mCherryLT, suggesting correct receptor recognition and lysosomal trafficking from synthesized hFTH-Mag to lysosomes.

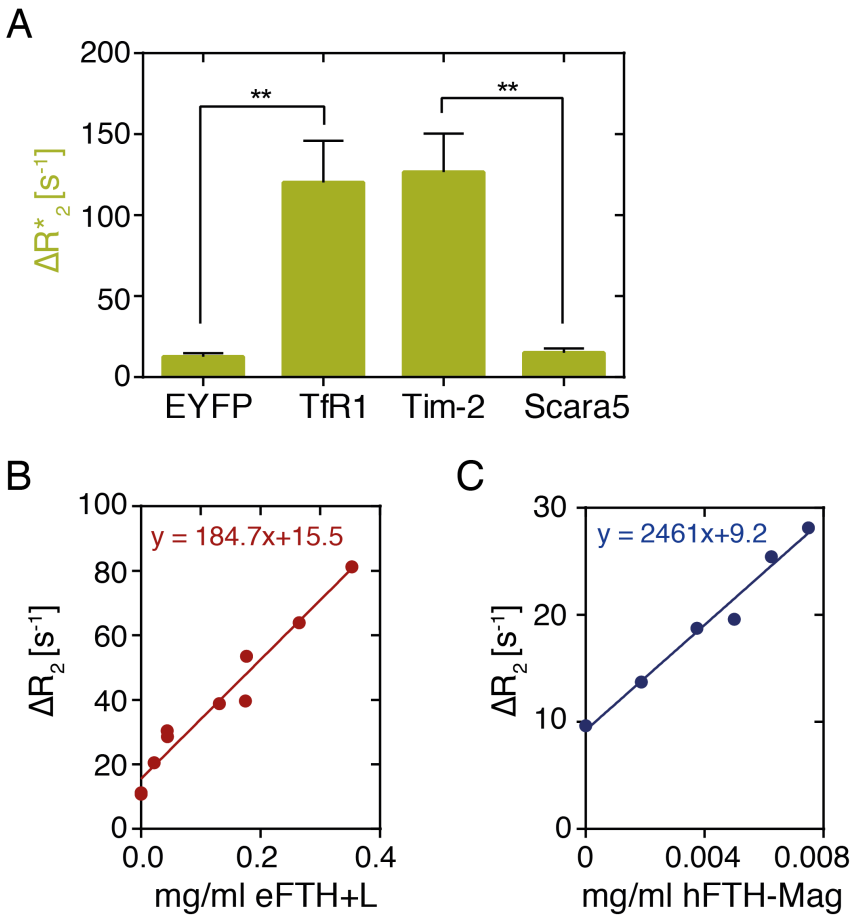

Figure 13: hFTH-Mag as interface for MRI and lysosomal signal enhancement. (A) Heavy chain ferritin receptors TfR1 and Tim-2 overexpressing cells showed strong MR-contrast enhancement. Light chain receptor Scara5 overexpressing did not increase MR-contrast. Error bar according to SEM. p=<0.01. (B) Titration of eFTH+L on Tim-2 overexpressing cells lead to a pseudo-relaxivity of 184.7 (mg/ml)s^{-1}. (C) Titration of hFTH-Mag on Tim2 overexpressing cells lead to a pseudo relaxivity of 2461 (mg/ml)s^{-1}. The ratio of these two pseudo-relaxivities is 13.32, whereas the ratio of the relaxivities of the protein solution is 1.81.

Magnetoferritin as an Actuator

Due to the superparamagnetic behavior of magnetoferrtin and the high cellular uptake, different possibilities of magnetic interaction were examined. Magnetic sorting over superparamagnetic columns could be realized. Magnetic sorting was achieved after the overexpression of heavy-chain ferritin receptors and hFTH-Mag loading (TfR1: 32 ± 3%, Tim-2: 35 ± 2%). However, it was not possible to sort significant amounts of cells after overexpression of the light chain receptor Scara5 or during the expression of any ferritin receptor expressing cells and incubation with eFTH+L (Figure 14).

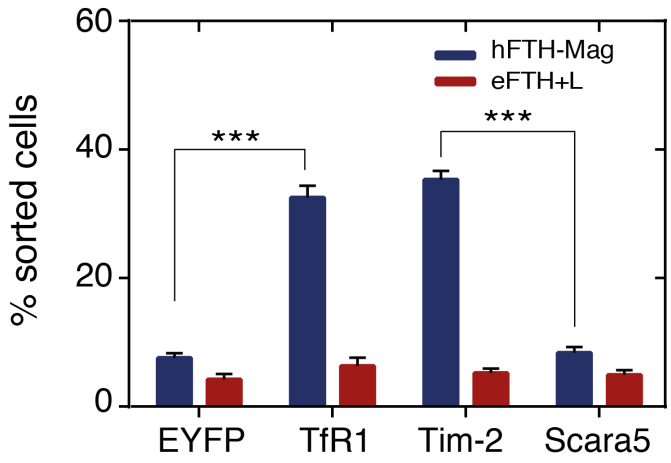

Figure 14: Magnetic sorting of ferritin loaded cells. Magnetic cell sorting of cells overexpressing different ferritin receptors and loaded with either eFTH+L or hFTH-Mag. Application of a static magnetic field to the column containing a superparamagnetic mesh resulted in magnetically sorting of TfR1 and Tim-2 overexpressing cells, after loading with hFTH-Mag. Error bars according to SEM. p=<0.001. n=3

Another form of magnetic interaction is heating through magnetic hyperthermia. It was tested whether is was possible to induce cell ablation with either of the two lysosomally targeted ferritin variants. Experiments show 12 ± 2% cell death 24 h after RF-treatment (18-20 mT for 30 min) of hFTH-Mag loaded Tim-2 overexpressing cells (Figure 15 A). It was only possible to detect 3 ± 2% cell death in eFTH+L, or 2 ± 1 % in apo-ferritin loaded cells after RF-treatment. Control cells, which did not undergo RF-treatment, were left outside of the incubator for the time the other cell received RF-treatment. These cells show approximately 4% cell death but the difference is not significant from RF-treated eFTH+L loaded cells. The dependence of cell death on the magnetic flux density was demonstrated during experiments in which hFTH-Mag incubated Tim-2 cells experienced 18-20 mT or 1.8 mT-2 mT for 30 min each (Figure 15 A). It was possible to induce approximately 9 ± 1% cell death in Tim-2 overexpressing cell after hFTH-Mag loading at 18-20 mT, but not at 1.8 mT- 2 mT. In contrast, cells loaded with eFTH+L could not be ablated significantly at any magnetic flux density used in our experimental setup. The temperature raise during the experiment with 18-20 mT was neglectable because the absolute temperature did not rise over 37 °C. Magnetic flux densities were simulated by the Trumpf-Huettinger GmbH and can be found in the appendix (Figure 19 in appendix).

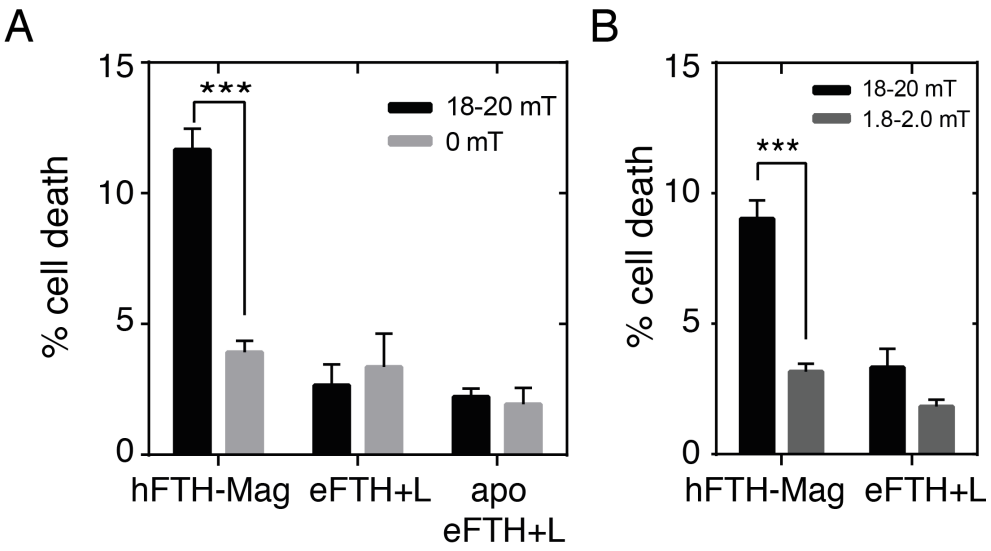

Figure 15: RF-induced hyperthermia. (A) RF-dependent cell death could be induced in Tim-2 overexpressing cells after loading with hFTH-Mag but not after loading with eFTH+L or apo eFTH+L at a field strength of 18-20 mT. Error bars according to SEM. p=<0.0001. n=6. (B) RF-dependent cell death was induced in a flux density-dependent way after hFTH-Mag uptake but not after eFTH+L uptake into Tim-2 overexpressing cells. Cell death could be induced with 18-21 mT but not with 1.8-2 mT. Error bars according to SEM. p=<0.0001. n=3

3.3.3 Ferritin as Optical Contrast Agent

Both ferritin variants have distinct colors. eFTH+L is brown-reddish, and hFTH-Mag appears black. The changes in optical properties, more precisely in absorbance and optical homogeneity were used for optoacoustic (OA) imaging and third harmonic generation (THG) based imaging.

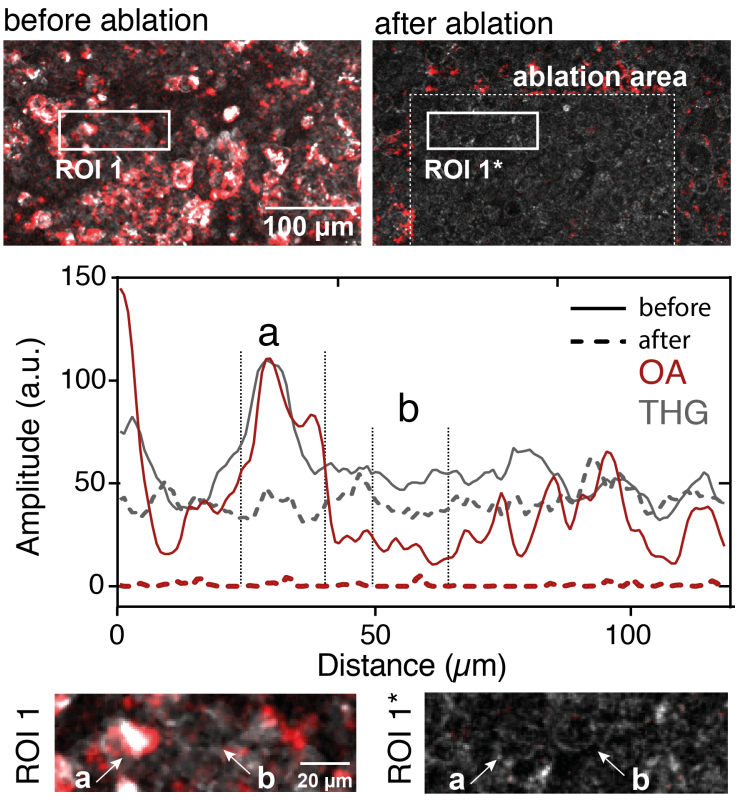

Figure 16: eFTH+L as an contrast agent for optical resolution optoacoustic and third harmonic generation microscopy, and actuator for controlled photoablation. Tim-2 overexpressing cells generate OA-contrast and enhance THG-contrast after take up of eFTH+L uptake. Imaging was conducted before and after locally confined ablation within the indicated area. OA-signal is displayed in red and THG in gray. Intensity profiles of representative cells (a+b) are shown above magnifications of regions of interest (ROIs). Cell a evokes ferritin based OA-and THG signals (solid lines), which are reduced to background after ablation (dashed line). Cell b does not show OA-signal, but the THG-signal remains comparable after ablation.

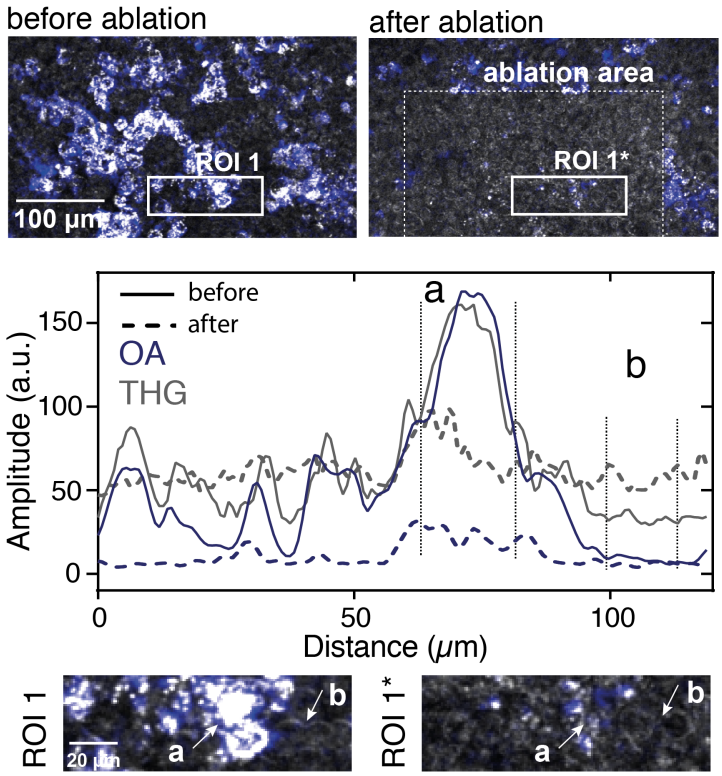

Figure 17: hFTH+L as an contrast agent for optical resolution optoacoustic and third harmonic generation microscopy, and actuator for controlled photoablation. Tim-2 overexpressing cells generate distinct OA-contrast and enhance THG-contrast due to hFTH+L uptake. Imaging was conducted before and after locally confined ablation within the indicated area. OA-signal is displayed in red and THG in gray. Intensity profiles of representative cells (a+b) are shown above magnifications of regions of interest (ROIs). Cell a evokes ferritin based OA-and THG signals (solid lines), which are reduced to background after ablation (dashed line). Cell b does not show OA-signal, but the THG-signal remains comparable after ablation.

Tim-2 overexpressing cells evoked OA-signal and showed enhanced THG-signal after incubation with eFTH+L (Figure 16) and hFTH-Mag (Figure 17). The OA-signal is only generated by ferritin, but THG is generated by every cell through the cell membrane and additionally enhanced by ferritin. After imaging, it was shown that specific cell ablation through energy absorption could be realized. The laser intensity of the OA laser was in-

creased in the area marked as “ablation area”. Cells loaded with either of the ferritin variants were selectively destroyed through photothermolysis, whereas non-loaded cells were not destroyed (Figure 16 ROI1+1*, Figure 17 ROI 1+1*). Cell ablation is shown with vanished OA as well as absent THG signal from cells that showed strong OA and THG signal before. Cells lacking OA contrast still showed normal morphology in THG and were therefore not damaged.

Chapter 4

Discussion

This doctoral thesis focused on the development of genetically encoded magnetic contrast agents and actuators for molecular imaging and cellular actuation. Genetically encoded magnetic particles combine magnetic features with unique genetic features like cell type specific addressability and delivery. Due to its magnetic properties, a targeted magnetic interface can be used in two ways. On the one hand, it can function as MRI contrast agent and therefore enable non-invasive molecular imaging with whole organ coverage [Pankhurst et al., 2003]. On the other hand, it can be used as an energy converter in the field of magnetogenetics to modulate cellular behavior through the application of mechanic forces or heat [Dobson, 2008; Jordan et al., 1999]. The magnetic contrast agents and actuators developed during this doctoral research project have also altered optical properties which could be used in combination with new emerging non-invasive imaging and actuation techniques.

The profound knowledge of systemic and especially cellular iron homeostasis, gathered through basis research over the past decades, were the bases for the bioengineering approaches in this project. To assess the maximum achievable effects ferritin can evoke in these systems CMV-promoter driven transient overexpression was used to deflect iron homeostasis from its highly-controlled equilibrium. High iron loading of ferritin is necessary for the assessment of its full potential as a genetically en-

coded biomagnetic contrast agent and actuator. To simplify the testing of the different approaches HEK293 and HEK293T cells were used as a eukaryotic model cell line, granting highly efficient transfections, followed by high protein expression. Furthermore, it enabled the assessment of different combinations of genetic constructs and other experimental conditions. These assessments mainly consisted of iron assays and cell pellet MR-measurements. These two analysis techniques were established for this thesis and carried out in a defined way to enable multiple comparisons of experiments.

4.1 Tf-dependent iron uptake pathways for bioengineering

Tf-dependent iron uptake is the most abundant pathway in vertebrates [Ganz & Nemeth, 2015]. The uptake of maximal two iron atoms per endocytosis cycle seems from a bioengineering point of view very inefficient. Considering that iron is irreplaceable for many cellular processes, but excess iron can harm cells through radical formation, a strong regulation of cellular and systemic iron uptake is vital [Aisen et al., 2001]. Furthermore, evolution had to solve the hurdle of iron accessibility. Ferrous iron is highly soluble and reactive in aqueous solution, but ferric iron is insoluble and stable [Aisen et al., 2001], creating a dilemma. The solution of this being the systemic mobilization of iron through the interaction of ferric iron with transferrin [Vulpe et al., 1999; Aisen et al., 1978]. In contrast, iron is mobilized inside the cell in its ferrous form, probably through the iron chaperones from the PCBP family [Leidgens et al., 2013]. Since a very fine balance of all these factors needs to be maintained, iron homeostasis on systemic and cellular levels is dominated by iron retention and recycling to keep the fine balance needed [Ganz & Nemeth, 2015]. The experiments shown in 3.1 suggest that it is possible to increase cellular iron loading through the addition of transferrin and ferric iron in the cell culture media. As a direct consequence T_2-derived MR-contrast was elevated. However, the

elevation of both was little and a specific further increase through overexpression of TfR1 could not be realized. Also, the introduction of an artificial iron sink through overexpression of different ferritin variants did not result in significantly increased cellular iron or MR-contrast. However, the increased cell proliferation during transferrin loading with ferric citrate hints to the successful loading of cells with iron via the canonical transferrin-dependent iron uptake pathway. These experiments are in accordance with many published data, were research groups repeatedly publish intracellular iron and MR-contrast elevation but fail to prove a genetic control over these conditions through TfR1 or even heavy chain ferritin expression [Pereira et al., 2016, 2015; Lee et al., 2017; Bernau et al., 2016]. For further evaluations of Tf-dependent iron uptake, cellular regulation mechanisms should be taken into focus. For instance, HFE diminishes binding of TfR1 to ferric iron-loaded transferrin through direct competition [Giannetti & Björkman, 2004]. This happens normally under low transferrin-bound iron conditions [Ganz & Nemeth, 2015]. Even though ferric iron and transferrin were supplemented in high concentrations, it might be that iron loading of transferrin was not efficient. *In-vivo* but also in cell culture the ferroxidase ceruloplasmin oxidizes ferrous iron to ferric iron and facilitates transferrin loading [Crielaard et al., 2017]. Since loading without the help of ceruloplasmin can take up to minutes, the supplemented ferric iron in combination with Tf could have led to a very slow iron loading of Tf and therefore a high concentration of non-iron bound transferrin. This would then cause HFE interaction with TfR1 and in consequence inhibition of iron uptake over TfR1. Even though ferric iron was theoretically the correct oxidation form of iron, the supplementation with ferrous iron for iron loading over TfR1 could be a promising starting point for further experiments.
For the bioengineering of biomagnetic contrast agents, which require high intracellular iron concentrations, this pathway did not seem to be efficient enough, and genetic control was lacking. This led to the use of the ferrous iron uptake pathway.

4.2 Ferrous iron transport

Through the overexpression of ferrous iron pumps in the cell membrane, the bypassing of the highly regulated Tf-dependent iron uptake pathway was realized. At first, the well-known iron transporter DMT1 was assessed.

DMT1

To my knowledge, the publication of [Kim et al., 2012] is the only published study using DMT1 in combination with its iron transport abilities in a bioengineering context. The artificial loading conditions, through the use of a loading buffer and the further *in vitro* loading of ferritin after protein extraction have to be taken into account for the evaluation of this approach for cell culture experiments at physiological conditions, as well as for *in vivo* experiments. In the experiments described in 3.2.1 a clear increase in intracellular iron could be detected which was correlated with the used DNA amount for transfections. However, iron loading was strongly correlated with cell death, suggesting mishandling of the artificially high iron concentrations inside the cell. The verification of the positive effect of nifedipine as claimed in [Kim et al., 2012] could not be verified if the loading control was considered. This lays in accordance with other published studies [Mackenzie et al., 2010]. After the first assessment of DMT1, the focus was shifted to Zip14. Zip14 has its pH optimum at pH 7.4 in contrast to DMT1 which has its pH optimum at pH 6.75.

Zip14

For the first time, Zip14 was used in a bioengineering context to load overexpressed ferritin inside cells and therefore alter their magnetic properties. Zip14 was trafficked to the cell membrane after transient overexpression. It was further shown, that intracellular iron could be gradually increased

through the increase of Zip14 coding DNA used during transfections and 3 mM FAS incubation. However, a pronounced cell death was observed indicating mishandling of iron and/or an overextension of cellular iron storage. The assessment of hFt and LHFT as iron storage proteins, during Zip14 and 1 mM FAS incubation, clearly suggested a rescue effect of hFt. Whereas the rescue effect of LHFT was not as pronounced but still significant comparing to cells not expressing an iron storage protein. The overexpression of hFt and LHFT had a positive impact on cell viability under these conditions, but the total iron loading of cells was with approx. 0.3 pg iron/cell relatively low and unsuitable for the high concentrations needed for a magnetic contrast agents. The difference in iron uptake, even though same amounts of Zip14 DNA were used, could be a result of differences in HFE interaction with Zip14. It is known that HFE interacts with Zip14 and causes its degradation, resulting in a diminishing NTBI-uptake [Gao et al., 2009]. The iron uptake could be further increased through the use of ascorbic acid as reduction agent during incubation with 1 mM FAS, reaching values comparable with 3 mM FAS incubation without ascorbic acid. Under physiological conditions, most ferrous iron oxidizes and forms low molecular weight complexes (e.g with citrate). This equilibrium is probably influenced through ascorbic acid, making ferrous iron more accessible to Zip14 [Pinilla-Tenas et al., 2011]. Nevertheless, the overexpression of hFT could not buffer the toxic effect of these high intracellular iron concentrations. This led to the conclusion that iron transport was not the bottleneck during Zip14-mediated iron import. Mainly because the transport could be boosted with the addition of ascorbic acid. Additionally, the effect of ascorbic acid can be enhanced through the use of 2-phosphoascorbate, which is more stable over time in cell culture media and therefore retains its reductive capabilities [Frikke-Schmidt & Lykkesfeldt, 2010]. The bottleneck appeared to be the safe handling of the newly introduced iron. To tackle this problem, higher protein titers of the transiently expressed proteins were produced through a different transfection protocol. By producing more ferritin, the iron toxicity could be controlled while increasing simultaneously intracellular iron, making a further step towards the prereq-

uisites of a magnetic contrast agents and actuators.
Through the novel transfection strategy, the amount of cellular iron could be raised during the incubation with 1 mM FAS loading. It was shown that overexpressed heavy chain ferritin (hFt) can be effectively loaded using Zip14, thereby making hFt a more robust and potent MRI gene reporter. However, the increase in iron loading of hFt did not resemble the increase in protein detected by Western blotting. This suggests that the loading of the overexpressed ferritin could be the bottleneck in this experimental approach. Recently it was reported, that each member of the Poly-r(C)-binding Protein (PCBP) functions as an iron chaperone and facilitate ferritin loading [Leidgens et al., 2013]. The overexpression of PCBP1 and PCBP2 -which have been reported to be the most effective ones- was carried out to enable higher iron loading of hFt. There was no clear evidence for the positive effect of these genes on ferritin loading in the experimental set-up. On the other hand, it could be shown that the amount of Zip14 encoding DNA could be reduced to a third of the total DNA without any negative effects on MR-contrast enhancement or iron loading. This suggests that the total amount of Zip14 encoding DNA and probably also the protein levels are not a limiting factor of iron loading. There are probably regulatory mechanisms in place which can alter iron transport even if there is CMV-driven overexpression, for instance, HFE [Gao et al., 2009]. Regulatory mechanisms also caused the upregulation of endogenous ferritin during Zip14 mediated iron loading while no hFt was transiently overexpressed. Nevertheless, elevated MR-contrast from only Zip14 overexpressing cells is probably a mixture of iron loaded upregulated ferritin and cytotoxicity induced by Fenton chemistry.
Zip14 proved to be an effective iron transporter under physiological conditions in cell culture. The bottleneck appeared the effective loading of hFt. For further experiments, iron loading kinetics of ferritin should be taken into account. Even in *in vitro* loading conditions native ferritin loading can take up to minutes [Chasteen & Harrison, 1999], whereas there are no studies to my knowledge about ferritin loading kinetics inside cells. A slower iron loading could lead to the desired high cellular iron concen-

tration without toxic effects. To test this, stable cell lines overexpressing different acceptors in combination with Zip14 could be generated for instance using the CRISPR/Cas technology. This would also reduce variability during these experiments and make the global readouts (iron assay and MR-measurements) more precise. If stable cell lines were used, also the impact of cell density during iron loading could be evaluated. The extent of cell death could be fluctuating caused by different cellular redox capacities as a result of cell density dependent cysteine-cystine cycling [Nkabyo et al., 2002]. Also, the ratio of Zip14 and hFt DNA can be changed, thereby producing more ferritin and importing less iron during the experiment. This would not directly solve the problem of inefficient ferritin loading but equip the cells with a higher iron buffer capacity and probably diminish cell death. If then, on the other hand, Zip14 is not negatively regulated by HFE, lower amounts of Zip14 could be sufficient. Additionally, the knowledge gathered about ferrous iron import could be the bases of iron loading of more suitable iron scaffold proteins like encapsulins [Giessen, 2016].

4.3 Ferritin Transport Pathway

The loading of overexpressed ferritin appeared to be a major obstacle to the use of the ferrous iron transport pathways for the development of a biomagnetic contrast agent. A different approach is the delivery of iron inside ferritin to the desired cells.

4.3.1 Native Ferritin

There are at least three receptors (murine Scara5, murine Tim-2, and human TfR1) that induce clathrin-coated pit-mediated endocytosis of ferritin upon its binding [Li et al., 2009, 2010; Chen et al., 2005]. This pathway can be more efficient than the Tf-dependent iron uptake pathway because up to 4500 Fe-atoms can be delivered into the cell with one single endocytosis cycle. The endocytosis of ferritin proved to be more efficient than

the iron uptake over Zip14 since similar amounts of iron inside the cells were achieved while using approx. a half of the iron concentration for incubation over the same period (eFTH+L≈1450 Fe/protein). Lacking regulatory mechanisms of heterologously expressed murine Tim-2 and Scara5 in HEK293T cells could also play a positive role in this approach. Even for human TfR1, the regulatory mechanisms described in literature affect only Tf binding e.g. through direct competition and ferritin binding probably appears at a different side as Tf binding happens [Giannetti & Björkman, 2004; Li et al., 2010]. Another positive aspect of ferritin uptake is the lack of toxicity. More precisely even proliferation of cells was observed to a certain extent. HEK293T cells have the inherent ability to take up ferritin over the endogenously expressed TfR1 which caused a strong increase of T_2-contrast. This effect could be enhanced and genetically controlled through the overexpression of TfR1, Tim-2 and Scara5. Since the iron delivered into cells is encapsulated inside ferritin, which is trafficked to the lysosomes after endocytosis, the cellular iron homeostasis did not seem to be massively deflected. Consequently the cells do not have to control vast amounts of free ferrous iron in the cytosol, which can cause toxic byproducts if not handled appropriately. Ferritin stayed mostly intact in the lysosomes and inhibition of lysosomal activity through bafilomycin A1 and chloroquine did not alter the MR-contrast. These experiments can lead to the conclusion that spatial vicinity or precipitation more than degradation of the ferritin shell amplifies the total magnetization and causes, therefore, higher T_2-derived MR-contrast.

It was tried to mimic the lysosomal ferritin clustering through the redirection of overexpressed hFt through the introduction of the peroxisomal targeting signal (PTS2) to the N-terminus of hFT. It is known that during the translocation into the peroxisome through this leader peptide the native protein conformation is kept, in contrast, to e.g. mitochondrial translocation [Dammai & Subramani, 2001]. Even though protein expression could be verified, iron loading or buffering of Zip14 mediated iron toxicity could not be detected. A possible explanation could be that ferritin was trafficked to the peroxisomes before iron loading could occur or that the N-terminal

modification blocked effective iron loading.
The uptake of ferritin proved to be an enormous step towards high cellular iron loading, combined with high viability. Furthermore, ferritin can be used as a nanocage carrying for instance highly magnetic metal cores or anti-cancerogenic substances and its potential ability to cross the blood-brain barrier could make it a powerful tool for preclinical studies [Cao et al., 2014; Crich et al., 2015; Fisher et al., 2007].

4.3.2 Magnetoferrtin

The use of ferrihydrite harboring ferritin as a biomagnetic actuator has clear physical limits due to the possible size and the magnetization of the iron core [Meister, 2016]. It is highly unlikely to exert a mechanical force, strong enough to open mechanosensitive ion channel or to raise the local temperature for the opening of heat-sensitive ion channels with as single ferritin particle a local energy converter [Meister, 2016]. Even if these single ferritins were carrying cobalt-doped magnetite cores with enhanced magnetization. The results shown in 3.1 and in 3.2 suggest that iron loading of overexpressed ferritin is challenging and has to be solved before ferritin can be used as an actuator. It was investigated if the limits of native ferritin could be overcome with the use of hFTH-Mag as an contrast agent and energy converter for magnetic interaction.
During receptor-mediated cellular ferritin uptake, an 80-fold lower concentration of hFTH-Mag evoked the same MR-contrast compared to experiments with eFTH+L. This enables possible targeting of single cells or cell clusters *in vivo* with this biosynthetic nanocage. This effect could be further enhanced if hFTH-Mag iron loading were elevated from 3000 Fe-atoms/protein to a published maximum of 7000 Fe-atoms/protein [Cai et al., 2015]. However, the synthesis procedure with an iron loading of 7000 Fe-atoms/protein resulted in a lower yield and requires more optimization. Even though the superparamagnetic behavior of the synthesized magnetite core could be determined, the strong contrast increase caused

by the use of hFTH-Mag was unexpected. It is known that clustering of T_2-contrast agents -like ferritin- has an amplifying effect in comparison to a non-clustered state of the same T_2-contrast agents [Bennett et al., 2008; Shapiro et al., 2009]. Through the use of hFTH-Mag, the contrast-enhancing effect of lysosomal ferritin entrapment was further evaluated. In experiments, in which a batch of hFTH-Mag was used that exhibited only a 1.8-fold increase of the relaxivity compared to eFTH+L in solution, a clustering effect through the lysosomes could be determined since the ratio increased to 13.32 after cellular uptake. If there were no enhancing effect, the ratios should remain the same or similar, because both contrast agents experience the same difference in the environment due to their uptake into the cells. A different affinity in the binding of eFTH+L and hFTH-Mag to Tim-2 could interfere with this reasoning, but increasing MR-contrast with increasing ferritin concentration of both variants, suggested a linear non-saturating range and thereby the complete uptake of the incubated ferritin. These results lead to the conclusion of a positive effect of lysosomal entrapment on T_2-derived MR-contrast. To test this hypothesis, further a release of ferritin form extracted lysosomes was conducted through the use of detergent. This would have allowed a comparison between lysosomally entrapped ferritin and the same concentration of disperse ferritin which underwent the same biochemical cellular pathways. However MR-measurements of these samples did not result in new insights, because detergent treatment of the samples resulted in a T_1-contrast enhancement, probably through increased interaction between exposed lipids and water protons. Additionally, the release of ferritin can be stimulated in further experiments through the use of endosomal/lysosomal escape peptides [Li et al., 2015; Nakase et al., 2010]. These peptides e.g. GALA or aurein 1.2 could be fused N-terminally to the precursor protein for hFTH-Mag. If a signal decrease in MRI correlated with a relocation of fluorescently labeled ferritin from the lysosomes to the cytosol, the enhancement of lysosomal entrapment would be further underlined.

The biggest difference between eFTH+L and hFTH-Mag is the possibility of magnetic interaction. Cells overexpressing TfR1 and Tim-2 could

be magnetically sorted after the uptake of hFTH-Mag, whereas these cells could not be sorted in significant amounts during the incubation with eFTH+L. Sorting efficiencies of approx. 30% in both cases is a combination of multiple factors. The theoretical size of the magnetite core (7-8 nm) only allows for superparamagnetic behavior and limits, therefore, the magnetic susceptibility. Secondly, the protein expression of Tim-2 underlies the limits of transient transfection, namely limitations in effectiveness and efficiency. A combination of these effects can result in seemingly low efficiency, during cellular analysis of the experimental outcome. On the other hand, the same effects also lower the actual experimental impact if the analysis methods take the whole cell population into account e.g., during MRI and iron assays. Stable cell lines, derived from single clones, would account for these methodological shortcomings.
Another form of magnetic interaction is heat-induced cell death via magnetic hyperthermia. This application is not as accurate as the control over ion channels as reported earlier, but physically more plausible [Stanley et al., 2016; Wheeler et al., 2016; Meister, 2016]. For cell ablation experiments, cell death was observed only if cells are overexpressing Tim-2, loaded with hFTH-Mag and experienced RF-treatment. The diminishing of the magnetic flux density from 18-20 mT to 1.8-2.0 mT resulted in the absence of observed cell death. It was recently reported that cobalt-doped magnetite nanoparticle could induce cell death solely after targeting the cell membrane and during RF-treatment with 17 kA/m and 183 kHz for 30 min [Fantechi et al., 2014]. The described cobalt-doping resulted in a strongly enhanced magnetic anisotropy and could, therefore, account for direct heat damage of the cell membrane and its proteins. Approaches, closer to ours, were used when lysosomally targeted magnetic nanoparticles, with a size comparable to the hFTH-Mag magnetite core (9 nm and 10 nm), caused lysosomal leakage and apoptotic cell death [Sanchez et al., 2014; Domenech et al., 2013]. It is well accepted that lysosomal membrane permeabilization actively contributes to apoptotic signaling pathways through the release of proteolytic lysosomal enzymes into the cytosol [Guicciardi et al., 2004]. In these studies, lysosomal leakage was

shown through the relocalization of fluorescently labeled nanoparticles from lysosomes to the cytosol and increased ROS production [Sanchez et al., 2014; Domenech et al., 2013]. As a further proof of lysosomal leakage, cell death could be abolished through the use of E64d, an inhibitor of cysteine proteases such as lysosomal cathepsins [Sanchez et al., 2014]. These approaches are similar to the approach with hFTH-Mag, however, the amplitude of the alternating magnetic field reached values of approx. 40 mT with a frequency of 275 kHz and 233 kHz, respectively [Sanchez et al., 2014; Domenech et al., 2013]. While our experimental setup only allowed for approx. 20 mT and 318 kHz without unspecific heating of the coil and the surrounding. Another big difference is the hydrodynamic diameter of the nanoparticles in use in our system. The mean hydrodynamic diameters of the particles used in the studies from Sanchez et al. and Domenech et al. were reaching values between 40 nm and 61 nm with large variations due to functionalization. The use of ferritin as a defined nanocage addresses these shortcomings and results in a very narrow size distribution of the magnetic core and the hydrodynamic size of approx. 12 nm. The 3 nm protein shell could increase the magnetic interactions between the magnetite cores, compared to the large distances between the functionalized magnetic particles used in studies mentioned. Also, a partial degradation of ferritin through lysosomal enzymes could cause the exposure of the magnetite cores and enable further magnetic interaction. Even though the phenomena of magnetic hyperthermia induced cell death caused by SPOIs in the size range of the ferritin core is reported repeatedly, the mechanism is still not understood. It is standing to reason that heat generation causes lysosomal leakage, however, a temperature rise was never reported, probably due to its very local appearance and the resulting difficulties in the determination. A temperature rise could explain a membrane leakage since for instance drug release from magnetic particle-loaded liposomes can be controlled through RF-treatment [Amstad et al., 2011]. The lipid phase transition can cause higher permeability in liposomes, but it appears more plausible that in mammalian membranes protein denaturation accounts for the difference in membrane stability if tem-

perature rise as little as 40-42℃ [Lepock, 1982, 2003]. Overall, it can be assumed that lysosomally trafficked hFTH-Mag caused lysosomal leakage during RF-treatment, which then caused cell death. The close vicinity of a vast amount of hFTH-Mag and/or the partial precipitation of hFTH-Mag in the lysosomes could be a possible explanation of this effect.

4.3.3 Ferritin as an Contrast Agent for OA and THG Microscopy

The introduction of metal-protein interfaces in cells caused an alternation of optical properties. The uptake of both ferritin variants during Tim-2 overexpression resulted in a genetically controlled increase of absorbance and enabled, therefore, optoacounstic imaging. This makes iron-loaded ferritin a suitable label for optoacoustic microscopy. However, the subcellular clustering of large amounts of ferritin inside the lysosomes has probably an enhancing effect on the optoacoustic signal. If the sensibility of the method could be further improved, ferritin iron loading dynamics could be studied through this method. This would be especially interesting in combination with the Zip14-mediated iron loading of overexpressed hFT, discussed in 4.2. Furthermore, it was possible to evoke ferritin derived THG signal. Since ferritin was targeted to the lysosomes, the total size of the THG interface reached about 1µm which is comparable to the focal size of the laser and therefore ideal for THG. The difference in refractive index, which is the leading cause of THG, was either evoked through the big amount of protein densely packed in the lysosome or through the metallic interface introduced via iron-loaded ferritin [Weigelin et al., 2016]. Without further modification, it was possible to use iron-loaded ferritin (eFTH+L and hFTH-Mag) as an constrast agent for two non-invasive imaging techniques, namely OA and THG.

Due to the ability of specific energy deposition in ferritin, selective cell ablation on OA signal evoking cells could be carried out. Therefore the laser power was increased to a threshold on which OA signal-evoking cell suffer thermal destruction whereas non-OA-evoking cell did not absorb enough

energy for the same phenomena to be observed. Cell ablation was shown with the absence of OA-signal in combination with vanished ferritin and cell membrane evoked THG signal. However, cells lacking OA contrast before the ablation, still showed normal morphology in THG after the ablation power was applied and were therefore not damaged.
The use of both ferritin variants as contrast agents for non-invasive optical imaging and actuators underlines the use of the genetic control over the ferritin uptake pathways for bioengineering purposes. For further studies, OA and THG could be used for the detection of hemosiderin during hemochromatosis or neurodegenerative diseases, in which lysosomal impairment causes ferritin agglomeration in lysosomes [**?**Zecca et al., 2004; Barnham et al., 2004; Greenough et al., 2013].

4.4 Bioengineering of Contrast Agents and Actuators

The terms bioengineering, cell engineering, and synthetic biology have very broad definitions, big overlaps and are mostly dependent on the educational background of the researchers. The concept of modularity and standardization that adapts logical operators is a key factor in the bioengineering branch of synthetic biology [Schwille, 2011]. In this thesis, the term bioengineering was used for the genetic alteration of cellular systems to function as an contrast agents and actuators for defined purposes. One of the big differences between classical engineering and bioengineering lies in the tools that are used. Whereas classical engineering uses tools that are designed from scratch for a certain purpose, bioengineers usually use tools designed by evolution and adapt them for their use [Schwille, 2011]. These tools are usually proteins. Since there is a profound knowledge about a vast amount of proteins, bioengineers pick described characteristics and use them for their purposes. The biggest difficulties are hidden in exactly this approach. Since some, but not all characteristics of the proteins are known, a bioengineer usually works with tools that have

the desired attributes, but at the same time, there is an introduction of unknown factors to the systems. Furthermore, the cellular systems are not as defined as systems in classical engineering and harbor many known and unknown regulatory abilities of variable efficiency.
During this project, the deflection of iron homeostasis was achieved only under extreme conditions like CMV-driven transient protein expression and the provision of big amounts of iron. Even under these conditions, endogenous regulatory mechanisms were able to interfere severely with the newly introduced approaches. This happened for instance through endogenous upregulation of ferritin and the abolishment of TfR1 induced iron uptake. Additionally, the interference with a highly regulated cellular process caused severe toxic effects whereas its anticipation and solution requires not only the knowledge of them, but probably also a systems biology approach to overcome these hurdles. Another possible solution to overcome regulatory mechanisms would be the design of orthogonal systems which interfere at only one point with the system of interest. A technology which uses the principle of orthogonality with great success is optogenetics. The use of optogenetic tools enables the sensing of unknown stimuli for the cells and evoke ion influx that resembles cellular stimulation or inhibition. This can be seen as the crossing of these two systems [Deisseroth, 2011].
Orthogonality is also one potential power of magnetogenetics. Additionally, magnetic fields do not suffer tissue attenuation and are therefore not limited in penetration depth [Pankhurst et al., 2003]. However, the interaction with magnetic field requires magnetic particles in one form or another, and the only element suitable as a building block is iron if a genetic approach is desired. The engineering of endogenous cellular iron homeostasis suffers from the lack of orthogonality. However, it provides more accessible tools than complete orthologue tools which inherently often deal with different iron redox chemistry [Yadav, 2010]. Magnetic contrast agents can already be used for several non-invasive imaging techniques as shown in 3.3.2 and 3.3.3, but still lack a translation to cellular actuation besides hyperthermic cell ablation (3.3.2) [Sanchez et al., 2014; Domenech et al.,

2013]. The translation of magnetic interaction to more precise interaction methods was addressed in earlier studies through the use of TRPV1 a heat-sensitive ion channel, and TRPV4 a mechanosensitive ion channel [Stanley et al., 2016; Wheeler et al., 2016]. With single native ferritins being the energy converters, these approaches seem physically not plausible, but could be rather artifacts of non-desired stimuli, e.g., change in ionic strength, pH change or unspecific heating [Meister, 2016; Chao, 2003; Ahern et al., 2005].

The limitations of non-orthogonal approaches in bioengineering can be illustrated through the use of the Tf-dependent iron uptake pathways and the ferrous iron uptake pathway described in this thesis. After the introduction of proteins or protein mechanisms that lack endogenous effective regulation and the use of hFTH-Mag, which harbors a non-accessible iron form, these limitations could be overcome and an contrast agent and actuator for multimodal non-invasive imaging and actuation was developed.

Bibliography

Ahern, G. P., Brooks, I. M., Miyares, R. L., & Wang, X.-b. (2005). Extracellular cations sensitize and gate capsaicin receptor trpv1 modulating pain signaling. *Journal of Neuroscience*, **25**(21), 5109–5116.

Aisen, P., Leibman, A., & Zweier, J. L. (1978). Stoichiometric and site characteristics of the binding of iron to human transferrin. *Journal of Biological Chemistry*, **253**(6), 1930–1937.

Aisen, P., Enns, C., & Wessling-Resnick, M. (2001). Chemistry and biology of eukaryotic iron metabolism. *The international journal of biochemistry & cell biology*, **33**(10), 940–959.

Amstad, E., Kohlbrecher, J., Muller, E., Schweizer, T., Textor, M., & Reimhult, E. (2011). Triggered release from liposomes through magnetic actuation of iron oxide nanoparticle containing membranes. *Nano letters*, **11**(4), 1664–1670.

Andersen, C. B. F., Torvund-Jensen, M., Nielsen, M. J., de Oliveira, C. L. P., Hersleth, H.-P., Andersen, N. H., Pedersen, J. S., Andersen, G. R., & Moestrup, S. K. (2012). Structure of the haptoglobin-haemoglobin complex. *Nature*, **489**(7416), 456–459.

Andrews, N. C. (1999). The iron transporter dmt1. *The international journal of biochemistry & cell biology*, **31**(10), 991–994.

Arredondo, M., Kloosterman, J., Núñez, S., Segovia, F., Candia, V., Flores, S., Le Blanc, S., Olivares, M., & Pizarro, F. (2008). Heme iron uptake by

caco-2 cells is a saturable, temperature sensitive and modulated by extracellular ph and potassium. *Biological trace element research*, **125**(2), 109–119.

Asano, T., Komatsu, M., Yamaguchi-Iwai, Y., Ishikawa, F., Mizushima, N., & Iwai, K. (2011). Distinct mechanisms of ferritin delivery to lysosomes in iron-depleted and iron-replete cells. *Molecular and cellular biology*, **31**(10), 2040–2052.

Barnham, K. J., Masters, C. L., & Bush, A. I. (2004). Neurodegenerative diseases and oxidative stress. *Nature reviews Drug discovery*, **3**(3), 205–214.

Batey, R., Fong, P. L. C., Shamir, S., & Sherlock, S. (1980). A non-transferrin-bound serum iron in idiopathic hemochromatosis. *Digestive diseases and sciences*, **25**(5), 340–346.

Begum, N. A., Kobayashi, M., Moriwaki, Y., Matsumoto, M., Toyoshima, K., & Seya, T. (2002). Mycobacterium bovis bcg cell wall and lipopolysaccharide induce a novel gene, bigm103, encoding a 7-tm protein: identification of a new protein family having zn-transporter and zn-metalloprotease signatures. *Genomics*, **80**(6), 630–645.

Belaidi, A. A. & Bush, A. I. (2016). Iron neurochemistry in alzheimer's disease and parkinson's disease: targets for therapeutics. *Journal of neurochemistry*.

Bellelli, R., Castellone, M. D., Guida, T., Limongello, R., Dathan, N. A., Merolla, F., Cirafici, A. M., Affuso, A., Masai, H., Costanzo, V., et al. (2014). Ncoa4 transcriptional coactivator inhibits activation of dna replication origins. *Molecular cell*, **55**(1), 123–137.

Bellelli, R., Federico, G., Colecchia, D., Iolascon, A., Chiariello, M., Santoro, M., De Franceschi, L., Carlomagno, F., et al. (2016). Ncoa4 deficiency impairs systemic iron homeostasis. *Cell reports*, **14**(3), 411–421.

Bennett, K. M., Shapiro, E. M., Sotak, C. H., & Koretsky, A. P. (2008). Controlled aggregation of ferritin to modulate mri relaxivity. *Biophysical journal*, **95**(1), 342–351.

Berg, D. & Youdim, M. B. (2006). Role of iron in neurodegenerative disorders. *Topics in Magnetic Resonance Imaging*, **17**(1), 5–17.

Bernau, K., Lewis, C. M., Petelinsek, A. M., Reagan, M. S., Niles, D. J., Mattis, V. B., Meyerand, M. E., Suzuki, M., & Svendsen, C. N. (2016). In vivo tracking of human neural progenitor cells in the rat brain using magnetic resonance imaging is not enhanced by ferritin expression. *Cell transplantation*, **25**(3), 575–592.

Bhatt, L., Horgan, C. P., & McCaffrey, M. W. (2009). Knockdown of β2-microglobulin perturbs the subcellular distribution of hfe and hepcidin. *Biochemical and biophysical research communications*, **378**(4), 727–731.

Bidmon, H.-J., Emde, B., Oermann, E., Kubitz, R., Witte, O. W., & Zilles, K. (2001). Heme oxygenase-1 (hsp-32) and heme oxygenase-2 induction in neurons and glial cells of cerebral regions and its relation to iron accumulation after focal cortical photothrombosis. *Experimental neurology*, **168**(1), 1–22.

Blasberg, R. G. & Gelovani-Tjuvajev, J. (2002). In vivo molecular-genetic imaging. *Journal of Cellular Biochemistry*, **87**(S39), 172–183.

Bloch, F. (1946). Nuclear induction. *Physical review*, **70**(7-8), 460.

Bloembergen, N., Purcell, E. M., & Pound, R. V. (1948). Relaxation effects in nuclear magnetic resonance absorption. *Physical review*, **73**(7), 679.

Bretscher, M. S. & Thomson, J. N. (1983). Distribution of ferritin receptors and coated pits on giant hela cells. *The EMBO journal*, **2**(4), 599.

Brissot, P., Wright, T. L., Ma, W.-L., & Weisiger, R. A. (1985). Efficient clearance of non-transferrin-bound iron by rat liver. implications for hep-

atic iron loading in iron overload states. *Journal of Clinical Investigation*, **76**(4), 1463.

Burdo, J., Menzies, S., Simpson, I., Garrick, L., Garrick, M., Dolan, K., Haile, D., Beard, J., & Connor, J. (2001). Distribution of divalent metal transporter 1 and metal transport protein 1 in the normal and belgrade rat. *Journal of neuroscience research*, **66**(6), 1198–1207.

Cai, Y., Cao, C., He, X., Yang, C., Tian, L., Zhu, R., & Pan, Y. (2015). Enhanced magnetic resonance imaging and staining of cancer cells using ferrimagnetic h-ferritin nanoparticles with increasing core size. *International journal of nanomedicine*, **10**, 2619.

Cao, C., Tian, L., Liu, Q., Liu, W., Chen, G., & Pan, Y. (2010). Magnetic characterization of noninteracting, randomly oriented, nanometer-scale ferrimagnetic particles. *Journal of Geophysical Research: Solid Earth*, **115**(B7).

Cao, C., Wang, X., Cai, Y., Sun, L., Tian, L., Wu, H., He, X., Lei, H., Liu, W., Chen, G., et al. (2014). Targeted in vivo imaging of microscopic tumors with ferritin-based nanoprobes across biological barriers. *Advanced materials*, **26**(16), 2566–2571.

Carrey, J., Mehdaoui, B., & Respaud, M. (2011). Simple models for dynamic hysteresis loop calculations of magnetic single-domain nanoparticles: Application to magnetic hyperthermia optimization. *Journal of Applied Physics*, **109**(8), 083921.

Chakravarti, S., Sabatos, C. A., Xiao, S., Illes, Z., Cha, E. K., Sobel, R. A., Zheng, X. X., Strom, T. B., & Kuchroo, V. K. (2005). Tim-2 regulates t helper type 2 responses and autoimmunity. *Journal of Experimental Medicine*, **202**(3), 437–444.

Chao, M. V. (2003). Neurotrophins and their receptors: a convergence point for many signalling pathways. *Nature Reviews Neuroscience*, **4**(4), 299–309.

Chasteen, N. D. & Harrison, P. M. (1999). Mineralization in ferritin: an efficient means of iron storage. *Journal of structural biology*, **126**(3), 182–194.

Cheepsunthorn, P., Palmer, C., Menzies, S., Roberts, R. L., & Connor, J. R. (2001). Hypoxic/ischemic insult alters ferritin expression and myelination in neonatal rat brains. *Journal of Comparative Neurology*, **431**(4), 382–396.

Chen, T. T., Li, L., Chung, D.-H., Allen, C. D., Torti, S. V., Torti, F. M., Cyster, J. G., Chen, C.-Y., Brodsky, F. M., Niemi, E. C., et al. (2005). Tim-2 is expressed on b cells and in liver and kidney and is a receptor for h-ferritin endocytosis. *The Journal of experimental medicine*, **202**(7), 955–965.

Cohen, B., Dafni, H., Meir, G., Harmelin, A., & Neeman, M. (2005). Ferritin as an endogenous mri reporter for noninvasive imaging of gene expression in c6 glioma tumors. *Neoplasia*, **7**(2), 109–117.

Cohen, B., Ziv, K., Plaks, V., Israely, T., Kalchenko, V., Harmelin, A., Benjamin, L. E., & Neeman, M. (2007). Mri detection of transcriptional regulation of gene expression in transgenic mice. *Nature medicine*, **13**(4), 498–503.

Cohen, L. A., Gutierrez, L., Weiss, A., Leichtmann-Bardoogo, Y., Zhang, D.-l., Crooks, D. R., Sougrat, R., Morgenstern, A., Galy, B., Hentze, M. W., et al. (2010). Serum ferritin is derived primarily from macrophages through a nonclassical secretory pathway. *Blood*, **116**(9), 1574–1584.

Collins, J. F., Xu, H., Kiela, P. R., Zeng, J., & Ghishan, F. K. (1997). Functional and molecular characterization of nhe3 expression during ontogeny in rat jejunal epithelium. *American Journal of Physiology-Cell Physiology*, **273**(6), C1937–C1946.

Connor, J., Menzies, S., St Martin, S., & Mufson, E. (1990). Cellular distribution of transferrin, ferritin, and iron in normal and aged human brains. *Journal of neuroscience research*, **27**(4), 595–611.

Connor, J., Snyder, B., Beard, J., Fine, R., & Mufson, E. (1992). Regional distribution of iron and iron-regulatory proteins in the brain in aging and alzheimer's disease. *Journal of neuroscience research*, **31**(2), 327–335.

Connor, J. R. & Menzies, S. L. (1995). Cellular management of iron in the brain. *Journal of the neurological sciences*, **134**, 33–44.

Connor, J. R. & Menzies, S. L. (1996). Relationship of iron to oligondendrocytes and myelination. *Glia*, **17**(2), 83–93.

Connor, J. R., Pavlick, G., Karli, D., Menzies, S. L., & Palmer, C. (1995). A histochemical study of iron-positive cells in the developing rat brain. *Journal of Comparative Neurology*, **355**(1), 111–123.

Cozzi, A., Corsi, B., Levi, S., Santambrogio, P., Albertini, A., & Arosio, P. (2000). Overexpression of wild type and mutated human ferritin h-chain in hela cells in vivo role of ferritin ferroxidase activity. *Journal of Biological Chemistry*, **275**(33), 25122–25129.

Creamer, B. (1967). The turnover of the epithelium of the small intestine. *British medical bulletin*, **23**(3), 226–230.

Crich, S. G., Cadenazzi, M., Lanzardo, S., Conti, L., Ruiu, R., Alberti, D., Cavallo, F., Cutrin, J., & Aime, S. (2015). Targeting ferritin receptors for the selective delivery of imaging and therapeutic agents to breast cancer cells. *Nanoscale*, **7**(15), 6527–6533.

Crielaard, B. J., Lammers, T., & Rivella, S. (2017). Targeting iron metabolism in drug discovery and delivery. *Nature Reviews Drug Discovery*.

Crowe, A. & Morgan, E. H. (1992). Iron and transferrrin uptake by brain and cerebrospinal fluid in the rat. *Brain research*, **592**(1), 8–16.

Dammai, V. & Subramani, S. (2001). The human peroxisomal targeting signal receptor, pex5p, is translocated into the peroxisomal matrix and recycled to the cytosol. *Cell*, **105**(2), 187–196.

De Domenico, I., Vaughn, M. B., Li, L., Bagley, D., Musci, G., Ward, D. M., & Kaplan, J. (2006). Ferroportin-mediated mobilization of ferritin iron precedes ferritin degradation by the proteasome. *The EMBO Journal*, **25**(22), 5396–5404.

Deans, A. E., Wadghiri, Y. Z., Bernas, L. M., Yu, X., Rutt, B. K., & Turnbull, D. H. (2006). Cellular mri contrast via coexpression of transferrin receptor and ferritin. *Magnetic resonance in medicine*, **56**(1), 51–59.

Deisseroth, K. (2011). Optogenetics. *Nature methods*, **8**(1), 26–29.

Deliolanis, N. C., Ale, A., Morscher, S., Burton, N. C., Schaefer, K., Radrich, K., Razansky, D., & Ntziachristos, V. (2014). Deep-tissue reporter-gene imaging with fluorescence and optoacoustic tomography: a performance overview. *Molecular Imaging and Biology*, **16**(5), 652–660.

Dhungana, S., Taboy, C. H., Zak, O., Larvie, M., Crumbliss, A. L., & Aisen, P. (2004). Redox properties of human transferrin bound to its receptor. *Biochemistry*, **43**(1), 205–209.

Dobson, J. (2008). Remote control of cellular behaviour with magnetic nanoparticles. *Nature nanotechnology*, **3**(3), 139–143.

Domenech, M., Marrero-Berrios, I., Torres-Lugo, M., & Rinaldi, C. (2013). Lysosomal membrane permeabilization by targeted magnetic nanoparticles in alternating magnetic fields. *ACS nano*, **7**(6), 5091–5101.

Donovan, A., Lima, C. A., Pinkus, J. L., Pinkus, G. S., Zon, L. I., Robine, S., & Andrews, N. C. (2005). The iron exporter ferroportin/slc40a1 is essential for iron homeostasis. *Cell metabolism*, **1**(3), 191–200.

Dowdle, W. E., Nyfeler, B., Nagel, J., Elling, R. A., Liu, S., Triantafellow, E., Menon, S., Wang, Z., Honda, A., Pardee, G., et al. (2014). Selective vps34 inhibitor blocks autophagy and uncovers a role for ncoa4 in ferritin degradation and iron homeostasis in vivo. *Nature cell biology*, **16**(11), 1069–1079.

Drayer, B., Burger, P., Darwin, R., Riederer, S., Herfkens, R., & Johnson, G. (1986). Mri of brain iron. *American Journal of Roentgenology*, **147**(1), 103–110.

Drysdale, J., Arosio, P., Invernizzi, R., Cazzola, M., Volz, A., Corsi, B., Biasiotto, G., & Levi, S. (2002). Mitochondrial ferritin: a new player in iron metabolism. *Blood Cells, Molecules, and Diseases*, **29**(3), 376–383.

Duffy, S. P., Shing, J., Saraon, P., Berger, L. C., Eiden, M. V., Wilde, A., & Tailor, C. S. (2010). The fowler syndrome-associated protein flvcr2 is an importer of heme. *Molecular and cellular biology*, **30**(22), 5318–5324.

Dunn, K. W., McGraw, T. E., & Maxfield, F. R. (1989). Iterative fractionation of recycling receptors from lysosomally destined ligands in an early sorting endosome. *The Journal of cell biology*, **109**(6), 3303–3314.

Eide, D. J. (2004). The slc39 family of metal ion transporters. *Pflügers Archiv*, **447**(5), 796–800.

Evstatiev, R. & Gasche, C. (2011). Iron sensing and signalling. *Gut*, pages gut–2010.

Fan, K., Cao, C., Pan, Y., Lu, D., Yang, D., Feng, J., Song, L., Liang, M., & Yan, X. (2012). Magnetoferritin nanoparticles for targeting and visualizing tumour tissues. *Nature nanotechnology*, **7**(7), 459–464.

Fantechi, E., Innocenti, C., Zanardelli, M., Fittipaldi, M., Falvo, E., Carbo, M., Shullani, V., Di Cesare Mannelli, L., Ghelardini, C., Ferretti, A. M., et al. (2014). A smart platform for hyperthermia application in cancer treatment: cobalt-doped ferrite nanoparticles mineralized in human ferritin cages. *ACS nano*, **8**(5), 4705–4719.

Feng, Y., Liu, Q., Zhu, J., Xie, F., & Li, L. (2012). Efficiency of ferritin as an mri reporter gene in npc cells is enhanced by iron supplementation. *BioMed Research International*, **2012**.

Fetcho, J. R., Cox, K. J., & O'malley, D. M. (1998). Monitoring activity in neuronal populations with single-cell resolution in a behaving vertebrate. *The Histochemical journal*, **30**(3), 153–167.

Finazzi, D. & Arosio, P. (2014). Biology of ferritin in mammals: an update on iron storage, oxidative damage and neurodegeneration. *Archives of toxicology*, **88**(10), 1787–1802.

Fisher, J., Devraj, K., Ingram, J., Slagle-Webb, B., Madhankumar, A., Liu, X., Klinger, M., Simpson, I. A., & Connor, J. (2007). Ferritin: a novel mechanism for delivery of iron to the brain and other organs. *American Journal of Physiology-Cell Physiology*, **293**(2), C641–C649.

Fleming, M. D., Trenor, C. C., Su, M. A., Foernzler, D., Beier, D. R., Dietrich, W. F., & Andrews, N. C. (1997). Microcytic anaemia mice have a mutation in nramp2, a candidate iron transporter gene. *Nature genetics*, **16**(4), 383–386.

Fleming, M. D., Romano, M. A., Su, M. A., Garrick, L. M., Garrick, M. D., & Andrews, N. C. (1998). Nramp2 is mutated in the anemic belgrade (b) rat: evidence of a role for nramp2 in endosomal iron transport. *Proceedings of the National Academy of Sciences*, **95**(3), 1148–1153.

Ford, G., Harrison, P., Rice, D., Smith, J., Treffry, A., White, J., & Yariv, J. (1984). Ferritin: design and formation of an iron-storage molecule. *Philosophical Transactions of the Royal Society of London B: Biological Sciences*, **304**(1121), 551–565.

Frazer, D. M. & Anderson, G. J. (2005). Iron imports. i. intestinal iron absorption and its regulation. *American Journal of Physiology-Gastrointestinal and Liver Physiology*, **289**(4), G631–G635.

Frikke-Schmidt, H. & Lykkesfeldt, J. (2010). Keeping the intracellular vitamin c at a physiologically relevant level in endothelial cell culture. *Analytical biochemistry*, **397**(1), 135–137.

Fukada, T. & Kambe, T. (2011). Molecular and genetic features of zinc transporters in physiology and pathogenesis. *Metallomics*, **3**(7), 662–674.

Ganz, T. (2013). Systemic iron homeostasis. *Physiological reviews*, **93**(4), 1721–1741.

Ganz, T. & Nemeth, E. (2006). Iron imports. iv. hepcidin and regulation of body iron metabolism. *American Journal of Physiology-Gastrointestinal and Liver Physiology*, **290**(2), G199–G203.

Ganz, T. & Nemeth, E. (2015). Iron homeostasis in host defence and inflammation. *Nature Reviews Immunology*, **15**(8), 500–510.

Gao, J., Chen, J., Kramer, M., Tsukamoto, H., Zhang, A.-S., & Enns, C. A. (2009). Interaction of the hereditary hemochromatosis protein hfe with transferrin receptor 2 is required for transferrin-induced hepcidin expression. *Cell metabolism*, **9**(3), 217–227.

Garrick, M. D. (2011). Human iron transporters. *Genes & nutrition*, **6**(1), 45–54.

Gelvan, D., Fibach, E., Meyron-Holtz, E. G., & Konijn, A. (1996). Ferritin uptake by human erythroid precursors is a regulated iron uptake pathway. *Blood*, **88**(8), 3200–3207.

Genove, G., DeMarco, U., Xu, H., Goins, W. F., & Ahrens, E. T. (2005). A new transgene reporter for in vivo magnetic resonance imaging. *Nature medicine*, **11**(4), 450–454.

Gerlach, M., Ben-Shachar, D., Riederer, P., & Youdim, M. (1994). Altered brain metabolism of iron as a cause of neurodegenerative diseases? *Journal of neurochemistry*, **63**(3), 793–807.

Ghosh, S., Hevi, S., & Chuck, S. L. (2004). Regulated secretion of glycosylated human ferritin from hepatocytes. *Blood*, **103**(6), 2369–2376.

Giannetti, A. M. & Björkman, P. J. (2004). Hfe and transferrin directly compete for transferrin receptor in solution and at the cell surface. *Journal of Biological Chemistry*, **279**(24), 25866–25875.

Giessen, T. W. (2016). Encapsulins: microbial nanocompartments with applications in biomedicine, nanobiotechnology and materials science. *Current opinion in chemical biology*, **34**, 1–10.

Goodfellow, F. T., Simchick, G. A., Mortensen, L. J., Stice, S. L., & Zhao, Q. (2016). Tracking and quantification of magnetically labeled stem cells using magnetic resonance imaging. *Advanced Functional Materials*.

Gossuin, Y., Gillis, P., Hocq, A., Vuong, Q. L., & Roch, A. (2009). Magnetic resonance relaxation properties of superparamagnetic particles. *Wiley Interdisciplinary Reviews: Nanomedicine and Nanobiotechnology*, **1**(3), 299–310.

Goswami, T. & Andrews, N. C. (2006). Hereditary hemochromatosis protein, hfe, interaction with transferrin receptor 2 suggests a molecular mechanism for mammalian iron sensing. *Journal of Biological Chemistry*, **281**(39), 28494–28498.

Greenough, M. A., Camakaris, J., & Bush, A. I. (2013). Metal dyshomeostasis and oxidative stress in alzheimer's disease. *Neurochemistry international*, **62**(5), 540–555.

Griffiths, P. & Crossman, A. (1993). Distribution of iron in the basal ganglia and neocortex in postmortem tissue in parkinson's disease and alzheimer's disease. *Dementia and Geriatric Cognitive Disorders*, **4**(2), 61–65.

Gruenheid, S., Cellier, M., Vidal, S., & Gros, P. (1995). Identification and characterization of a second mouse nramp gene. *Genomics*, **25**(2), 514–525.

Guerinot, M. L. (2000). The zip family of metal transporters. *Biochimica et Biophysica Acta (BBA)-Biomembranes*, **1465**(1), 190–198.

Guicciardi, M. E., Leist, M., & Gores, G. J. (2004). Lysosomes in cell death. *Oncogene*, **23**(16), 2881–2890.

Gunshin, H., Mackenzie, B., Berger, U. V., Gunshin, Y., Romero, M. F., Boron, W. F., Nussberger, S., Gollan, J. L., & Hediger, M. A. (1997). Cloning and characterization of a mammalian proton-coupled metal-ion transporter. *Nature*, **388**(6641), 482–488.

Gunshin, H., Fujiwara, Y., Custodio, A. O., DiRenzo, C., Robine, S., & Andrews, N. C. (2005). Slc11a2 is required for intestinal iron absorption and erythropoiesis but dispensable in placenta and liver. *The Journal of clinical investigation*, **115**(5), 1258–1266.

Ha, S. H., Carson, A. R., & Kim, K. (2012). Ferritin as a novel reporter gene for photoacoustic molecular imaging. *Cytometry Part A*, **81**(10), 910–915.

Haacke, E. M., Cheng, N. Y., House, M. J., Liu, Q., Neelavalli, J., Ogg, R. J., Khan, A., Ayaz, M., Kirsch, W., & Obenaus, A. (2005). Imaging iron stores in the brain using magnetic resonance imaging. *Magnetic resonance imaging*, **23**(1), 1–25.

Hallberg, L., Brune, M., & Rossander, L. (1986). Effect of ascorbic acid on iron absorption from different types of meals. studies with ascorbic-acid-rich foods and synthetic ascorbic acid given in different amounts with different meals. *Human nutrition. Applied nutrition*, **40**(2), 97–113.

Han, J., Day, J. R., Connor, J. R., & Beard, J. L. (2003). Gene expression of transferrin and transferrin receptor in brains of control vs. iron-deficient rats. *Nutritional neuroscience*, **6**(1), 1–10.

Hare, D. J., Arora, M., Jenkins, N. L., Finkelstein, D. I., Doble, P. A., & Bush, A. I. (2015). Is early-life iron exposure critical in neurodegeneration? *Nature Reviews Neurology*, **11**(9), 536–544.

Harrison, P. M. & Arosio, P. (1996). The ferritins: molecular properties, iron storage function and cellular regulation. *Biochimica et Biophysica Acta (BBA)-Bioenergetics*, **1275**(3), 161–203.

Heinlein, C. A., Ting, H.-J., Yeh, S., & Chang, C. (1999). Identification of ara70 as a ligand-enhanced coactivator for the peroxisome proliferator-activated receptor γ. *Journal of Biological Chemistry*, **274**(23), 16147–16152.

Hentze, M. W., Caughman, S. W., Casey, J. L., Kodier, D. M., Rouault, T. A., Harford, J. B., & Klausner, R. D. (1988). A model for the structure and functions of iron-responsive elements. *Gene*, **72**(1), 201–208.

Heyn, C., Ronald, J. A., Mackenzie, L. T., MacDonald, I. C., Chambers, A. F., Rutt, B. K., & Foster, P. J. (2006). In vivo magnetic resonance imaging of single cells in mouse brain with optical validation. *Magnetic Resonance in Medicine*, **55**(1), 23–29.

Hopkins, C. R. (1983). Intracellular routing of transferrin and transferrin receptors in epidermoid carcinoma a431 cells. *Cell*, **35**(1), 321–330.

Hove, J. R., Köster, R. W., Forouhar, A. S., Acevedo-Bolton, G., Fraser, S. E., & Gharib, M. (2003). Intracardiac fluid forces are an essential epigenetic factor for embryonic cardiogenesis. *Nature*, **421**(6919), 172–177.

Huang, H., Delikanli, S., Zeng, H., Ferkey, D. M., & Pralle, A. (2010). Remote control of ion channels and neurons through magnetic-field heating of nanoparticles. *Nature nanotechnology*, **5**(8), 602–606.

Huang, P., Rong, P., Jin, A., Yan, X., Zhang, M. G., Lin, J., Hu, H., Wang, Z., Yue, X., Li, W., et al. (2014). Dye-loaded ferritin nanocages for multimodal imaging and photothermal therapy. *Advanced Materials*, **26**(37), 6401–6408.

Hughes, S., McBain, S., Dobson, J., & El Haj, A. J. (2008). Selective activation of mechanosensitive ion channels using magnetic particles. *Journal of The Royal Society Interface*, **5**(25), 855–863.

Hulet, S., Hess, E., Debinski, W., Arosio, P., Bruce, K., Powers, S., & Connor, J. (1999). Characterization and distribution of ferritin binding sites in the adult mouse brain. *Journal of neurochemistry*, **72**(2), 868–874.

Hulet, S., Heyliger, S., Powers, S., & Connor, J. (2000). Oligodendrocyte progenitor cells internalize ferritin via clathrin-dependent receptor mediated endocytosis. *Journal of neuroscience research*, **61**(1), 52–60.

Hvidberg, V., Maniecki, M. B., Jacobsen, C., Højrup, P., Møller, H. J., & Moestrup, S. K. (2005). Identification of the receptor scavenging hemopexin-heme complexes. *Blood*, **106**(7), 2572–2579.

Inoue, K., Nakai, Y., Ueda, S., Kamigaso, S., Ohta, K.-y., Hatakeyama, M., Hayashi, Y., Otagiri, M., & Yuasa, H. (2008). Functional characterization of pcft/hcp1 as the molecular entity of the carrier-mediated intestinal folate transport system in the rat model. *American Journal of Physiology-Gastrointestinal and Liver Physiology*, **294**(3), G660–G668.

Iordanova, B. & Ahrens, E. T. (2012). In vivo magnetic resonance imaging of ferritin-based reporter visualizes native neuroblast migration. *Neuroimage*, **59**(2), 1004–1012.

Iordanova, B., Robison, C. S., & Ahrens, E. T. (2010). Design and characterization of a chimeric ferritin with enhanced iron loading and transverse nmr relaxation rate. *JBIC Journal of Biological Inorganic Chemistry*, **15**(6), 957–965.

Iordanova, B., Hitchens, T. K., Robison, C. S., & Ahrens, E. T. (2013). Engineered mitochondrial ferritin as a magnetic resonance imaging reporter in mouse olfactory epithelium. *PloS one*, **8**(8), e72720.

Jain, R. K., Munn, L. L., & Fukumura, D. (2002). Dissecting tumour pathophysiology using intravital microscopy. *Nature Reviews Cancer*, **2**(4), 266–276.

Jathoul, A. P., Laufer, J., Ogunlade, O., Treeby, B., Cox, B., Zhang, E., Johnson, P., Pizzey, A. R., Philip, B., Marafioti, T., et al. (2015). Deep in vivo photoacoustic imaging of mammalian tissues using a tyrosinase-based genetic reporter. *Nature Photonics*.

Jenkitkasemwong, S., Wang, C.-Y., Mackenzie, B., & Knutson, M. D. (2012). Physiologic implications of metal-ion transport by zip14 and zip8. *Biometals*, **25**(4), 643–655.

Jiang, Y., Oliver, P., Davies, K. E., & Platt, N. (2006). Identification and characterization of murine scara5, a novel class a scavenger receptor that is expressed by populations of epithelial cells. *Journal of Biological Chemistry*, **281**(17), 11834–11845.

Jiang, Y., Sigmund, F., Reber, J., Deán-Ben, X. L., Glasl, S., Kneipp, M., Estrada, H., Razansky, D., Ntziachristos, V., & Westmeyer, G. G. (2015). Violacein as a genetically-controlled, enzymatically amplified and photobleaching-resistant chromophore for optoacoustic bacterial imaging. *Scientific reports*, **5**.

Johnson, M. B., Chen, J., Murchison, N., Green, F. A., & Enns, C. A. (2007). Transferrin receptor 2: evidence for ligand-induced stabilization and redirection to a recycling pathway. *Molecular biology of the cell*, **18**(3), 743–754.

Jordan, A., Scholz, R., Wust, P., Fähling, H., & Felix, R. (1999). Magnetic fluid hyperthermia (mfh): Cancer treatment with ac magnetic field induced excitation of biocompatible superparamagnetic nanoparticles. *Journal of Magnetism and Magnetic Materials*, **201**(1), 413–419.

Kang, J. H. & Chung, J.-K. (2008). Molecular-genetic imaging based on reporter gene expression. *Journal of Nuclear Medicine*, **49**(Suppl 2), 164S–179S.

Kawabata, H., Yang, R., Hirama, T., Vuong, P. T., Kawano, S., Gombart, A. F., & Koeffler, H. P. (1999). Molecular cloning of transferrin receptor 2 a new member of the transferrin receptor-like family. *Journal of Biological Chemistry*, **274**(30), 20826–20832.

Kawabata, H., Nakamaki, T., Ikonomi, P., Smith, R. D., Germain, R. S., & Koeffler, H. P. (2001). Expression of transferrin receptor 2 in normal and neoplastic hematopoietic cells. *Blood*, **98**(9), 2714–2719.

Keel, S. B., Doty, R. T., Yang, Z., Quigley, J. G., Chen, J., Knoblaugh, S., Kingsley, P. D., De Domenico, I., Vaughn, M. B., Kaplan, J., et al. (2008). A heme export protein is required for red blood cell differentiation and iron homeostasis. *Science*, **319**(5864), 825–828.

Kidane, T. Z., Sauble, E., & Linder, M. C. (2006). Release of iron from ferritin requires lysosomal activity. *American Journal of Physiology-Cell Physiology*, **291**(3), C445–C455.

Kim, T., Moore, D., & Fussenegger, M. (2012). Genetically programmed superparamagnetic behavior of mammalian cells. *Journal of biotechnology*, **162**(2), 237–245.

Kobayashi, K. (1978). Fine structure of the mammalian renal capsule: the atypical smooth muscle cell and its functional meaning. *Cell and tissue research*, **195**(3), 381–394.

Krieger, M. (1994). Structures and functions of multiligand lipoprotein receptors: macrophage scavenger receptors and ldl receptor-related protein (lrp). *Annual review of biochemistry*, **63**(1), 601–637.

Krieger, M. (1997). The other side of scavenger receptors: pattern recognition for host defense. *Current opinion in lipidology*, **8**(5), 275–280.

Kristiansen, M., Graversen, J. H., Jacobsen, C., Sonne, O., Hoffman, H.-J., Law, S. A., & Moestrup, S. K. (2001). Identification of the haemoglobin scavenger receptor. *Nature*, **409**(6817), 198–201.

Lakshmanan, A., Farhadi, A., Nety, S. P., Lee-Gosselin, A., Bourdeau, R. W., Maresca, D., & Shapiro, M. G. (2016). Molecular engineering of acoustic protein nanostructures. *ACS nano*, **10**(8), 7314–7322.

Lane, D. J., Robinson, S. R., Czerwinska, H., Bishop, G. M., & Lawen, A. (2010). Two routes of iron accumulation in astrocytes: ascorbate-dependent ferrous iron uptake via the divalent metal transporter (dmt1) plus an independent route for ferric iron. *Biochemical Journal*, **432**(1), 123–132.

Lane, D. J., Chikhani, S., Richardson, V., & Richardson, D. R. (2013). Transferrin iron uptake is stimulated by ascorbate via an intracellular reductive mechanism. *Biochimica et Biophysica Acta (BBA)-Molecular Cell Research*, **1833**(6), 1527–1541.

Lanzino, M., De Amicis, F., McPhaul, M. J., Marsico, S., Panno, M. L., & Andò, S. (2005). Endogenous coactivator ara70 interacts with estrogen receptor α (erα) and modulates the functional erα/androgen receptor interplay in mcf-7 cells. *Journal of Biological Chemistry*, **280**(21), 20421–20430.

Lauffer, R. B. (1987). Paramagnetic metal complexes as water proton relaxation agents for nmr imaging: theory and design. *Chemical Reviews*, **87**(5), 901–927.

Le Blanc, S., Garrick, M. D., & Arredondo, M. (2012). Heme carrier protein 1 transports heme and is involved in heme-fe metabolism. *American Journal of Physiology-Cell Physiology*, **302**(12), C1780–C1785.

Lee, C. W., Choi, S. I., Lee, S. J., Oh, Y. T., Park, G., Park, N. Y., Yoon, K.-A., Kim, S., Kim, D., Kim, Y.-H., et al. (2017). The effectiveness of ferritin as a contrast agent for cell tracking mri in mouse cancer models. *Yonsei medical journal*, **58**(1), 51–58.

Leidgens, S., Bullough, K. Z., Shi, H., Li, F., Shakoury-Elizeh, M., Yabe, T., Subramanian, P., Hsu, E., Natarajan, N., Nandal, A., et al. (2013).

Each member of the poly-r (c)-binding protein 1 (pcbp) family exhibits iron chaperone activity toward ferritin. *Journal of Biological Chemistry*, **288**(24), 17791–17802.

Leimberg, J., Konijn, A., & Fibach, E. (2003). Developing human erythroid cells grown in transferrin-free medium utilize iron originating from extracellular ferritin. *American journal of hematology*, **73**(3), 211–212.

Leimberg, M. J., Prus, E., Konijn, A. M., & Fibach, E. (2008). Macrophages function as a ferritin iron source for cultured human erythroid precursors. *Journal of cellular biochemistry*, **103**(4), 1211–1218.

Lepock, J. R. (1982). Involvement of membranes in cellular responses to hyperthermia. *Radiation Research*, **92**(3), 433–438.

Lepock, J. R. (2003). Cellular effects of hyperthermia: relevance to the minimum dose for thermal damage. *International Journal of Hyperthermia*, **19**(3), 252–266.

Levy, J. E., Jin, O., Fujiwara, Y., Kuo, F., & Andrews, N. (1999). Transferrin receptor is necessary for development of erythrocytes and the nervous system. *Nature genetics*, **21**(4), 396–399.

Li, J. Y., Paragas, N., Ned, R. M., Qiu, A., Viltard, M., Leete, T., Drexler, I. R., Chen, X., Sanna-Cherchi, S., Mohammed, F., et al. (2009). Scara5 is a ferritin receptor mediating non-transferrin iron delivery. *Developmental cell*, **16**(1), 35–46.

Li, L., Fang, C. J., Ryan, J. C., Niemi, E. C., Lebrón, J. A., Björkman, P. J., Arase, H., Torti, F. M., Torti, S. V., Nakamura, M. C., et al. (2010). Binding and uptake of h-ferritin are mediated by human transferrin receptor-1. *Proceedings of the National Academy of Sciences*, **107**(8), 3505–3510.

Li, M., Tao, Y., Shu, Y., LaRochelle, J. R., Steinauer, A., Thompson, D., Schepartz, A., Chen, Z.-Y., & Liu, D. R. (2015). Discovery and characterization of a peptide that enhances endosomal escape of delivered

proteins in vitro and in vivo. *Journal of the American Chemical Society*, **137**(44), 14084–14093.

Lin, J. Y. (2011). A user's guide to channelrhodopsin variants: features, limitations and future developments. *Experimental physiology*, **96**(1), 19–25.

Lin, L., Valore, E. V., Nemeth, E., Goodnough, J. B., Gabayan, V., & Ganz, T. (2007). Iron transferrin regulates hepcidin synthesis in primary hepatocyte culture through hemojuvelin and bmp2/4. *Blood*, **110**(6), 2182–2189.

Liuzzi, J. P., Aydemir, F., Nam, H., Knutson, M. D., & Cousins, R. J. (2006). Zip14 (slc39a14) mediates non-transferrin-bound iron uptake into cells. *Proceedings of the National Academy of Sciences*, **103**(37), 13612–13617.

Ludwiczek, S., Theurl, I., Muckenthaler, M. U., Jakab, M., Mair, S. M., Theurl, M., Kiss, J., Paulmichl, M., Hentze, M. W., Ritter, M., et al. (2007). Ca2+ channel blockers reverse iron overload by a new mechanism via divalent metal transporter-1. *Nature medicine*, **13**(4), 448–454.

Mack, U., Powell, L. W., & Halliday, J. (1983). Detection and isolation of a hepatic membrane receptor for ferritin. *Journal of Biological Chemistry*, **258**(8), 4672–4675.

Mackenzie, B., Shawki, A., Ghio, A. J., Stonehuerner, J. D., Zhao, L., Ghadersohi, S., Garrick, L. M., & Garrick, M. D. (2010). Calcium-channel blockers do not affect iron transport mediated by divalent metal-ion transporter-1. *Blood*, **115**(20), 4148–4149.

Madsen, E. & Gitlin, J. D. (2007). Copper and iron disorders of the brain. *Annu. Rev. Neurosci.*, **30**, 317–337.

Mancias, J. D., Wang, X., Gygi, S. P., Harper, J. W., & Kimmelman, A. C. (2014). Quantitative proteomics identifies ncoa4 as the cargo receptor mediating ferritinophagy. *Nature*, **509**(7498), 105–109.

Mancuso, J. J., Kim, J., Lee, S., Tsuda, S., Chow, N. B., & Augustine, G. J. (2011). Optogenetic probing of functional brain circuitry. *Experimental physiology*, **96**(1), 26–33.

Mank, M., Santos, A. F., Direnberger, S., Mrsic-Flogel, T. D., Hofer, S. B., Stein, V., Hendel, T., Reiff, D. F., Levelt, C., Borst, A., et al. (2008). A genetically encoded calcium indicator for chronic in vivo two-photon imaging. *Nature methods*, **5**(9), 805–811.

Mannix, R. J., Kumar, S., Cassiola, F., Montoya-Zavala, M., Feinstein, E., Prentiss, M., & Ingber, D. E. (2008). Nanomagnetic actuation of receptor-mediated signal transduction. *Nature nanotechnology*, **3**(1), 36–40.

Matsumoto, Y., Chen, R., Anikeeva, P., & Jasanoff, A. (2015). Engineering intracellular biomineralization and biosensing by a magnetic protein. *Nature communications*, **6**.

McCarthy, R. C. & Kosman, D. J. (2013). Ferroportin and exocytoplasmic ferroxidase activity are required for brain microvascular endothelial cell iron efflux. *Journal of Biological Chemistry*, **288**(24), 17932–17940.

McCarthy, R. C. & Kosman, D. J. (2015). Iron transport across the blood–brain barrier: development, neurovascular regulation and cerebral amyloid angiopathy. *Cellular and Molecular Life Sciences*, **72**(4), 709–727.

McCarthy, R. C., Park, Y.-H., & Kosman, D. J. (2014). sapp modulates iron efflux from brain microvascular endothelial cells by stabilizing the ferrous iron exporter ferroportin. *EMBO reports*, page e201338064.

McKie, A. T., Marciani, P., Rolfs, A., Brennan, K., Wehr, K., Barrow, D., Miret, S., Bomford, A., Peters, T. J., Farzaneh, F., et al. (2000). A novel duodenal iron-regulated transporter, ireg1, implicated in the basolateral transfer of iron to the circulation. *Molecular cell*, **5**(2), 299–309.

Meguro, R., Asano, Y., Odagiri, S., Li, C., Iwatsuki, H., & Shoumura, K. (2007). Nonheme-iron histochemistry for light and electron microscopy:

a historical, theoretical and technical review. *Archives of histology and cytology*, **70**(1), 1–19.

Meister, M. (2016). Physical limits to magnetogenetics. *Elife*, **5**, e17210.

Meyron-Holtz, E., Vaisman, B., Cabantchik, Z., Fibach, E., Rouault, T., Hershko, C., & Konijn, A. (1999). Regulation of intracellular iron metabolism in human erythroid precursors by internalized extracellular ferritin. *Blood*, **94**(9), 3205–3211.

Miyazaki, E., Kato, J., Kobune, M., Okumura, K., Sasaki, K., Shintani, N., Arosio, P., & Niitsu, Y. (2002). Denatured h-ferritin subunit is a major constituent of haemosiderin in the liver of patients with iron overload. *Gut*, **50**(3), 413–419.

Moos, T., Nielsen, T. R., Skjørringe, T., & Morgan, E. H. (2007). Iron trafficking inside the brain. *Journal of neurochemistry*, **103**(5), 1730–1740.

Morgan, E. H. & Oates, P. S. (2002). Mechanisms and regulation of intestinal iron absorption. *Blood Cells, Molecules, and Diseases*, **29**(3), 384–399.

Moss, D., Powell, L., Arosio, P., & Halliday, J. (1992). Characterization of the ferritin receptors of human t lymphoid (molt-4) cells. *The Journal of laboratory and clinical medicine*, **119**(3), 273–279.

Muller, R., Roch, A., Colet, J., Ouakssim, A., & Gillis, P. (2001). Particulate magnetic contrast agents. *The chemistry of contrast agents in medical magnetic resonance imaging. Wiley, New York*, pages 417–435.

Nagel, G., Ollig, D., Fuhrmann, M., Kateriya, S., Musti, A. M., Bamberg, E., & Hegemann, P. (2002). Channelrhodopsin-1: a light-gated proton channel in green algae. *Science*, **296**(5577), 2395–2398.

Nakai, J., Ohkura, M., & Imoto, K. (2001). A high signal-to-noise ca2+ probe composed of a single green fluorescent protein. *Nature biotechnology*, **19**(2), 137–141.

Nakai, Y., Inoue, K., Abe, N., Hatakeyama, M., Ohta, K.-y., Otagiri, M., Hayashi, Y., & Yuasa, H. (2007). Functional characterization of human proton-coupled folate transporter/heme carrier protein 1 heterologously expressed in mammalian cells as a folate transporter. *Journal of Pharmacology and experimental Therapeutics*, **322**(2), 469–476.

Nakase, I., Kobayashi, S., & Futaki, S. (2010). Endosome-disruptive peptides for improving cytosolic delivery of bioactive macromolecules. *Peptide Science*, **94**(6), 763–770.

Naumova, A. V., Reinecke, H., Yarnykh, V., Deem, J., Yuan, C., & Murry, C. E. (2010). Ferritin overexpression for noninvasive magnetic resonance imaging–based tracking of stem cells transplanted into the heart. *Molecular imaging*, **9**(4), 7290–2010.

Nemeth, E., Tuttle, M. S., Powelson, J., Vaughn, M. B., Donovan, A., Ward, D. M., Ganz, T., & Kaplan, J. (2004). Hepcidin regulates cellular iron efflux by binding to ferroportin and inducing its internalization. *science*, **306**(5704), 2090–2093.

Nkabyo, Y. S., Ziegler, T. R., Gu, L. H., Watson, W. H., & Jones, D. P. (2002). Glutathione and thioredoxin redox during differentiation in human colon epithelial (caco-2) cells. *American Journal of Physiology-Gastrointestinal and Liver Physiology*, **283**(6), G1352–G1359.

Ntziachristos, V. (2010). Going deeper than microscopy: the optical imaging frontier in biology. *Nature methods*, **7**(8), 603–614.

Ntziachristos, V., Ripoll, J., Wang, L. V., & Weissleder, R. (2005). Looking and listening to light: the evolution of whole-body photonic imaging. *Nature biotechnology*, **23**(3), 313–320.

Padmanaban, G., Venkateswar, V., & Rangarajan, P. (1989). Haem as a multifunctional regulator. *Trends in biochemical sciences*, **14**(12), 492–496.

Pankhurst, Q. A., Connolly, J., Jones, S. K., & Dobson, J. (2003). Applications of magnetic nanoparticles in biomedicine. *Journal of physics D: Applied physics*, **36**(13), R167.

Paraskeva, E. & Hentze, M. W. (1996). Iron-sulphur clusters as genetic regulatory switches: the bifunctional iron regulatory protein-1. *FEBS letters*, **389**(1), 40–43.

Patel, B. N., Dunn, R. J., Jeong, S. Y., Zhu, Q., Julien, J.-P., & David, S. (2002). Ceruloplasmin regulates iron levels in the cns and prevents free radical injury. *Journal of Neuroscience*, **22**(15), 6578–6586.

Patrick, P. S., Rodrigues, T. B., Kettunen, M. I., Lyons, S. K., Neves, A. A., & Brindle, K. M. (2015). Development of timd2 as a reporter gene for mri. *Magnetic resonance in medicine*.

Pearson, A. M. (1996). Scavenger receptors in innate immunity. *Current opinion in immunology*, **8**(1), 20–28.

Pereira, S. M., Moss, D., Williams, S. R., Murray, P., & Taylor, A. (2015). Overexpression of the mri reporter genes ferritin and transferrin receptor affect iron homeostasis and produce limited contrast in mesenchymal stem cells. *International journal of molecular sciences*, **16**(7), 15481–15496.

Pereira, S. M., Herrmann, A., Moss, D., Poptani, H., Williams, S. R., Murray, P., & Taylor, A. (2016). Evaluating the effectiveness of transferrin receptor-1 (tfr1) as a magnetic resonance reporter gene. *Contrast media & molecular imaging*.

Picard, V., Govoni, G., Jabado, N., & Gros, P. (2000). Nramp 2 (dct1/dmt1) expressed at the plasma membrane transports iron and other divalent cations into a calcein-accessible cytoplasmic pool. *Journal of Biological Chemistry*, **275**(46), 35738–35745.

Pinilla-Tenas, J. J., Sparkman, B. K., Shawki, A., Illing, A. C., Mitchell, C. J., Zhao, N., Liuzzi, J. P., Cousins, R. J., Knutson, M. D., & Mackenzie, B.

(2011). Zip14 is a complex broad-scope metal-ion transporter whose functional properties support roles in the cellular uptake of zinc and nontransferrin-bound iron. *American Journal of Physiology-Cell Physiology*, **301**(4), C862–C871.

Pountney, D., Trugnan, G., Bourgeois, M., & Beaumont, C. (1999). The identification of ferritin in the nucleus of k562 cells, and investigation of a possible role in the transcriptional regulation of adult beta-globin gene expression. *Journal of cell science*, **112**(6), 825–831.

Pu, Y. & Psaltis, D. (2013). Seeing through turbidity with harmonic holography [invited]. *Applied optics*, **52**(4), 567–578.

Qiu, A., Jansen, M., Sakaris, A., Min, S. H., Chattopadhyay, S., Tsai, E., Sandoval, C., Zhao, R., Akabas, M. H., & Goldman, I. D. (2006). Identification of an intestinal folate transporter and the molecular basis for hereditary folate malabsorption. *Cell*, **127**(5), 917–928.

Radisky, D. C. & Kaplan, J. (1998). Iron in cytosolic ferritin can be recycled through lysosomal degradation in human fibroblasts. *Biochemical Journal*, **336**(1), 201–205.

Raffin, S. B., Woo, C. H., Roost, K. T., Price, D. C., & Schmid, R. (1974). Intestinal absorption of hemoglobin iron-heme cleavage by mucosal heme oxygenase. *Journal of Clinical Investigation*, **54**(6), 1344.

Rajagopal, A., Rao, A. U., Amigo, J., Tian, M., Upadhyay, S. K., Hall, C., Uhm, S., Mathew, M., Fleming, M. D., Paw, B. H., et al. (2008). Haem homeostasis is regulated by the conserved and concerted functions of hrg-1 proteins. *Nature*, **453**(7198), 1127–1131.

Ramos-Gómez, M. & Martínez-Serrano, A. (2016). Tracking of iron-labeled human neural stem cells by magnetic resonance imaging in cell replacement therapy for parkinson's disease. *Neural regeneration research*, **11**(1), 49.

Recalcati, S., Invernizzi, P., Arosio, P., & Cairo, G. (2008). New functions for an iron storage protein: the role of ferritin in immunity and autoimmunity. *Journal of autoimmunity*, **30**(1), 84–89.

Rennert, P. D., Ichimura, T., Sizing, I. D., Bailly, V., Li, Z., Rennard, R., McCoon, P., Pablo, L., Miklasz, S., Tarilonte, L., et al. (2006). T cell, ig domain, mucin domain-2 gene-deficient mice reveal a novel mechanism for the regulation of th2 immune responses and airway inflammation. *The Journal of Immunology*, **177**(7), 4311–4321.

Richter, G. W. (1986). Studies of iron overload: lysosomal proteolysis of rat liver ferritin. *Pathology-Research and Practice*, **181**(2), 159–167.

Riemer, J., Hoepken, H. H., Czerwinska, H., Robinson, S. R., & Dringen, R. (2004). Colorimetric ferrozine-based assay for the quantitation of iron in cultured cells. *Analytical biochemistry*, **331**(2), 370–375.

Roch, A., Muller, R. N., & Gillis, P. (1999). Theory of proton relaxation induced by superparamagnetic particles. *The Journal of chemical physics*, **110**(11), 5403–5411.

Rodrigue, K. M., Haacke, E. M., & Raz, N. (2011). Differential effects of age and history of hypertension on regional brain volumes and iron. *Neuroimage*, **54**(2), 750–759.

Romero, A., Ramos, E., Los Ríos, C., Egea, J., Pino, J., & Reiter, R. J. (2014). A review of metal-catalyzed molecular damage: protection by melatonin. *Journal of pineal research*, **56**(4), 343–370.

Rosensweig, R. E. (2002). Heating magnetic fluid with alternating magnetic field. *Journal of magnetism and magnetic materials*, **252**, 370–374.

Roskams, A. & Connor, J. (1992). Transferrin receptor expression in myelin deficient (md) rats. *Journal of neuroscience research*, **31**(3), 421–427.

Rucker, P., Torti, F. M., & Torti, S. V. (1997). Recombinant ferritin: modulation of subunit stoichiometry in bacterial expression systems. *Protein engineering*, **10**(8), 967–973.

Rudin, M. & Weissleder, R. (2003). Molecular imaging in drug discovery and development. *Nature reviews Drug discovery*, **2**(2), 123–131.

Rusakov, D. A. (2006). Ca2+-dependent mechanisms of presynaptic control at central synapses. *The Neuroscientist*, **12**(4), 317–326.

Salahudeen, A. A., Thompson, J. W., Ruiz, J. C., Ma, H.-W., Kinch, L. N., Li, Q., Grishin, N. V., & Bruick, R. K. (2009). An e3 ligase possessing an iron-responsive hemerythrin domain is a regulator of iron homeostasis. *Science*, **326**(5953), 722–726.

Salvador, G. A. (2010). Iron in neuronal function and dysfunction. *BioFactors*, **36**(2), 103–110.

San Martin, C. D., Garri, C., Pizarro, F., Walter, T., Theil, E. C., & Núñez, M. T. (2008). Caco-2 intestinal epithelial cells absorb soybean ferritin by μ2 (ap2)-dependent endocytosis. *The Journal of nutrition*, **138**(4), 659–666.

Sanchez, C., El Hajj Diab, D., Connord, V., Clerc, P., Meunier, E., Pipy, B., Payré, B., Tan, R. P., Gougeon, M., Carrey, J., et al. (2014). Targeting a g-protein-coupled receptor overexpressed in endocrine tumors by magnetic nanoparticles to induce cell death. *Acs Nano*, **8**(2), 1350–1363.

Sanchez, M., Galy, B., Dandekar, T., Bengert, P., Vainshtein, Y., Stolte, J., Muckenthaler, M. U., & Hentze, M. W. (2006). Iron regulation and the cell cycle identification of an iron-responsive element in the 3-untranslated region of human cell division cycle 14a mrna by a refined microarray-based screening strategy. *Journal of Biological Chemistry*, **281**(32), 22865–22874.

Schwille, P. (2011). Bottom-up synthetic biology: engineering in a tinkerer's world. *Science*, **333**(6047), 1252–1254.

Shapiro, M. G., Szablowski, J. O., Langer, R., & Jasanoff, A. (2009). Protein nanoparticles engineered to sense kinase activity in mri. *Journal of the American Chemical Society*, **131**(7), 2484–2486.

Shaw, G. C., Cope, J. J., Li, L., Corson, K., Hersey, C., Ackermann, G. E., Gwynn, B., Lambert, A. J., Wingert, R. A., Traver, D., et al. (2006). Mitoferrin is essential for erythroid iron assimilation. *Nature*, **440**(7080), 96–100.

Shawki, A., Anthony, S. R., Nose, Y., De Renshaw, T. B., Thiele, D. J., & Mackenzie, B. (2012). Intestinal divalent metal-ion transporter-1 is critical for iron homeostasis but is not required for maintenance of cu or zn. *The FASEB Journal*, **26**(1 Supplement), 1112–2.

Shayeghi, M., Latunde-Dada, G. O., Oakhill, J. S., Laftah, A. H., Takeuchi, K., Halliday, N., Khan, Y., Warley, A., McCann, F. E., Hider, R. C., et al. (2005). Identification of an intestinal heme transporter. *Cell*, **122**(5), 789–801.

Sibille, J., Ciriolo, M., Kondo, H., Crichton, R., & Aisen, P. (1989). Subcellular localization of ferritin and iron taken up by rat hepatocytes. *Biochemical Journal*, **262**(2), 685–688.

Simpson, I. A., Ponnuru, P., Klinger, M. E., Myers, R. L., Devraj, K., Coe, C. L., Lubach, G. R., Carruthers, A., & Connor, J. R. (2015). A novel model for brain iron uptake: introducing the concept of regulation. *Journal of Cerebral Blood Flow & Metabolism*, **35**(1), 48–57.

Singh, N., Haldar, S., Tripathi, A. K., Horback, K., Wong, J., Sharma, D., Beserra, A., Suda, S., Anbalagan, C., Dev, S., et al. (2014). Brain iron homeostasis: from molecular mechanisms to clinical significance and therapeutic opportunities. *Antioxidants & redox signaling*, **20**(8), 1324–1363.

Stanley, S. A., Gagner, J. E., Damanpour, S., Yoshida, M., Dordick, J. S., & Friedman, J. M. (2012). Radio-wave heating of iron oxide nanoparticles can regulate plasma glucose in mice. *Science*, **336**(6081), 604–608.

Stanley, S. A., Sauer, J., Kane, R. S., Dordick, J. S., & Friedman, J. M. (2015). Remote regulation of glucose homeostasis in mice using genetically encoded nanoparticles. *Nature medicine*, **21**(1), 92–98.

Stanley, S. A., Kelly, L., Latcha, K. N., Schmidt, S. F., Yu, X., Nectow, A. R., Sauer, J., Dyke, J. P., Dordick, J. S., & Friedman, J. M. (2016). Bidirectional electromagnetic control of the hypothalamus regulates feeding and metabolism. *Nature*, **531**(7596), 647–650.

Stosiek, C., Garaschuk, O., Holthoff, K., & Konnerth, A. (2003). In vivo two-photon calcium imaging of neuronal networks. *Proceedings of the National Academy of Sciences*, **100**(12), 7319–7324.

Takeda, A., Devenyi, A., & Connor, J. R. (1998). Evidence for non-transferrin-mediated uptake and release of iron and manganese in glial cell cultures from hypotransferrinemic mice. *Journal of neuroscience research*, **51**(4), 454–462.

Taylor, K. M., Morgan, H. E., Smart, K., Zahari, N. M., Pumford, S., Ellis, I. O., Robertson, J. F., & Nicholson, R. I. (2007). The emerging role of the liv-1 subfamily of zinc transporters in breast cancer. *MOLECULAR MEDICINE-CAMBRIDGE MA THEN NEW YORK-*, **13**(7/8), 396.

Theil, E. C. & Eisenstein, R. S. (2000). Combinatorial mrna regulation: iron regulatory proteins and iso-iron responsive elements (iso-ires). *Journal of Biological Chemistry*.

Thompson, K., Molina, R. M., Donaghey, T., Brain, J. D., & Wessling-Resnick, M. (2007). Iron absorption by belgrade rat pups during lactation. *American Journal of Physiology-Gastrointestinal and Liver Physiology*, **293**(3), G640–G644.

Tian, L., Hires, S. A., Mao, T., Huber, D., Chiappe, M. E., Chalasani, S. H., Petreanu, L., Akerboom, J., McKinney, S. A., Schreiter, E. R., et al. (2009). Imaging neural activity in worms, flies and mice with improved gcamp calcium indicators. *Nature methods*, **6**(12), 875–881.

Todorich, B., Zhang, X., Slagle-Webb, B., Seaman, W. E., & Connor, J. R. (2008). Tim-2 is the receptor for h-ferritin on oligodendrocytes. *Journal of neurochemistry*, **107**(6), 1495–1505.

Towe, K. (1981). Structural distinction between ferritin and iron-dextran (imferon). an electron diffraction comparison. *Journal of Biological Chemistry*, **256**(18), 9377–9378.

Vashisht, A. A., Zumbrennen, K. B., Huang, X., Powers, D. N., Durazo, A., Sun, D., Bhaskaran, N., Persson, A., Uhlen, M., Sangfelt, O., et al. (2009). Control of iron homeostasis by an iron-regulated ubiquitin ligase. *Science*, **326**(5953), 718–721.

Vera, N. P. M., Schmidt, R., Langer, K., Zlatev, I., Wronski, R., Auer, E., Havas, D., Windisch, M., von Briesen, H., Wagner, S., et al. (2014). Tracking of magnetite labeled nanoparticles in the rat brain using mri. *PloS one*, **9**(3), e92068.

von Haehling, S., Jankowska, E. A., van Veldhuisen, D. J., Ponikowski, P., & Anker, S. D. (2015). Iron deficiency and cardiovascular disease. *Nature Reviews Cardiology*, **12**(11), 659–669.

Vulpe, C. D., Kuo, Y.-M., Murphy, T. L., Cowley, L., Askwith, C., Libina, N., Gitschier, J., & Anderson, G. J. (1999). Hephaestin, a ceruloplasmin homologue implicated in intestinal iron transport, is defective in the sla mouse. *Nature genetics*, **21**(2), 195–199.

Wang, C.-Y., Jenkitkasemwong, S., Duarte, S., Sparkman, B. K., Shawki, A., Mackenzie, B., & Knutson, M. D. (2012). Zip8 is an iron and zinc transporter whose cell-surface expression is up-regulated by cellular iron loading. *Journal of Biological Chemistry*, **287**(41), 34032–34043.

Wang, N. & Ingber, D. E. (1995). Probing transmembrane mechanical coupling and cytomechanics using magnetic twisting cytometry. *Biochemistry and Cell Biology*, **73**(7-8), 327–335.

Wang, N., Butler, J. P., Ingber, D. E., et al. (1993). Mechanotransduction across the cell surface and through the cytoskeleton. *Science*, **260**(5111), 1124–1127.

Ward, R. J., Legssyer, R., Henry, C., & Crichton, R. R. (2000). Does the haemosiderin iron core determine its potential for chelation and the development of iron-induced tissue damage? *Journal of inorganic biochemistry*, **79**(1), 311–317.

Ward, R. J., Zucca, F. A., Duyn, J. H., Crichton, R. R., & Zecca, L. (2014). The role of iron in brain ageing and neurodegenerative disorders. *The Lancet Neurology*, **13**(10), 1045–1060.

Weigelin, B., Bakker, G.-J., & Friedl, P. (2016). Third harmonic generation microscopy of cells and tissue organization. *J Cell Sci*, **129**(2), 245–255.

Wheeler, M. A., Smith, C. J., Ottolini, M., Barker, B. S., Purohit, A. M., Grippo, R. M., Gaykema, R. P., Spano, A. J., Beenhakker, M. P., Kucenas, S., et al. (2016). Genetically targeted magnetic control of the nervous system. *Nature neuroscience*, **19**(5), 756–761.

White, C., Yuan, X., Schmidt, P. J., Bresciani, E., Samuel, T. K., Campagna, D., Hall, C., Bishop, K., Calicchio, M. L., Lapierre, A., et al. (2013). Hrg1 is essential for heme transport from the phagolysosome of macrophages during erythrophagocytosis. *Cell metabolism*, **17**(2), 261–270.

Willmann, J. K., Van Bruggen, N., Dinkelborg, L. M., & Gambhir, S. S. (2008). Molecular imaging in drug development. *Nature reviews Drug discovery*, **7**(7), 591–607.

Wong, B. X. & Duce, J. A. (2015). The iron regulatory capability of the major protein participants in prevalent neurodegenerative disorders. *The Importance Of Iron In Pathophysiologic Conditions*, page 368.

Worthen, C. A. & Enns, C. A. (2014). The role of hepatic transferrin receptor 2 in the regulation of iron homeostasis in the body.

Worthington, M. T., Browne, L., Battle, E. H., & Luo, R. Q. (2000). Functional properties of transfected human dmt1 iron transporter. *Ameri-*

can Journal of Physiology-Gastrointestinal and Liver Physiology, **279**(6), G1265–G1273.

Wu, L. J.-c., Leenders, A. M., Cooperman, S., Meyron-Holtz, E., Smith, S., Land, W., Tsai, R. Y., Berger, U. V., Sheng, Z.-H., & Rouault, T. A. (2004). Expression of the iron transporter ferroportin in synaptic vesicles and the blood–brain barrier. *Brain research*, **1001**(1), 108–117.

Yadav, S. (2010). Heavy metals toxicity in plants: an overview on the role of glutathione and phytochelatins in heavy metal stress tolerance of plants. *South African Journal of Botany*, **76**(2), 167–179.

Yamashiro, D. J., Tycko, B., Fluss, S. R., & Maxfield, F. R. (1984). Segregation of transferrin to a mildly acidic (ph 6.5) para-golgi compartment in the recycling pathway. *Cell*, **37**(3), 789–800.

Yang, Z. & Klionsky, D. J. (2010). Eaten alive: a history of macroautophagy. *Nature cell biology*, **12**(9), 814–822.

Yao, J., Kaberniuk, A. A., Li, L., Shcherbakova, D. M., Zhang, R., Wang, L., Li, G., Verkhusha, V. V., & Wang, L. V. (2016). Multiscale photoacoustic tomography using reversibly switchable bacterial phytochrome as a near-infrared photochromic probe. *Nature methods*, **13**(1), 67–73.

Yoo, S.-S., Bystritsky, A., Lee, J.-H., Zhang, Y., Fischer, K., Min, B.-K., McDannold, N. J., Pascual-Leone, A., & Jolesz, F. A. (2011). Focused ultrasound modulates region-specific brain activity. *Neuroimage*, **56**(3), 1267–1275.

Yuste, R., Peinado, A., & Katz, L. C. (1992). Neuronal domains in developing neocortex. *Science*, **257**(5070), 665–669.

Zecca, L., Gallorini, M., Schünemann, V., Trautwein, A. X., Gerlach, M., Riederer, P., Vezzoni, P., & Tampellini, D. (2001). Iron, neuromelanin and ferritin content in the substantia nigra of normal subjects at different ages: consequences for iron storage and neurodegenerative processes. *Journal of neurochemistry*, **76**(6), 1766–1773.

Zecca, L., Youdim, M. B., Riederer, P., Connor, J. R., & Crichton, R. R. (2004). Iron, brain ageing and neurodegenerative disorders. *Nature Reviews Neuroscience*, **5**(11), 863–873.

Zhang, X., Surguladze, N., Slagle-Webb, B., Cozzi, A., & Connor, J. (2006). Cellular iron status influences the functional relationship between microglia and oligodendrocytes. *Glia*, **54**(8), 795–804.

Zhao, N., Gao, J., Enns, C. A., & Knutson, M. D. (2010). Zrt/irt-like protein 14 (zip14) promotes the cellular assimilation of iron from transferrin. *Journal of Biological Chemistry*, **285**(42), 32141–32150.

Zhao, Y., Araki, S., Wu, J., Teramoto, T., Chang, Y.-F., Nakano, M., Abdelfattah, A. S., Fujiwara, M., Ishihara, T., Nagai, T., et al. (2011). An expanded palette of genetically encoded ca2+ indicators. *Science*, **333**(6051), 1888–1891.

Appendix

Chemicals

Table 2: Chemicals

Chemical	Manufacturer	Order number
10x Tris/Glycine/SDS	Bio-Rad	1610732
16 % Formaldehyd Solution (w/v)	Thermo Fisher Scientific	28908
"3-(2-Pyridyl)-5,6-diphenyl-1,2,4-triazine-p,p-disulfonic acid monosodium salt hydrate (Ferrozine)"	Sigma-Aldrich	160601
3,3-Diaminobenzidine tetrahydrochloride hydrate	Sigma-Aldrich	32750
Ammonium acetate	Sigma-Aldrich	A1542
Ammonium iron(II) sulfate hexahydrate	Sigma-Aldrich	1.03792
Ampicilin	Sigma-Aldrich	A5354
apo-Transferrin human	Sigma-Aldrich	T2036
cOmplete™, EDTA-free Protease Inhibitor Cocktail	Roche	11873580001
Coomassie Brilliant Blue R-250	Bio-Rad	161-0436
Ferric citrate	Sigma-Aldrich	F3388
Geneticin	Sigma-Aldrich	4727878001
Ferritin from equine spleen	Sigma-Aldrich	F4503
HEPES	Carl Roth	HN77.3
Hoechst 33342 Solution	Thermo Fisher Scientific	62249

Hydrochloric acid	Sigma-Aldrich	H1758
Hydrogen peroxide solution	Sigma-Aldrich	H1009
Hygromycin B	Sigma-Aldrich	H0654
IPTG	Sigma-Aldrich	I6758
Kanamycin	Sigma-Aldrich	K0129
L-Ascorbic acid	Sigma-Aldrich	A5960
Mini-PROTEAN® TGX™ Precast Gels	Bio-Rad	4561041
M-PER™ Mammalian Protein Extraction Reagent	Thermo Fisher Scientific	78501
Native Sample Buffer	Bio-Rad	161-0738
Neocuproine	Sigma-Aldrich	N1501
Nitric acid	Sigma-Aldrich	364576
Non-fat Milk	Carl Roth	T145.2
Poly-L-lysine solution	Sigma-Aldrich	P8920
Potassium hexacyanoferrate(III)	Sigma-Aldrich	208019
Potassium permanganate	Sigma-Aldrich	60459
Protease Inhibitor Cocktail	Sigma-Aldrich	P8340
Roti®garose (Agarose)	Carl Roth	3810
Sample Buffer, Laemmli 2× Concentrate	Sigma-Aldrich	S3401
Sodium chloride	Carl Roth	962.1
Sodium citrate	Sigma-Aldrich	1613859
Sodium hydroxide	Sigma-Aldrich	757527
Transferrin human	Sigma-Aldrich	T3705
TRIS Hydrochlorid	Carl Roth	9090.2
Triton™ X-100	Sigma-Aldrich	X100
Trypan Blue Solution, 0.4%	Thermo Fisher Scientific	15250061

Molecular Biological and Analytical Kits and Reagents

Table 3: Molecular biological and analytical kits and reagents

Kit/Reagent	Manufacturer	Order nummer
Alexa Fluor® 488 NHS Ester (Succinimidyl Ester)	Thermo Fisher Scientific	A20000
Anti-Ferritin Heavy Chain antibody	abcam	ab65080
Anti-Mouse IgG	Sigma-Aldrich	A9044
Anti-Rabbit IgG	abcam	ab6721
Aqua-Poly/Mount	Polyscience, Inc.	18606
Cytotoxicity Detection Kit (LDH)	ROCHE	11644793001
ECL Prime Western Blotting detection reagent	Amersham	RPN2232
Immun-Blot® PVDF Membrane	Bio-Rad	1620177
Lysosome Isolation Kit	Sigma-Aldrich	LYSISO1-1KT
Monoclonal ANTI-FLAG® M2 antibody	Sigma-Aldrich	F3165
NEBuilder® HiFi DNA Assembly Master Mix	NEB	E2621L
One Shot® TOP10 Chemically Competent	Thermo Fisher Scientific	C404006
PCR Master Mix (2X)	Genaxxon	M3014.0100
Pierce™ BCA Protein Assay Kit	Thermo Fisher Scientific	23225
Q5® High-Fidelity 2X Master Mix	NEB	M0492S
QIAGEN Plasmid Plus Maxi Kit	Qiagen	12963
QIAprep Spin Miniprep Kit	Qiagen	27104
SuperBlock™ (TBS) Blocking Buffer	Thermo Fisher Scientific	37537

Hardware

Table 4: Hardware

Hardware	Manufacturer	Order nummer
Countess II FL Automated Cell Counter	Thermo Fisher Scientific	AMQAF1000
10 ml Pipet	Greiner-Bio one	607 107
25 ml Pipet	Greiner-Bio one	760 180
50 ml Pipet	Greiner-Bio one	768 180
ÄKTA pure 25	Thermo Fisher Scientific	29018226
Bruker BioSpec 94/20USR, 9.4 T	Bruker	
Corning® Costar® center well culture dish	Corning	CLS3260
COUNTING CHAMBER (C-Chip)	biochrom	P DHC-N01
Dialysis membrane Spectra/Por® - MWCO 300 000	Carl Roth	8977
Dounce tissue grinder set	Sigma-Aldrich	D9938
Eppendorf Research® plus 3-pack	Eppendorf	3120000909
EVOS FL Auto Cell Imaging System	Thermo Fisher Scientific	AMAFD1000
FUSION-FX7 SPECTRA	Vilber	VILB151115461
Greiner CELLSTAR® dish 10 cm	Greiner-Bio one	P7612
Leica SP5	Leica	
Macs MS Columns	Miltenyi Biotec	130-042-201
Mastercycler Gradient	Eppendorf	6321000019
Mini-PROTEAN® Tetra Vertical Electrophoresis Cell	Bio-Rad	1658004
minispin; Rotor: F-45-12-11	Eppendorf	5452000018
Multipette® E3	Eppendorf	4987000010
Nunc™ 384-Well Optical Bottom Plates	Thermo Fisher Scientific	142761
Nunc™ Coded Cryobank Vial Systems	Thermo Fisher Scientific	374088
OctoMACS™ Separator	Miltenyi Biotec	130-042-108
PIPETBOY	Integra Biosciences	613-4437

Poly-L-Lysine Coated Glass Coverslips (12 mm Round)	BD Biosciences	354085
RES 400 1H 112/072 Quad TR AD	Bruker	
S20-Seven Easy	Mettler Toledo	51302803
Sartorius Basic	Sartorius	BA 210 S
SpectraMax M5	moleculardevices	
Superdex 200 Increase 10/300 GL	GE Healthcare	28990944
TitroLine 7000	SI Analytics	TL 7000-M2/20
Tru Heat 3010 generator	Trumpf-Hüttinger	
Varifuge 3.0 R; Rotor: 8074	Heraeus	26049

Antibiotics

Table 5: Antibiotica concentrations

Antibiotic	Final concentration
Ampicilin	100 µ/ml
G418	700 µg/ml
Kanamycin	50 µg/ml
Hygromycin B	50 µ/ml

Cell Culture Item

Table 6: Cell culture items

Item	Manufacturer	Order nummer
Accutase	Thermo Fisher Scientific	AT104
Advanced DMEM	Thermo Fisher Scientific	12491023
Ampicillin	Sigma-Aldrich	A5354
Fetal Bovine Serum	Thermo Fisher Scientific	10082139
G418 Solution	Sigma-Aldrich	G418-RO
Gluta-Max	Thermo Fisher Scientific	35050061
Kanamycin solution	Sigma-Aldrich	K0254
Lipofectamine® 3000	Thermo Fisher Scientific	L3000001
Penicillin-Streptomycin	Thermo Fisher Scientific	10378016
Synth-a-Freeze	Thermo Fisher Scientific	A1254201
Xfect™ Transfection Reagent	Takara	631317

Primer

Table 7: Primer

Construct	forward (5'-3')	reverse (5'-3')
TfR1 into pcDNA3	GCG CGC GAA TTC ATG ATG GAT CAA GCT AGA TC	GCG CGC CTC GAG TTA AAA CTC ATT GTC AAT GT
PCBP amplification	GAA TTC GCC GCC ACC ATG	CTC GAG TCA GCT GCT CC
Fusion of P2A to Zip14 (1)	TGA AAC AGG CCG GCG ACG TGG AAG AGA AC CCT GGC CCT ATG AAG AGA CTG CAC CCT	TCA CTT GTC GTC GTC GTC C
Fusion of P2A to Zip14 (2)	GGC AGC GGC GCC ACC AAC TTC AGC CTG CTG AAA CAG GCC GGC GAC	TCA CTT GTC GTC GTC GTC C
P2A Zip14 into pcDNA-hFT (1)	GAC AGT GAT AAT GAA AGC GGC AGC GGC GCC ACC AAC	TCG AGG CTG ATC AGC TCA CTT GTC GTC GTC GTC CTT GTA GTC
P2A Zip14 into pcDNA3-hFt (2)	GCT GAT CAG CCT CGA CTG	GCT TTC ATT ATC ACT GTC TCC
P2A Zip14 into pcDNA3-LHFT (1)	AGC GAC AAC GAG AGC GGC AGC GGC GCC ACC AAC	CTA TAG AAT AGG GCC CTC ACT TGT CGT CGT CGT CCT TGT AGT C
P2A Zip14 into pDNA3-LHFT (2)	GGG CCC TAT TCT ATA GTG TC	GCT CTC GTT GTC GCT GTC
P2A fusion to TfR1 (1)	TGA AAC AGG CCG GCG ACG TGG AAG AGA ACC CTG GCC CTA TGA TGG ATC AAG CTA GAT CAG	TTA AAA CTC ATT GTC AAT GTC CCA AAC
P2A fusion to TfR1 (2)	GTC GCC GGC CTG TTT CAG CAG GCT GAA GTT GGT GGC GCC GCT GCC	GGC AGC GGC GCC ACC AAC TTC AGC CTG CTG AAA CAG GCC GGC GAC

P2A TfR1 into pcDNA3-hFt (1)	GAC AGT GAT AAT GAA AGC GGC AGC GGC GCC ACC AAC	TCG AGG CTG ATC AGC TTA AAA CTC ATT GTC AAT GTC CCA AAC GTC ACC AG
P2A TfR1 into pcDNA3-hFt (2)	GCT GAT CAG CCT CGA CTG	GCT TTC ATT ATC ACT GTC TCC
P2A TfR into pcDNA3-LHFT (1)	AGC GAC AAC GAG AGC GGC AGC GGC GCC ACC AAC	CTA TAG AAT AGG GCC CTT AAA ACT CAT TGT CAA TGT CCC AAA CGT CAC CAG
P2A TfR into pcDNA3-LHFT (2)	GGG CCC TAT TCT ATA GTG TC	GCT CTC GTT GTC GCT GTC
QC pcDNA-LHFTP2AZip14	GGC AGC GGC GCC ACC AAC	GCT CTC GTT GTC GCT GTC GCC
QC pcDNA3-hFTP2PZip14	GGC AGC GGC GCC ACC AAC	GCT TTC ATT ATC ACT GTC TCC CAG GGT G
PTS2 into pcDNA3-hFT	CCG GCC GAT CCG GCT GGA TGC CGC AGG CCG CGC CTT GCA TGA CGA CCG CGT CCA CC	ACC CCT CAG GTG GCC CAG CAC TAC CTG CAG CCT CTG CAT AAG CTT GGG TCT CCC TAT AGT G
hFT into pET151 (1)	GGA ATT GAT CCC TTC ACC ATG ACG ACC GCG TCC ACC	ATC TGA GCT CGC CCT TTT AGC TTT CAT TAT CAC TGT CTC
hFT into pET151 (2)	AAG GGC GAG CTC AGA TCC G	GGT GAA GGG ATC AAT TCC CTG
QC hFT w/o His-tag	ATT GAT CCC TTC ACC ATG ACG ACC G	CAT ATG TAT ATC TCC TTC TTA AAG TTA AAC

Geometrical RF-coil Drawing

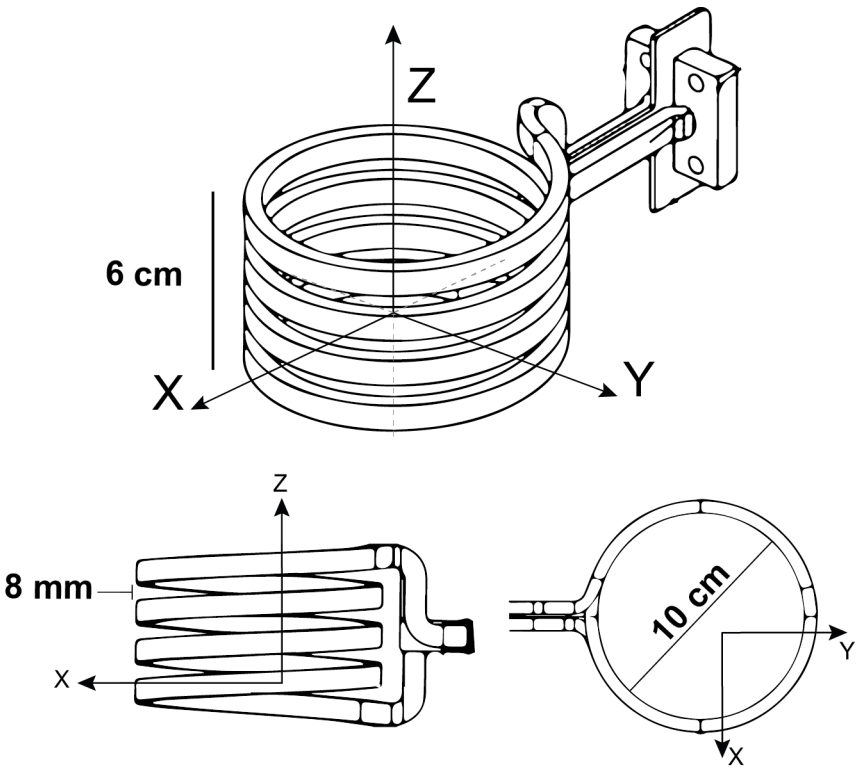

Figure 18: Schematic depiction of RF-coil

Magnetic Flux Density Simulation

The numerical magnetic flux density simulation was carried out by Jens-Uwe Mohring from the Trumpf-Huettinger GmbH with the comsol simulation software.

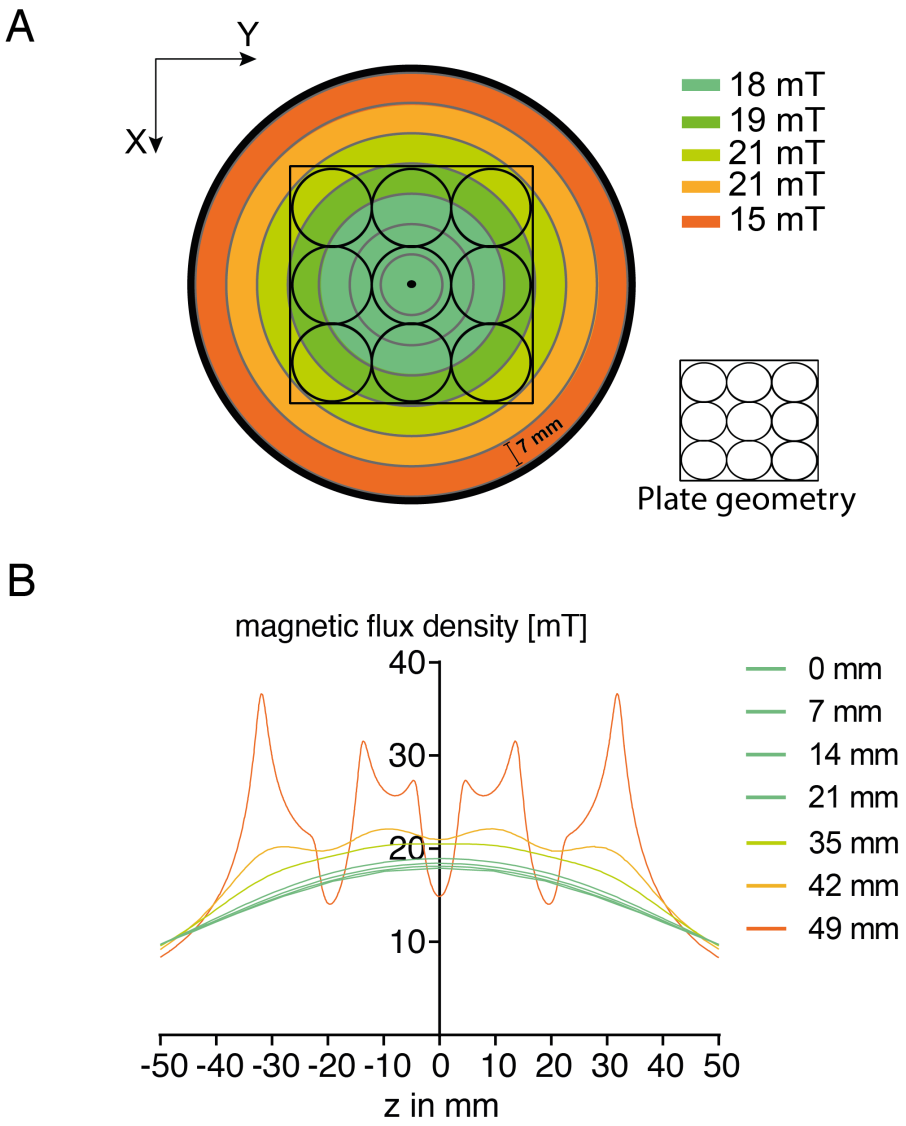

Figure 19: Magnetic flux densitiy simulation. (A) Magntic flux density distribution at 462 A and 319 kHz in xy plane at z=0. The plate geometry used for the experiments is depicted. (B) Magnetic flux density in z direction.

Ferritin Localization

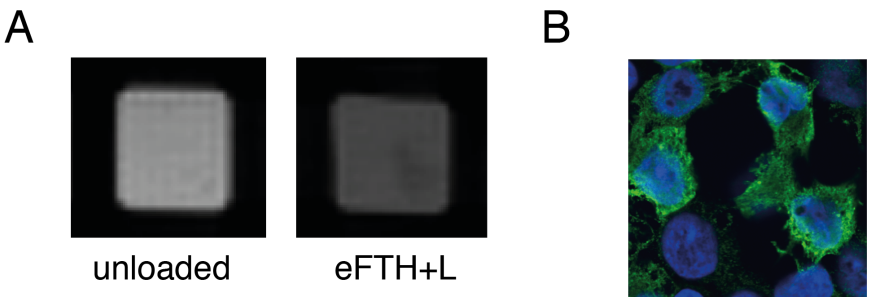

Figure 20: Ferritin localization. (A) MR-measurements of lysosomal fractions with and without ferritin loading after Tim-2 expression. (B) Cytosolic localization of overexpressed hFt.

hFTH-Mag Size Exclusion Chromatography

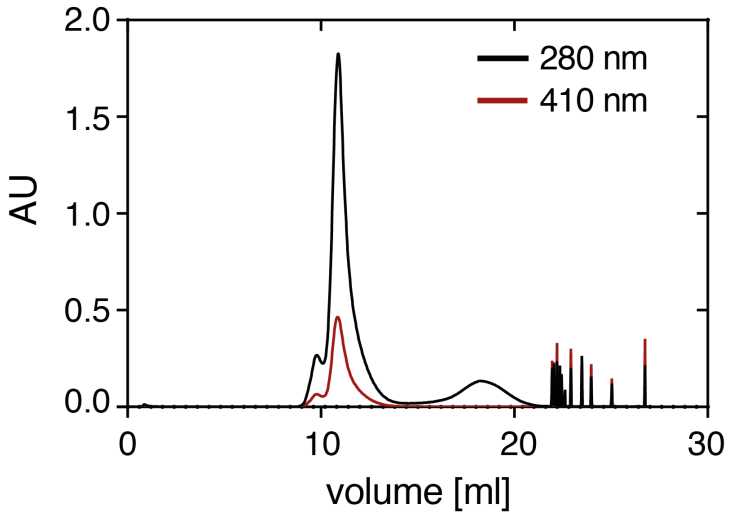

Figure 21: Size exclusion chromatography of hFTH-Mag. Absorption at a wavelenght of 280 nm is correlated with protein absorption. Absorption at a wavelenght of 410 nm is correlated with iron absorption.

Acknowledgments

The time of my doctoral studies was the most instructive period of life until now. I am grateful to Gil Westmeyer who gave me the opportunity to conduct my research in a extremely interdisciplinary field of life science. At all times the equipment, the scientific possibilities and freedom in the research conducted were extraordinary. He thought me important principles of science, beginning from detailed experimental setups and ending with big picture thinking. During the entire period he was always kind, polite and helpful whenever I needed his help.
Furthermore I want to thank Wolfgang Wurst who was my second supervisor. His critical questions during the thesis committee meeting were always helpful for the reevaluation of the project and gave me the right direction for further experiments. Another member of my thesis committee was Michael Winklhofer. I admire his clear, analytically thinking and I am grateful for the close scientific exchange and especially his advises during the last year. Without the experiments he conducted and his help, my research would not have been as exciting as it was.
I am grateful to all our collaborators who helped us with important experiments and enabled experiments and analytic methods we could not conduct in our laboratory. I thank Markus Seeger for the OA and THG measurements and their analysis. It was a pleasure to work with him, because of this clear thinking and his vigorous work attitude.
I thank the lab members Yuan Yuan, Ahne, Anurag, Sherly, Michele and Jeff for the scientific discussions and the fun moments we all spent together. I am grateful to Antonella who had very important suggestions for the manuscripts of the paper and who gave me numerous times valuable

scientific advice. I want to thank Giorgio for introducing me to the field of MRI and teaching me the basics. Also I want to thank Hannes for being a helpful member of the lab, who always gave me a hand when ever I wanted to do more experiments I could handle. I am especially grateful to Anja. I enjoyed working with her very much and she was always a funny and understanding companion in our coffee breaks. I also want to thank Panos a lot for his scientific and non-scientific discussions. I probably owe him a Christmas bonus worth of coffee, but since he is a very generous soul, I assume that he is fine with it. The next person I want to thank is Felix. Felix was mentally, emotionally and scientifically and enormous help to me. He is probably one of the best scientist I know. I appreciated always his profound knowledge and his ability to wrap his mind around problem to finally solve them. I am really happy that we spent this many hours together at the HMGU. Furthermore, I want to thank Carlos who I liked to "bother" during my incubation times. Also, I thank Susanne who was at first my Master's student and then a very good colleague. Without her constant effort in the synthesis of magnetoferritin and her conduction of experiments, little of the ferritin work could have been done.
Undoubtedly the biggest help for me outside for the HMGU was Mariona. She stood by me in difficult times and always found a way to cheer me up even in desperate situations. More importantly, she showed me how to enjoy the good moments of life and celebrate them as they come. I am very grateful to my parents who always supported me during the whole time of my education and during more exotic endeavors. I want to thank also especially Frederik who is not only my brother but one of my closest and best friends. The time we spent together was always relaxing and enjoyable. I am grateful to Lourdes, Joan and to all the members of Mariona's family who were always caring and very welcoming when ever we visited them in Spain. I also want to thank Mira for the nice moments we shared and for the excellent food she provides whenever we meet. I am happy that I've found good friends here in Munich like Wolfi, Mariel, Chris, Nagore, Paul and Joana. I very much enjoyed the trips we did and the dinners we had together. Furthermore I want to give a big thanks to my

group of regulars. Christian, Hannes, Dave, Flo, Michi, Tobi, Tommy and Thorsten were always understanding if I missed out on meetings and they cheered me up every time we met. These meetings, full of positive energy and laughter, were always a highlight for me. I am very grateful to have such a good friend as Ignacio. We shared a lot of fun and contemplating moments in the flat share, the mountains and Spain together. I also thank Karo for spicing up our tips and dinners with her incredible energy. Mario's company was always fun and inspiring at the same time. I thanks Ahmed for showing me that there is always a way. I want to thank Beni for this long friendship and his ability to make the time we spend together such a nice experience. Last but not least I want to thank Nico for his long lasting friendship and his advice in all matters of life.

To all the people mentioned and too many more who accompanied me during this journey of my doctoral studies I am very much grateful. **Thank you!**

Munich, July 2017